The continuum limit and integer-valued vacuum charge

A. Calogeracos[a)]
Low Temperature Laboratory, Helsinki University of Technology, FIN-02015 HUT, Finland

N. Dombey
Centre for Theoretical Physics, University of Sussex, Brighton, BN1 9QJ, UK

(Submitted 14 July 1998, resubmitted 6 August 1998)
Pis'ma Zh. Éksp. Teor. Fiz. **68**, No. 5, 353–358 (10 September 1998)

We consider a topologically trivial field theory defined in a large box of size L and exploit the enumeration of states to point out that the vacuum charge is integral, contrary to what a commonly used formula seems to suggest. We show that the large L limit is subtle: Standard anticommutation relations require the presence of a somewhat unfamiliar normalization factor which in turn leads to observable effects for the vacuum charge density. © *1998 American Institute of Physics.* [S0021-3640(98)00117-0]

PACS numbers: 03.70.+k, 11.15.Ha

INTRODUCTION

In this note we consider the continuum limit of a field theory defined in a large box of size L. In the limit $L\to\infty$, all discrete states apart from bound states become continuum states. According to most textbooks, quantum field theory is supposed to be well understood in this limit. We show, however, that the limiting procedure is subtle, and unless proper care is exercized the usual prescriptions may give incorrect results. In particular, we show an example where the charge of the system seems to be a continuous function of the background field, whereas it should be integer-valued.

An example which we have discussed in previous papers (which are referred to as CDI[1] and CD2[2]) is provided by the second-quantized Dirac theory in the presence of a one-dimensional four-vector potential vanishing at spatial infinity. The usual limiting procedure for counting states in the continuum limit is given by

$$\sum\ (\text{states})\to\frac{1}{\pi}\int^{\infty}dk\left(L+\frac{d\delta}{dk}\right), \tag{1}$$

where $\delta(k)$ is the scattering phase shift for a particle of momentum k in that limit. Yet as we (and many others) have argued the vacuum charge Q_0 of the system defined in the normal way by the spectral asymmetry

$$Q_0=\frac{1}{2}\left\{\sum_k\ (\text{states with } E>0)-\sum_k\ (\text{states with } E<0)\right\}, \tag{2}$$

which is obviously integer-valued in a box of finite size L, is given in the continuum limit with the use of Eq. (1) by

$$Q_0=\frac{1}{2}\left\{\frac{1}{\pi}(\delta_+(\infty)-\delta_+(0)-\delta_-(\infty)+\delta_-(0))+N_+-N_-\right\}, \tag{3}$$

where $+$ and $-$ refer to electron and positron scattering phase shifts and N_+ and N_- are the number of positive and negative energy bound states. Since in one dimension (see CDI)

$$\delta_\pm(\infty)=\pm\int_{-\infty}^{\infty}V(z)dz,$$

this implies for the potential $V(z)=\lambda\,\delta(z)$ that $Q_0=\lambda/\pi$, which is a continuous function of λ. The correct result is calculated using Eq. (2) in CD2 and is found to be

$$Q_0=\mathrm{Int}\left[\frac{\lambda}{\pi}+\frac{1}{2}\right], \tag{4}$$

where Int denotes the integral part, which is obviously an integer. The erroneous result of Eq. (3) for the vacuum charge for this model is found in many places besides CDI — for example, in Refs. 3 and 4. The same error may also be responsible for similar results where other quantized quantities such as baryon charge or angular momentum seem to be given non-quantized values[5,6] for no apparent reason. It is interesting that in the same context an explicit counting argument gives quantized values, as expected.[6]

In CDI, following Barton,[7] we counted states and showed that the number of both positive and negative energy states is unchanged when a potential is switched on from zero. Thus the vacuum charge is still zero in the presence of a small potential: there is a bound state, but the number of continuum states has decreased by one. As the potential increases in strength, Q_0 changes by one, according to Eq. (2), whenever a state crosses $E=0$. So why is the erroneous result obtained, and how can it be avoided? We now turn to these points.

In order to quantize the model consistently with standard anticommutation relations it is essential that the eigenfunctions be normalized to unity. We shall see that to ensure correct normalization we have to include an unfamiliar normalization factor N which reduces to unity as $L\to\infty$; in fact $N^2=1+\tilde{O}(1/L)$. It turns out that the expression for N^2 involves the phase shifts in a way reminiscent of the incorrect result of Eq. (3). We obtain a new expression for the charge density, differing from the conventional one by terms of order $\sim 1/L$. We find a finite change in the vacuum charge (defined as the space integral of the vacuum charge density) induced by the spectral asymmetry residing in a certain region of space of the system. It is crucial to get this $1/L$ behavior correct if we wish to sum over states and convert sums to integrals via

$$\sum_k \to \frac{L}{\pi}\int_0^\infty dk. \tag{5}$$

There are topologically nontrivial models where the Dirac particle is coupled to a soliton; the attending zero modes induce non-integer values for the vacuum charge.[8] However, in problems with trivial topology such as ours, Q_0 is integral.

THE NORMAL MODES

The potential $V(z)$ is symmetric and is taken to vanish for $|z|>a$. We take the system in a box of length $2L$ with periodic boundary conditions $\psi(-L)=\psi(L)$. The wave functions are classified according to the magnitude of the wave vector outside the well and their parity. Positive energy solutions outside the potential take the form

$$u_{e,k}(z)=\frac{N_{e+}(k)}{\sqrt{L}}\sqrt{\frac{E+m}{2E}}\begin{pmatrix}\cos(kz\pm\Delta_{e+})\\ 0\\ \dfrac{ik}{E+m}\sin(kz\pm\Delta_{e+})\\ 0\end{pmatrix}, \tag{6}$$

$$u_{o,k}(z)=\frac{N_{o+}(k)}{\sqrt{L}}\sqrt{\frac{E+m}{2E}}\begin{pmatrix}i\sin(kz\pm\Delta_{o+})\\ 0\\ \dfrac{k}{E+m}\cos(kz\pm\Delta_{o+})\\ 0\end{pmatrix}. \tag{7}$$

The subscript $+$ in the phase shifts Δ refers to the sign of the energy. Similar expressions are valid for negative energy states $v_{e,k}$, $v_{o,k}$ provided we replace E by $|E|$ and change notation from Δ_{e+}, Δ_{o+}, $N_{e+}(k)$, $N_{o+}(k)$ to Δ_{e-}, Δ_{o-}, $N_{e-}(k)$, $N_{o-}(k)$. We also quote for future reference the form of the even bound-state wave function outside the well:

$$u_b(|z|>a)=C\begin{pmatrix}1\\ 0\\ i\dfrac{m-E_b}{\kappa}\\ 0\end{pmatrix}e^{-\kappa z},\quad \kappa=\sqrt{m^2-E_b^2}. \tag{8}$$

We impose the normalization

$$\int_{-L}^{L}dz\;\psi_k^{\dagger}(z)\psi_k(z)=1 \tag{9}$$

for all eigenstates of the Hamiltonian. For the bound state the appropriate value of C to ensure correct normalization depends on the detailed behavior of the potential.

The Landau–Lifshitz–Stone lemma. We rederive a result originally due to Stone[9] which itself is based on a problem in Landau and Lifshitz.[10] We start with the Dirac equation; the argument is equally valid for either positive or negative energy solutions (thus $E_k=\pm\sqrt{k^2+m^2}$),

$$\frac{1}{i}\alpha_z\frac{du_{k'}}{dz}+m\beta u_{k'}=E_{k'}u_{k'}+V(z)u_{k'}, \tag{10}$$

and left-multiply by $u_k^{\dagger}$,

$$\frac{1}{i}u_k^\dagger \alpha_z \frac{du_{k'}}{dz} + mu_k^\dagger \beta u_{k'} = E_{k'} u_k^\dagger u_{k'} + V(z) u_k^\dagger u_{k'}. \tag{11}$$

We then write the Dirac equation for u_k, take the Hermitian conjugate, and right-multiply by $u_{k'}$:

$$-\frac{1}{i}\frac{du_k^\dagger}{dz}\alpha_z u_{k'} + mu_k^\dagger \beta u_{k'} = E_k u_k^\dagger u_{k'} + V(z) u_k^\dagger u_{k'}\,. \tag{12}$$

Subtracting (12) from (11), we get

$$\frac{1}{i}\frac{d}{dz}(u_k^\dagger \alpha_z u_{k'}) = (E_{k'} - E_k) u_k^\dagger u_{k'}\,. \tag{13}$$

We integrate over z from z_1 to z_2:

$$\frac{1}{i}[u_k^\dagger \alpha_z u_{k'}]_{z_1}^{z_2} = (E_{k'} - E_k)\int_{z_1}^{z_2} u_k^\dagger u_{k'} dz\,. \tag{14}$$

We now take $k' = k + dk$ in the above equation and divide by dk:

$$\frac{1}{i}\left[u_k^\dagger \alpha_z \frac{du_k}{dk}\right]_{z_1}^{z_2} = \frac{dE}{dk}\int_{z_1}^{z_2} u_k^\dagger u_k dz \quad \text{or} \quad \frac{1}{i}\left[u_k^\dagger \alpha_z \frac{du_k}{dk}\right]_{z_1}^{z_2} = \frac{k}{E}\int_{z_1}^{z_2} u_k^\dagger u_k dz. \tag{15}$$

This is the key equation. Its power lies in the fact that to evaluate the left-hand side for $|z_1|, |z_2| > a$ it suffices to use the asymptotic expressions (6), (7) for the wave functions, where only the phase shifts appear.

Normalization of eigenfunctions. Note that the normalization condition (9) together with periodic boundary conditions entail restrictions on k. We apply relation (15) at the end points $z_1 = -L$, $z_2 = L$. Then in the left-hand side we only need the asymptotic expressions (6), (7), and on the right-hand side we can use Eq. (9) to set the integral equal to unity. The evaluation of the left-hand side simplifies because of the periodic boundary conditions. We thus obtain

$$N_{e,o\pm}(k) = \frac{1}{\sqrt{1 + \frac{1}{L}\frac{d\Delta_{e,o\pm}}{dk}}} \tag{16}$$

and therefore

$$N_{e,o\pm}^2(k) = \frac{1}{1 + \frac{1}{L}\frac{d\Delta_{e,o\pm}}{dk}} \simeq 1 - \frac{1}{L}\frac{d\Delta_{e,o\pm}}{dk} \tag{17}$$

for L large. Note that the quantities $N_{e,o\pm}^2(k) - 1$ vanish both when $V = 0$ and in the limit $L \to \infty$. Equation (16) is the main result of this note.

2. THE VACUUM CHARGE DENSITY

We focus on the charge density

$$\rho_k(z) = \psi_k^\dagger(z)\psi_k(z) \tag{18}$$

of an eigenstate $\psi_k(z)$ (of definite parity and sign of energy) corresponding to a particular wave vector k. An expression for $\rho_k(z)$ for the scattering states can be written for $|z|>a$ by using the asymptotic forms (6) and (7) of the wave functions. The charge density outside the well in the case of a positive-energy, even-parity wave function is given by

$$\rho_{e+}(k,z)=\frac{1}{2L}\left(1-\frac{1}{L}\frac{d\Delta_{e+}}{dk}\right)\cdot\left(1+\frac{m}{E}\cos(2kz+\Delta_{e+}(k))\right) \tag{19}$$

(the even-parity, negative-energy and the odd-parity wave functions give similar expressions). Equation (19) consists of the expected $1/2L$ part, an oscillating part, and a constant background $-(1/2L^2)d\Delta_{e+}/dk$. The latter is purely a consequence of the somewhat unfamiliar normalization factor. Integration over k via Eq. (5) and subtraction of the analogous contribution from negative energy states leads to an observable distortion of the vacuum charge density.

The charge $Q_{k,\mathrm{ext}}$ outside the well due to this state is given by

$$Q_{k,\mathrm{ext}}=\left(\int_{-\infty}^{-a}+\int_{a}^{\infty}\right)dz\,\rho_k(z)=2\int_{a}^{\infty}dz\,\rho_k(z), \tag{20}$$

since V is symmetric. To order $1/L$

$$Q_{k,\mathrm{ext,even},\pm}=1-\frac{a}{L}-\frac{m}{2LEk}\sin 2(ka+\Delta_{e\pm}(k))-\frac{1}{L}\frac{d\Delta_{e\pm}}{dk}, \tag{21}$$

$$Q_{k,\mathrm{ext,odd},\pm}=1-\frac{a}{L}+\frac{m}{2LEk}\sin 2(ka+\Delta_{o\pm}(k))-\frac{1}{L}\frac{d\Delta_{o\pm}}{dk}. \tag{22}$$

The charge of the bound state outside the well can be calculated from Eq. (8),

$$Q_{b,\mathrm{ext}}=C^2\frac{2m}{\kappa(E+m)}e^{-2\kappa a}. \tag{23}$$

In the absence of the potential the first two terms in Eqs. (21), (22) would still be there. We wish to calculate $Q_{0,\mathrm{ext}}$ defined as the part of Q_0 residing outside the well. (Since Q_0 itself vanishes, this charge is cancelled exactly by an opposite charge residing inside the well.) We see that the continuum contribution to the vacuum charge outside the well resulting from the last term in (21), (22) is given by

$$Q_{0,\mathrm{ext}}=\frac{1}{2\pi}(\delta_+(\infty)-\delta_+(0)-\delta_-(\infty)+\delta_-(0)) \tag{24}$$

(where the phase shifts δ refer, as before,[1] to the sum of the even and odd phase shifts), an expression which is very similar to Eq. (3) and which will in general give non-integral values for $Q_{0,\mathrm{ext}}$. To get the total continuum contribution we must integrate over the terms that depend on the mass explicitly. The final result is in general non-integral, since there is no reason why the charge inside or outside a particular region of space should be integer-valued.

CONCLUSION

We investigate a commonly used formula which seems to give non-integral vacuum charge in the continuum limit. Enumeration of the states established a one-to-one corre-

spondence between states for different values of the potential (including $V=0$), thus ensuring that the vacuum charge is integer-valued. We showed that consistency with standard anticommutation relations requires the presence of a somewhat unfamiliar normalization factor which modifies the charge density pertaining to a particular wave vector by a position-independent addend of order $1/L^2$. This term is sensitive to the violation of charge conjugation by the potential and leads to observable effects upon summation over all wave vectors. This is relevant to the calculation of the vacuum charge residing in a certain region of space. The existence of this localized charge is due to the distortion of the Dirac sea induced by the potential.

ACKNOWLEDGMENTS

We would like to thank Gabriel Barton, Fred Goldhaber, and Mike Birse for their help and encouragement. One of us (AC) wishes to thank Professor Volovik and the Low Temperature Laboratory of Helsinki University of Technology for their hospitality, and the EU Training and Mobility of Researches Program Contract #ERBFMGECT980122 for its support.

[a)]Permanent Address, NCA Research Associates, PO Box 61147, Maroussi 151 01, Athens, Greece

---

[1] A. Calogeracos, N. Dombey, and K. Imagawa, Yad. Fiz. **59**, 1331 (1996) [Phys. At. Nucl. **59**, 1275 (1996)].
[2] A. Calogeracos and N. Dombey, ''Klein tunnelling and the Klein paradox,'' Int. J. Mod. Phys. A (to be published); http://xxx.lanl.gov/abs/quant-ph/9806052.
[3] R. K. Bhaduri, *Models of the Nucleon: From Quarks to Soliton*, Addison-Wesley, Redwood City, Calif., 1988, pp 329–330.
[4] W. Greiner, B. Muller, and J. Rafelski, *Quantum Electrodynamics of Strong Fields*, Springer-Verlag, Berlin 1985, Eq. (9.150).
[5] J. Garriga and T. Vachaspati, Nucl. Phys. B **438**, 161 (1995).
[6] G. E. Volovik and T. Vachaspati, Int. J. Mod. Phys. B **10**, 471 (1996).
[7] G. Barton, J. Phys. A **18**, 479 (1985).
[8] J. Goldstone and F. Wilczek, Phys. Rev. Lett. **47**, 986 (1981).
[9] M. Stone, Phys. Rev. B **31**, 6112 (1985).
[10] L. D. Landau and E. M. Lifshitz, *Quantum Mechanics: Non-Relativistic Theory*, 3rd ed., Pergamon Press, Oxford, 1997 (Problem 2, § 133: Resonance scattering at low energies) [Russian original, Nauka, Moscow, 1974].

Published in English in the original Russian journal. Edited by Steve Torstveit.

Coherent effects in ultrashort pulse propagation through an optically thick three-level medium

V. V. Kozlov

Department of Physics, Texas A&M University, College Station, Texas 77843, USA; Physics Research Institute, St. Petersburg State University, 198904 St. Petersburg, Russia

E. E. Fradkin

Physics Research Institute, St. Petersburg State University, 198904 St. Petersburg, Russia

(Submitted 27 July 1998)
Pis'ma Zh. Éksp. Teor. Fiz. **68**, No. 5, 359–363 (10 September 1998)

A theoretical study is made of the propagation of a weak ultrashort pulse through an optically thick, inhomogeneously broadened three-level medium of the *V* configuration driven by a self-induced transparency pulse on the coupled transition. The weak coherent pulse experiences a greatly enhanced transparency. The new transparency effect is discussed in detail and the results are found to be in good agreement with recent experimental observations. © *1998 American Institute of Physics.* [S0021-3640(98)00217-5]

PACS numbers: 42.50.Md, 42.65.Re, 42.65.Tg

The pioneering work of McCall and Hahn on self-induced induced transparency (SIT)[1] was followed by a number of theoretical and experimental works on pulse propagation through systems of two-level atoms. The most exciting feature of this phenomenon is that above a critical power threshold a short coherent pulse can propagate with anomalously small energy loss while at resonance with a two-level system of absorbers. Recently a variety of new coherent nonlinear quantum optical phenomena have been found, in which a secondary optical pulse cooperates with or even controls a primary pulse, such as electromagnetically induced transparency (EIT),[2] simulton propagation,[3] Raman solitons,[4] and efficient upper-state excitation by counterintuitive pulse sequencing.[5]

In most cases the pulses are to be injected into a medium of atoms that are well approximated as a three-level Λ system. The majority of the effects are closely related to the phenomenon of EIT, which arises due to an excitation of a superposition wave function, often termed as a population-trapped or dark state.[6] In the bare atomic basis, this wave function contains no upper-state component and therefore, once prepared, is immune to any kind of decay which affects only the upper state. This kind of transparency is of little importance in a *V*-type system, if for no other reason than the trapped state for a *V*-type medium requires all the atoms to be in a superposition of the two upper states, $|a\rangle$ and $|c\rangle$. This is evidently not a case of practical interest, because normally all the atoms are initially prepared in the lower state $|b\rangle$. In this Letter we come back to the classical SIT effect and show on the basis of this effect how a new type of transparency originates in a three-level configuration of the *V* type.

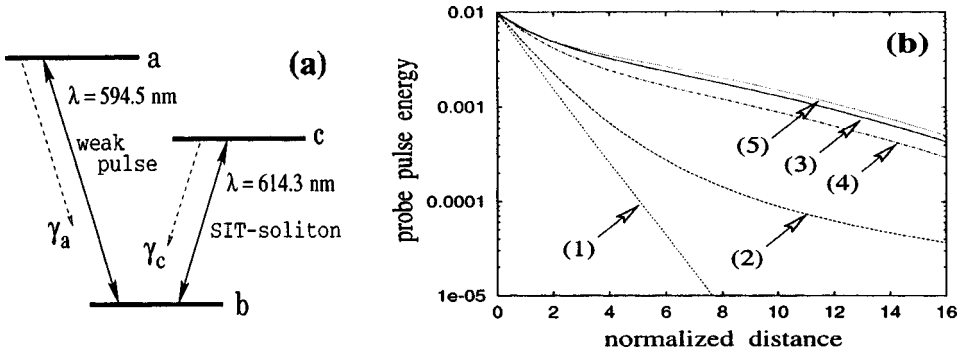

FIG. 1. a: Schematic level diagram of the absorbing medium in Ref. 7. The population decay rates (indicated with unidirectional arrows) are $\gamma_a = \gamma_c = 19$ ns. The relaxation times of all the polarizations, ρ_{ab}, ρ_{cb} and ρ_{ac}, are 11 ns, the inhomogeneous spectral width (FWHM) is 1400 MHz. b: Energy versus propagation distance: *1* — Beer's law; *2* — weak pulse in a two-level medium. Weak pulse in a *V*-type medium, driven by a SIT soliton: *3* — the peaks of the pulses coincide at the entrance; *4*,*5* — the weak pulse has a delay or advance, respectively, of 0.5 ns. For all figures: both pulses are sech-shaped; the durations of the weak and SIT pulses are 0.5 ns and 1 ns, respectivley, and the initial detuning is 290 MHz (750 MHz). Distances are normalized to the linear absorption coefficient on the $|a\rangle - |b\rangle$ transition, κ_{ab} (the linear absorption coefficient on the $|c\rangle - |b\rangle$ transition is $\kappa_{cb} = 2.14\,\kappa_{ab}$).

This letter is motivated by recent experiments[7] on the simultaneous propagation of two pulses through an inhomogeneously broadened *V*-type absorbing medium (the plasma of a positive glow-discharge neon column), see Fig. 1a. One of the pulses (the driving pulse), with a shape close to that of a SIT soliton and with a small detuning from the exact resonance, propagated at the resonant wavelength $\lambda = 614.3$ nm. Simultaneously, the other pulse (the probe pulse) was launched into the absorbing medium at the resonant wavelength $\lambda = 594.5$ nm and passed through it, attenuating by only a factor of 8. When the same probe pulse propagated independently it was absorbed so strongly that the experimenters were unable to detect the pulse at all at the output of the cell. Note that in the experiments the optical thickness $\kappa_{ab}L$ at $\lambda = 594.5$ nm was equal to 15, so that weak cw radiation should have been attenuated by a factor of $\exp(-15)$.

Our model for numerical calculations is based on the simultaneous solution of two Maxwell equations for the driving and probe fields, in the form of plane waves, and the density matrix equations for a three-level *V*-type absorber. It incorporates all the decay processes and the inhomogeneous broadening, the values of which are taken from the experiment of Ref. 7 (see figure captions for details).

Figure 1b displays the changes in energy with propagation distance. The abrupt absorption of weak cw radiation represents the familiar Beer's law of exponential energy decay; see curve *1*. Curve *2* shows how a short pulse attenuates during propagation in a two-level subsystem $|a\rangle - |b\rangle$, when the driving pulse is switched off. A strong deviation from Beer's law arises from the fact that the pulse is short and has a spectral width (''input'' in Fig. 3b), which is comparable to the width of the inhomogeneously broadened line (absorption spectrum in Fig. 3b). The additional transparency is due to a lower absorption of the spectral wings of the pulse. This effect, known as *abnormal classical absorption,* was described by Crisp in Ref. 8.

Curves *3*, *4*, and *5* in Fig. 1b correspond to the propagation of the probe pulse when

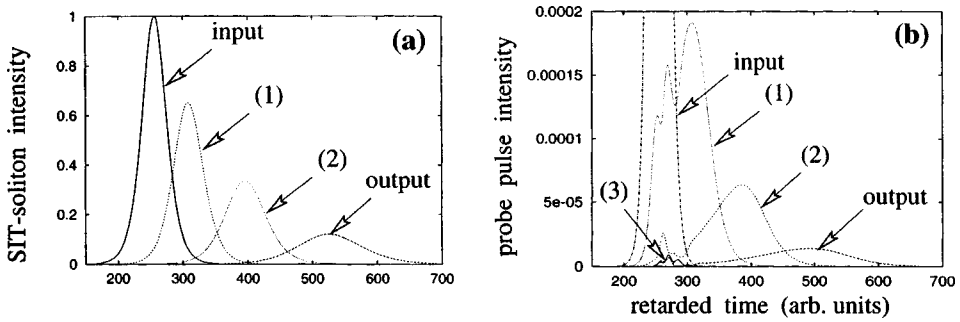

FIG. 2. a: SIT soliton shape for different propagation distances $\kappa_{ab} L$: *1* — 5; *2* — 10; ''output'' — 15. b: The same, for a weak pulse. Curve *3* shows the pulse shape at $\kappa_{ab} L = 15$ in a two-level configuration.

a drive pulse in the form of a SIT soliton is simultaneously launched into the medium on the adjacent transition. For curve *3* the two pulse peaks coincide at the entrance of the medium, while for curve *5* the probe pulse experiences an advance of 0.5 ns and for curve *4* a delay of the same magnitude. Transparency enhancement takes place for all three cases, and the most favorable conditions are established when the probe pulse goes ahead of the SIT soliton. One can see the order-of-magnitude increase in transparency in comparison with the case of independent pulse propagation [compare curves *2* and *3*].

The temporal shapes of the two pulses for four different propagation distances are plotted in Fig. 2. A SIT soliton propagates through the medium, demonstrating the familiar features of the SIT effect. As a result of relaxation of the atomic polarization between the $|a\rangle$ and $|b\rangle$ states and the decay of the $|a\rangle$ state, it gradually decreases in amplitude, with a corresponding increase in duration in order to keep its area equal to 2π. On the other hand, the probe pulse exhibits unusual behavior, clearly splitting into two parts. One part propagates with the velocity of light (without retardation in Fig. 2b) and is attenuated essentially in the same manner as if the pulse were propagating in the absence of a SIT soliton (compare the left-hand part of the ''output'' with curve *3*). The other, larger part is trapped by the SIT soliton and experiences a large delay. It is this part of the probe pulse that provides the transparency enhancement.

As is shown in Fig. 2a, the SIT pulse repeatedly reproduces itself while propagating through the medium. The theory of the classic SIT effect teaches us that the leading edge of a SIT soliton transfers the population from a lower state to an upper state, and then the second half of the pulse coherently restores the excited atoms to their original position. This energy exchange takes a finite interval of time, providing a significant pulse delay. The temporal evolution of the polarization executes a cycle, developing an absorptive portion at the leading edge and an identical gain portion at the trailing edge. Moreover, the polarization of *each* frequency group of inhomogeneously broadened line oscillates *in phase* with that of any other frequency group, providing complete transparency for the SIT soliton. In a two-level medium the ''phase locking'' mechanism turns on only for a sufficiently strong pulse with area greater than π.

Now, comparing all stages of the reshaping displayed in the two plots of Fig. 2, one can see that the probe pulse also experiences a delay, associated with the absorption of the leading edge and the subsequent reradiation energy at the trailing edge, just as for a

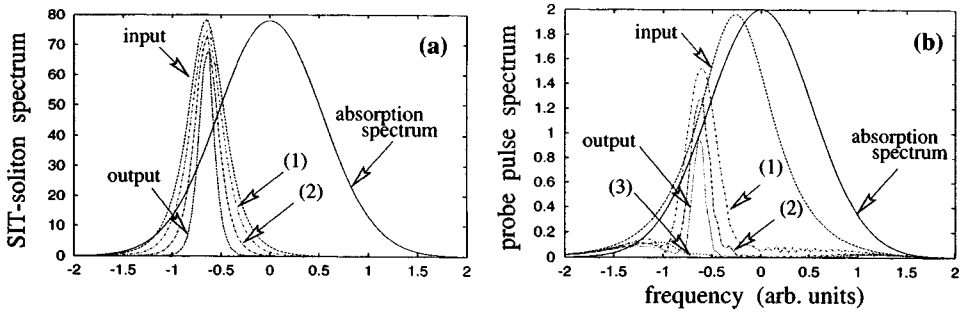

FIG. 3. The same as in Fig. 2, for the spectra of the pulses.

SIT soliton. Based on this similarity we conclude, and this is the key point of this paper, that the polarizations of the atoms of all frequency groups within the inhomogeneously broadened line are ''locked'' together, i.e., oscillate in phase with one another. This differs dramatically from the conventional picture of the interaction of a weak pulse with a two-level system. Since the dipoles have different detunings from a center of an atomic line, they oscillate at different frequencies and cannot interfere constructively, and so the net atomic polarization, obtained as a summation over all frequency groups, quickly vanishes. In a three-level configuration a SIT pulse on the adjacent transition provides an additional ''phase locking'' mechanism between all dipoles on the $|a\rangle - |b\rangle$ transition, allowing a weak pulse to propagate without absorption. So, in some sense, we are dealing with an extension of the SIT effect for weak coherent pulses.

Spectral measurements[7] have revealed a new effect, involving a shift of the probe pulse spectrum towards the carrier frequency of the SIT pulse. Figure 3a shows how an initially detuned SIT pulse keeps its carrier frequency and shape unchanged, while its spectral width gradually decreases with distance. This fact is due to the unique correspondence between a temporal shape and its Fourier transform, such that spreading in the time domain corresponds to contraction in the frequency domain. Also, a probe pulse spectrum does not have any striking features if its propagation is not accompanied by a SIT pulse. The absorbing medium ''burns a hole'' in the probe spectrum, such that only far off-resonant frequency components can survive (curve *3* in Fig. 3b).

In the presence of a SIT soliton the evolution of the probe pulse spectrum becomes more complicated and manifests two pronounced tendencies: (i) pulling of the spectral peak towards the carrier frequency of the SIT pulse, in accordance with the experimental observations; (ii) amplification of those frequency components which are arranged about the center of the SIT pulse spectrum. The surprising thing is that the whole frequency region exhibits a real amplification and grows within the place where the spectral components vanish without the SIT pulse (compare to curve *3*). Of course, this fact does not violate energy conservation, and the net pulse energy gradually decreases with propagation, as is shown in Fig. 1b. The amplification of some spectral components is due to the SIT pulse, which induces a nonlinear frequency conversion involving the transfer of energy from some spectral regions to another.

In conclusion, we have demonstrated a new type of transparency for a weak coherent pulse — transparency induced by a SIT soliton propagating on the adjacent transition

of a three-level system. The SIT pulse induces correlations between dipoles oscillating with different frequencies. It is these correlations that underlie the physics of the new transparency effect. An impressive rearrangement of the probe pulse spectrum and a frequency pulling effect accompany the new phenomenon.

The authors are pleased to acknowledge a fruitful discussion with V. S. Egorov and N. M. Reutova. This work was supported by RFBR (97-02-16013-a). V. V. K is also grateful for financial support from the Grant Center for Natural Sciences of St. Petersburg.

[1] S. L. McCall and E. L. Hahn, Phys. Rev. Lett. **18**, 908 (1967); Phys. Rev. **183**, 457 (1969).
[2] K.-J. Boller, A. Imamoglu, and S. E. Harris, Phys. Rev. Lett. **66**, 2593 (1991); S. E. Harris, Phys. Rev. Lett. **70**, 552 (1993).
[3] M. J. Konopnicki and J. H. Eberly, Phys. Rev. A **24**, 2567 (1981); L. A. Bolshov and V. V. Likhanskii, Kvant. Elektron. **12**, 1339 (1985) [Sov. J. Quantum Electron. **15**, 889 (1985)].
[4] K. Drühl, R. G. Wentzel, and J. E. Carlsten, Phys. Rev. Lett. **51**, 1171 (1983).
[5] J. R. Kuklinski, U. Gaubatz, F. T. Hioe, and K. Bergmann, Phys. Rev. A **40**, 6741 (1989).
[6] G. Alzetta, A. Gozzini, L. Moi, and G. Orriols, Nuovo Cimento B **36**, 5 (1976); R. M. Whitley and C. R. Stroud Jr., Phys. Rev. A **14**, 1498 (1976).
[7] N. V. Denisova, V. S. Egorov, V. V. Kozlov *et al.*, Zh. Éksp. Teor. Fiz. **113**, 71 (1998) [JETP **86**, 39 (1998)].
[8] M. D. Crisp, Phys. Rev. A **1**, 1604 (1970); L. Allen and J. H. Eberly, *Optical Resonance and Two-Level Atoms*, Wiley, New York, 1975.

Published in English in the original Russian journal. Edited by Steve Torstveit.

Gain without inversion in a medium of 1/2→1/2 atoms

N. P. Konopleva and A. M. Tumaĭkin
Novosibirsk State University,[a] 630090 Novosibirsk, Russia

(Submitted 24 July 1998)
Pis'ma Zh. Éksp. Teor. Fiz. **68**, No. 5, 364–369 (10 September 1998)

Amplification of a probe field without inversion in a medium of nondegenerate two-level atoms pumped by a circularly polarized optical field in resonance with a 1/2→1/2 atomic transition in the presence of a dc magnetic field orthogonal to the wave vector of the pump field is demonstrated. It is shown that gain without inversion is possible in strong optical and magnetic fields in the case of a pump with a finite spectral width which can be much greater than the natural width of the excited level. © *1998 American Institute of Physics.*
[S0021-3640(98)00317-X]

PACS numbers: 32.80.Bx, 42.50.Gy

Coherent effects in atomic systems can lead to a variety of physical phenomena, such as transparency induced by an electromagnetic field, an increase of the refractive index, and gain without a population inversion in the medium. Gain arising in noninverted atomic media in the presence of an interaction of a strong coherent field and a pump field has been investigated in detail for two-level[1,2] and various schemes employing three-level atoms with Λ, Ξ, and V configurations.[3–9] In general, gain without inversion can be interpreted as a nonlinear interference effect[10] resulting in amplification of a probe field in some regions of the spectrum. In this case, the total absorption coefficient is determined only by the population difference (for three-level systems see also Ref. 11). The physical processes leading to gain without inversion have a different origin in different systems. For example, the Raman resonance in the absorption spectrum of a probe field for a two-level atom (see, for example, Ref. 12) or gain without inversion in Λ and V systems, studied in Refs. 3, 5, and 8, can be interpreted as being a manifestation of a ''hidden'' inversion which exists in the basis of dressed states. For the three-level Λ scheme proposed in Ref. 6, inversion in the basis of dressed states is absent. In this case amplification in the basis of dressed states can be interpreted as a coherent effect caused by the probe field (''light amplification by coherence'').[13]

In the present letter we present a new amplification scheme for two-level nondegenerate atoms. In contrast to the works cited above, in the scheme considered below the strong optical field need not be coherent. Coherent atomic effects leading to gain without inversion arise when the atoms interact with a wide-band pump field in the presence of a dc magnetic field. The width of the spectrum of the pump field can be much greater than the natural width of the excited state.

STATEMENT OF THE PROBLEM

We are considering the propagation of a probe field in a medium consisting of two-level atoms with a ground state $J_e=1/2$ and excited state $J_g=1/2$ which are degenerate with respect to the projection of the angular momentum. Pumping is performed with a circularly polarized resonant optical field. The system is placed in a magnetic field directed perpendicular to the wave vector of the pump field. The probe field propagates along the magnetic field. The Hamiltonian of the atom can be written in the form

$$\hat{H}=\hat{H}_0+\hat{H}_1+\hat{H}_2+\hat{V}=\hat{H}'+\hat{V}, \tag{1}$$

where $\hat{H}_0$ is the Hamiltonian of the stationary atom, $\hat{H}_1$ and $\hat{H}_2$ are the Hamiltonians describing the interaction of the atom with the pump field and with the magnetic field, and $\hat{V}$ is the Hamiltonian of the interaction with the probe field. For definiteness, we shall assume that the σ^+ polarized pump field propagates along the z axis and that the magnetic field has a nonzero projection on the x axis: $\mathbf{H}=H\mathbf{e}_x$. Choosing the quantization axis along the wave vector of the pump field, we have

$$\hat{H}_0=\hbar\omega_0(|3\rangle\langle 3|+|4\rangle\langle 4|), \tag{2}$$

$$\hat{H}_1=\hbar(W(t)e^{-i(\omega t-kz)}|3\rangle\langle 1|+\text{h.c.}), \tag{3}$$

$$\hat{H}_2=\hbar(\Omega|1\rangle\langle 2|+\Omega_1|4\rangle\langle 3|+\text{h.c.}), \tag{4}$$

where the Hamiltonian $\hat{H}_1$ is written in the rotating-wave approximation. In Eqs. (2)–(4)

$$|1\rangle=|J_g=1/2,-1/2\rangle,|2\rangle=|J_g=1/2,1/2\rangle,$$

$$|3\rangle=|J_e=1/2,1/2\rangle,|4\rangle=|J_e=1/2,-1/2\rangle; \tag{5}$$

ω_0 and ω are the frequencies of the atomic transition and the pump field, $W(t)=\langle 1/2||d||1/2\rangle E=\exp[i\phi(t)]/\hbar\sqrt{3}$ is the Rabi frequency, where E is the amplitude of the pump field, $\langle 1/2||d||1/2\rangle$ is the reduced matrix element of the dipole moment operator of the atom; $\Omega=-\mu_0 gH/\hbar\sqrt{2}$ and $\Omega_1=-\mu_0 g_1 H/\hbar\sqrt{2}$ are the Larmor frequencies of the ground and excited states, and g and g_1 are the g factors of the ground and excited states. The phase factor containing $\phi(t)$ describes fluctuations of the phase in the case of a pump with a wide spectrum. For a coherent pump $\phi(t)=0$ and without loss of generality the Rabi frequency W can be assumed to be real and positive.

The Hamiltonian $\hat{V}$ in the rotating-wave approximation has the form

$$\hat{V}=\hbar(V_z e^{-i(\omega_p t-k_p x)}(|3\rangle\langle 2|-|4\rangle\langle 1|)+V_y e^{-i(\omega_p t-k_p x)}(|3\rangle\langle 1|-|4\rangle\langle 2|)+\text{h.c.}), \tag{6}$$

where ω_p is the frequency of the probe field. The probe field in Eq. (6) is represented in the form of components which are linearly polarized along the z and y axes and have Rabi frequencies $V_z=-\langle 1/2||d||1/2\rangle E_z/\hbar\sqrt{6}$ and $V_y=i\langle 1/2||d||1/2\rangle E_y/\hbar\sqrt{6}$, respectively.

The interaction of the atom with the probe field was studied in the standard manner using perturbation theory. The systems of equations for the density matrix in the zeroth, $\hat{\rho}^{(0)}$, and first, $\hat{\rho}^{(1)}$, orders in the probe field are

$$\frac{\partial}{\partial t}\hat{\rho}^{(0)}=-\frac{i}{\hbar}[\hat{H}',\hat{\rho}^{(0)}]+\hat{\Gamma}\hat{\rho}^{(0)}, \tag{7}$$

$$\frac{\partial}{\partial t}\hat{\rho}^{(1)} = -\frac{i}{\hbar}[\hat{H}', \hat{\rho}^{(1)}] + -\frac{i}{\hbar}[\hat{V}, \hat{\rho}^{(0)}] + \hat{\Gamma}\hat{\rho}^{(1)}, \tag{8}$$

The term $\hat{\Gamma}\hat{\rho}$ in Eqs. (7) and (8) describes radiative relaxation. For the transition under study

$$(\hat{\Gamma}\hat{\rho})_{mn} = -\gamma/2\rho_{mn}, \quad m=1,2, \ n=3,4 \quad (m=3,4, \ n=1,2);$$

$$(\hat{\Gamma}\hat{\rho})_{mn} = -\gamma\rho_{mn}, \quad m=3,4, \ n=3,4;$$

$$(\hat{\Gamma}\hat{\rho})_{11\ (22)} = 2\gamma/3\rho_{33\ (44)} + \gamma/3\rho_{44\ (33)}, (\hat{\Gamma}\hat{\rho})_{12} = \gamma/3\rho_{43},$$

where γ is the natural width of the excited level.

In studying a pump with a wide spectrum, we assumed that the phase fluctuations are a Markov random process and satisfy the stochastic equation

$$d\phi = \sqrt{2b}dw, \tag{9}$$

where w is a normal Wiener process.[14] Equation (9) corresponds to the Fokker–Planck equation with diffusion coefficient b. The autocorrelation function in this case is

$$\langle W^*(t)W(t+\tau)\rangle = |W|^2 e^{-2b\tau}. \tag{10}$$

One can see that b determines the width of the spectrum of the pump wave. The limit $b \to 0$ corresponds to a coherent pump field.

When the phase fluctuations of the pump wave (9) are taken into account, the equations for the density matrix (7) and (8) transform into a system of stochastic equations. The equations for the density matrix elements $\overline{\rho_{ij}}$ averaged over the fluctuations were obtained using the corresponding Fokker–Planck equation for the distribution functions $f(\rho_{ij}^{(0)}, \rho_{ij}^{(1)}, \phi, t)$, $i,j=1,4$ (see, for example, Ref. 14).

The propagation of the probe field in the steady-state case is described by the following system of abridged equations:

$$\frac{\partial}{\partial x}\begin{pmatrix} V_z \\ V_y \end{pmatrix} = -i4\pi\frac{nk_p|\langle 1/2||d||1/2\rangle|^2}{6\hbar}\begin{pmatrix} r_{32}-r_{41} \\ r_{31}-r_{42} \end{pmatrix}, \tag{11}$$

where n is the density of atoms and $\overline{\rho_{ij}^{(1)}} = r_{ij}\exp[-i(\omega_p t - k_p x)]$ $(i=3,4; \ j=1,2)$ are the fluctuation-averaged stationary amplitudes of the optical coherences at the frequency of the probe field. After obtaining the stationary solutions of the equations for the matrix elements of the density matrix, averaged over the fluctuations of the phase of the pump field, to zeroth and first orders in the probe field, we found the absorption coefficients (gains) of the normal modes.

RESULTS AND DISCUSSION

In a $\sigma+$-polarized pump field in the absence of a magnetic field the atoms optically pump the Zeeman sublevel $|2\rangle$ of the ground state (Fig. 1). As a result, orientation along the wave vector of the pump field arises. Such a medium is obviously transparent to the $\sigma+$-polarized probe field. For other polarizations the probe field will be absorbed. When a magnetic field is switched on, the atomic magnetic moment starts to precess around the direction of the magnetic field. In a basis tied to the pump field, this is expressed as

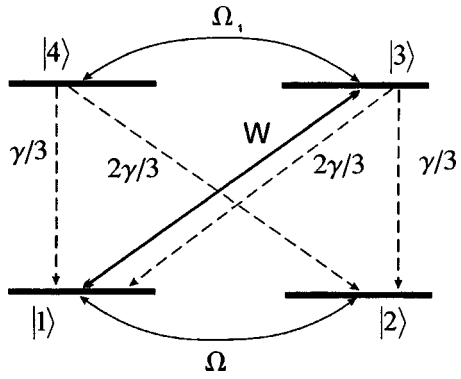

FIG. 1. Diagram of the atomic levels and transitions with the quantization axis along the wave vector of the pump field: The thick line shows transitions induced by the pump field, the dashed lines show spontaneous transitions, and the fine lines show transitions caused by a magnetic field.

transitions between the Zeeman sublevels (see Fig. 1). As a result of the combined action of the light and magnetic fields, all sublevels of the ground and excited states will be populated, and the optical coherences and the coherences between the Zeeman sublevels will also be nonzero. In such a complicated four-level system, the optical properties of the medium with respect to the probe field will change substantially: One of the normal modes can be amplified in the absence of inversion between the ground and excited states and of inversion between any pair of sublevels of the ground and excited states.

a) Coherent pump field. For a coherent pump field we found the susceptibility tensor of the medium in analytical form at exact resonance of the pump field and a probe field in the case of equal g factors of the ground and excited states ($\Omega_1=\Omega$). The linear absorption coefficients (gains) of the normal modes of the probe field were found. It was found that one of the normal modes can be amplified. For this mode, an equation determining the boundary between the regions of absorption and amplification for one of the normal modes was found. This equation is a polynomial of degree 10 in $(|W|/\gamma)^2$ and $(\Omega/\gamma)^2$; we do not present it here because of its complexity. As numerical calculations show, only one root of the equation is physically meaningful. The computational results are presented in Fig. 2. As one can see, amplification of the probe field is possible, including in weak magnetic fields, $\Omega \ll \gamma$. In this case gain occurs when the Rabi frequency of the pump field is greater than a critical value $|W|_c \approx 1.95\sqrt{\gamma\Omega}$. In strong magnetic fields ($\Omega \gg \gamma$) gain occurs if $|W|>|W_c|\approx 1.19\sqrt{\gamma\Omega}$. As numerical calculations of the line shape of the probe field showed, at exact resonance of the pump field the gain is maximum at line center.

To interpret the effect we examined amplification in a basis of dressed states (eigenstates of the Hamiltonian $\hat{H}'$) in the limit of strong fields $|W|$, $\Omega \gg \gamma$. We found that amplification does not reduce to inversion in the basis of dressed states. Therefore even in the basis of dressed states amplification is a consequence of coherence effects in a four-level atomic system.

The results presented above were all obtained without taking into account the motion of the atoms. It is clear that in a Doppler-broadened medium with orthogonal propa-

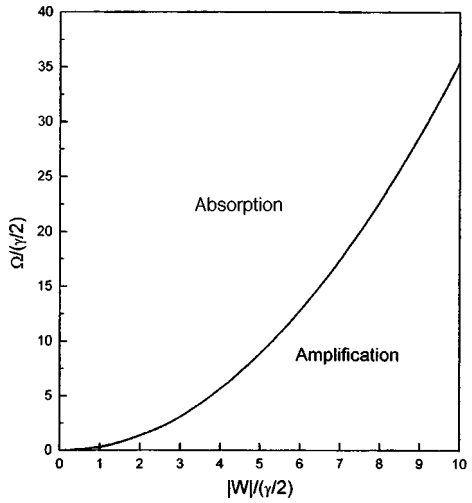

FIG. 2. Regions of absorption and amplification of a normal mode in the case of a coherent pump field and equal g factors of the ground and excited states.

gation of optical fields, the pump and probe fields will interact with different velocity groups of atoms. This can result in a decrease or vanishing of the amplification of the probe field. Thus it is of interest to examine the case of pumping with a wide spectrum.

b) Pump field with a wide spectrum. In studying the interaction of atoms with a wide-band pump, we assumed that the spectrum is narrower than the splitting between

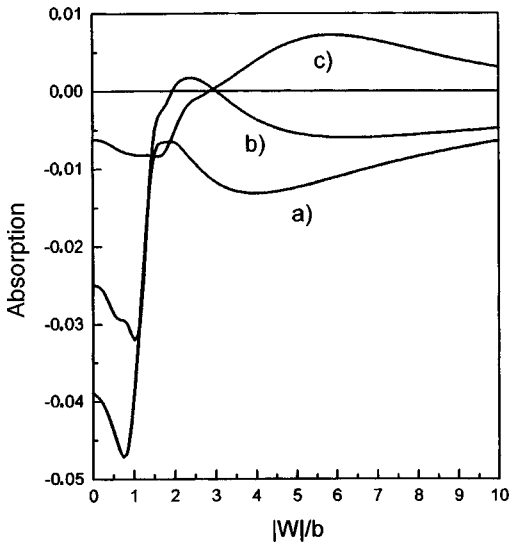

FIG. 3. Numerical calculations of the linear absorption coefficient for a normal mode as a function of the Rabi frequency for different values of the Larmor frequency: a) $\Omega = 0.8b$; b) $\Omega = b$; c) $\Omega = 2b$. The regions where the coefficient is positive correspond to amplification.

fine (hyperfine) structure components, and the two-level atom approximation is valid. In the limit $b \gg \gamma$, Ω, W (i.e., $b \to \infty$), both normal modes are absorbed. However, in the case $b \gg \gamma$ and strong optical and magnetic fields, $\Omega \sim b$, $W \sim b$, one of the normal modes can be amplified (Fig. 3). This is the main difference from the case of coherent pumping, where gain is possible in weak fields. Thus, as long as the diffusion of the phase of the pump field is comparable to the precession frequency and the Rabi frequency, atomic coherence effects can cause absorption to give way to amplification. Just as a for a coherent pump field, the gain is maximum at exact resonance for the probe field.

In conclusion, we note that atomic coherence effects in schemes for gain without inversion, where a strong coherent ''control'' field is used, depend strongly on the fluctuations of the ''control'' field. A strong decrease in the gain when the width of the spectrum of the ''control'' field becomes of the order of the radiation width of the excited level was demonstrated in Refs. 15 and 16 for Λ and V schemes. In our scheme the atomic coherence effects are due to the combined action of the pump field and a dc magnetic field. In this case the amplification of the probe field can occur in the presence of pumping of atoms by an optical field with a spectrum of finite width. In addition, in strong optical and magnetic fields the width of the spectrum can be much greater than the radiation width of the excited level. In this case an atomic medium acts as a ''converter'' of partially coherent into coherent light.

[a)]e-mail: llf@admin.nsu.ru

[1] S. G. Rautian and I. I. Sobel'man, Zh. Éksp. Teor. Fiz. **41**, 456 (1961) [Sov. Phys. JETP **14**, 328 (1962)].
[2] B. R. Mollow, Phys. Rev. A **5**, 2217 (1972).
[3] O. A. Kocharovskaya and Ya. I. Khanin, JETP Lett. **48**, 630 (1988).
[4] S. E. Harris, Phys. Rev. Lett. **62**, 1033 (1989).
[5] M. O. Scully, S. Y. Zhy, and A. Gavrielides, Phys. Rev. Lett. **62**, 2813 (1989).
[6] A. Imamoglu, J. E. Field, and S. E. Harris, Phys. Rev. Lett. **66**, 1154 (1991).
[7] G. Bhanu Prasad and G. S. Agarwal, Opt. Commun. **86**, 409 (1991).
[8] S. Basil and P. Lambropoulos, Opt. Commun. **78**, 163 (1990).
[9] Y. Zhy, Phys. Rev. A **45**, R6149 (1992).
[10] S. G. Rautian, G. I. Smirnov, and A. M. Shalagin, *Nonlinear Resonances in the Spectra of Atoms and Molecules* [in Russian], Nauka, Nobosibirsk, 1979.
[11] A. K. Popov, V. M. Kuchin, and S. A. Myslovets, Zh. Éksp. Teor. Fiz. **113**, 455 (1998) [JETP **86**, 244 (1998)].
[12] C. Cohen-Tannoudji and S. Reynaud, J. Phys. B **10**, 345 (1977).
[13] G. S. Agarwal, Phys. Rev. A **44**, R28 (1991).
[14] C. W. Gardiner, *Handbook of Stochastic Methods for Physics, Chemistry, and the Natural Sciences*, Springer-Verlag, Berlin, 1985 [Russian translation, Mir, Moscow, 1986].
[15] S. Sultana and M. S. Zubary, Phys. Rev. A **49**, 438 (1994).
[16] S. Gong and Z. Xu, Opt. Commun. **115**, 65 (1995).

Translated by M. E. Alferieff

Special features of wide-band EPR spectroscopy of singlet states in weak magnetic fields

V. F. Tarasov[a)]

Kazan Physicotechnical Institute, Kazan Science Center, Russian Academy of Sciences, 420029 Kazan, Russia

(Submitted 24 July 1998)
Pis'ma Zh. Éksp. Teor. Fiz. **68**, No. 5, 370–375 (10 September 1998)

A resonance change in microwave absorption in zero magnetic field, which is not due to magnetic-field dependence of the energy levels of the spin systems, is observed for a number of non-Kramers paramagnetic ions (Cr^{2+}, Ni^{2+}, Fe^{2+}) in synthetic forsterite. It is shown that these signals could be due to narrowing of the homogeneous spin packet of an inhomogeneously broadened EPR line in zero magnetic field. © *1998 American Institute of Physics.*
[S0021-3640(98)00417-4]

PACS numbers: 76.30.−v, 33.35.+r

Electron paramagnetic resonance (EPR), which was discovered in 1944, is now one of the most informative physical methods for investigating paramagnetic centers in solids at the microscopic level. However, this is completely true only for Kramers ions, with an odd number of electrons. For non-Kramers ions, with an integral magnetic moment, the system of electronic spin levels in crystal fields of low symmetry often splits into singlets. The energy splitting between these singlets depends on the structure of the crystal and the nature of the paramagnetic center, and it can vary over wide limits. Often it is too large to detect resonance transitions between these levels by means of ordinary EPR spectrometers.

In this connection, wideband tunable quasioptical spectrometers with coherent microwave radiation generators based on backward wave tubes provide great possibilities for studying non-Kramers ions in low-symmetry crystal fields.[1–4] Their frequency can be tuned over a quite wide continuous range, making it possible to perform investigations in a range of frequencies from 50 to 1000 GHz. Wideband EPR spectroscopy makes it possible to detect resonance transitions in zero magnetic field. In many cases, this expands and supplements information obtained about spin systems when studying resonance transitions in high fields.[5] However, EPR spectroscopy of singlet states in weak magnetic fields has certain peculiarities. This is due to the fact that in the absence of a magnetic field the magnetic moment μ of a singlet state equals zero. For this reason, the energy of an isolated singlet level does not depend on the magnetic field. In a system consisting of two singlet states with wave functions ψ_1 and ψ_2 a dependence of the level energies on the magnetic field appears if the magnetic moment operator **J** possesses

nonzero off-diagonal matrix elements $M_{12}=\langle\psi_1|\mathbf{J}|\psi_2\rangle$. Then the difference of the level energies in a magnetic field is determined by the expression

$$W=\sqrt{(\Delta)^2+(2g\beta B)^2|M_{12}|^2}, \tag{1}$$

where Δ is the energy difference between the levels, g is the spectroscopic splitting factor, β is the Bohr magneton, and B is the magnetic induction. In weak magnetic fields, when $g\beta B|M_{12}|\ll\Delta/2$, the splitting between the levels depends quadratically on the magnetic field:

$$W=\Delta\left(1+2\frac{g^2\beta^2|M_{12}|^2B^2}{\Delta^2}\right). \tag{2}$$

If the number of spin levels whose states are mixed by the magnetic field is greater than two, the dependence of W on B can be quite complicated. Nonetheless, in weak magnetic fields the energy of a singlet state is, to a good approximation, proportional to B^2. In standard EPR spectrometers the magnetic field dependence of the microwave absorption is measured. In addition, as a rule, the magnetic field is modulated in magnitude and the spectrum has the form of the derivative of the absorption signal. If the standard procedure is used for spectroscopy of singlet states in weak magnetic fields, the resonance lines will be broadened, while their intensity should drop as the frequency at which the spectrum is recorded approaches the splitting in a crystal field. No signals should be observed near zero magnetic field, since $dW/dB\sim 0$. Despite this, we have previously observed experimentally additional resonance signals due to a strong change in the resonant microwave absorption by paramagnetic ions[6] in zero magnetic field for a number of non-Kramers ions of the iron group in synthetic forsterite (Cr^{2+}, Ni^{2+}, and Fe^{2+}).

In the present work we have made a detailed experimental investigation of such signals for a resonance transition with $\Delta=96.4$ GHz. Here we propose a possible mechanism for the formation of these signals. Earlier, we identified this transition tentatively as a transition between the states $|\pm 2\rangle$ of the Fe^{2+} ion in an octahedrally coordinated position $M1$. The crystal lattice of forsterite has four magnetically nonequivalent centers of this type, the projections of whose principal axes are tilted away from the **a** axis of the lattice by angles of $\pm 3.5°$ and $\pm 13°$ in the *ab* and *ac* planes, respectively.[7] The experiments were performed in the Voigt geometry, i.e., the wave vector **k** of plane-polarized microwave radiation was perpendicular to the vector **B**. The orientation of the sample corresponded to $\mathbf{k}\|\mathbf{c}$ and $\mathbf{B}\|\mathbf{a}$, and the microwave magnetic field vector $\mathbf{B}_1$ could rotate in the *ab* plane. Figure 1 shows examples of the spectra at different frequencies for a sample at temperature 4.2 K. One can see that, just as expected, as the spectrometer frequency decreases, the resonance field decreases and the linewidth in the magnetic scan increases. Additional signals at $B=0$ are present in the spectra *c* and *d*. Investigation of the characteristics of these signals showed that they are observed in a narrow frequency range corresponding to the width of the resonance transition line in zero magnetic field. In contrast to ordinary EPR signals, for them the line center always corresponds to $B=0$. The amplitude of the signals depended strongly on the orientation of the sample in the magnetic field. In addition, for some orientations the phase of the signal was inverted. Further investigations led us to conclude that the zero-field resonance lines are a combination of at least two different signals. A signal of the first type is shown in spectrum *e*

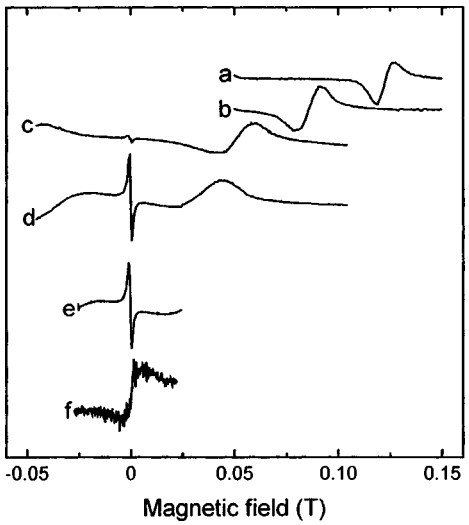

FIG. 1. EPR signals of a center with 96.4 GHz splitting in a crystal field in synthetic forsterite at different frequencies: a) 97.5 GHz, b) 97.0 GHz, c) 96.6 GHz, d) 96.5 GHz, e) 96.4 GHz ($\Delta B_0 = 8$ G), f) 96.4 GHz ($\Delta B_0 = 0.25$ G).

in Fig. 1. It is approximately Lorentzian with the peaks of the derivative separated by 12 G. The spectrum was recorded with a modulation amplitude of the magnetic field $\Delta B = 8$ G. As ΔB decreases, the amplitude of the signal of the first type decreases rapidly, and at the same time a signal of the second type with wide wings appears. Figure 1f, where the scale is increased by a factor of 30, shows this signal recorded with $\Delta B = 0.25$ G. Aside from the shape, the signals of different types differ in the dependences of the amplitude on the orientation of the vector $\mathbf{B}_1$ relative to the crystallographic axes. As $\mathbf{B}_1$ rotates in the *ab* plane, the signal of the first type does not change polarity; its polarity corresponds to a decrease in the zero-field absorption coefficient, and its amplitude I_1 is described quite well by the dependence $I_1 \sim \cos^4\theta$, where θ is the angle between the directions of $\mathbf{B}_1$ and $\mathbf{B}$ ($\mathbf{B} \| \mathbf{a}$). The dependence of the amplitude of signals of the second type on the orientation of $\mathbf{B}_1$ in the *ab* plane is complicated and cannot be described by simple functions for arbitrary orientation of the sample in a magnetic field. Characteristically, the polarity of these signals changes as the vector $\mathbf{B}_1$ rotates, i.e., a maximum or minimum of absorption can occur in zero magnetic field. We note that for $\mathbf{B}_1$ orientations in which signals of the first type are weak, signals of the second type are detected for large values of ΔB also.

The nature of signals of the second type has not yet been determined. Further investigations are required to determine the mechanism leading to their formation. Only the nature of signals of the first type will be discussed below. In our opinion, these signals appear in connection with a characteristic feature of the singlet states of paramagnetic ions in weak magnetic fields, specifically, the dependence of μ on B. For singlet states with $g\beta B|M_{12}| \ll \Delta/2$ the magnetism is of a polarizational character, and μ is proportional to the magnetic field

$$\mu = 4\frac{g^2\beta^2|M_{12}|^2}{\Delta^2}B. \tag{3}$$

For this reason the secular part of the dipole–dipole interactions at $B=0$ vanishes. The nonsecular part of the dipole–dipole interactions does not depend on the magnetic field, but it is small for an inhomogeneously broadened line. For this reason, for $B=0$ strong narrowing of a homogeneous packet occurs. Since the secular part of the dipole–dipole interactions is proportional to μ^2, the dependence of the width of the homogeneous packet on the field can be written in the form $\delta = C + D \cdot B^2$, where C is the magnitude of the homogeneous broadening due to the mechanisms which are unrelated with the secular part of the dipole–dipole interaction, and D is a coefficient of proportionality.

At the same time, it is well known that for an inhomogeneously broadened EPR line, the resonance absorption coefficient depends on the spin–spin and spin–lattice relaxation times T_2 and T_1 when saturation effects are taken into account.[8,9] In Ref. 9, for $S=1/2$ and a Lorentzian form of the homogeneous packet, a simple expression was obtained for the resonance contribution to the magnetic susceptibility:

$$\chi = \frac{1}{2}\chi_0\omega h(\omega-\omega_0)\frac{1}{(1+\gamma^2B_1^2T_1T_2)^{1/2}}. \tag{4}$$

Here χ_0 is the static magnetic susceptibility, ω_0 is the resonance frequency, and $h(\omega - \omega_0)$ is the shape of the inhomogeneously broadened EPR line. Extending this expression to arbitrary spin[10] gives an expression for the microwave power absorbed by the spin system per unit time:

$$P = \frac{1}{4}\chi_0\omega h(\omega-\omega_0)\frac{B_1^2}{(1+\gamma^2B_1^2|M_{1,2}|^2T_1T_2)^{1/2}}. \tag{5}$$

The physical picture of the T_2 dependence of the absorbed power is quite simple.[11] Only resonant spins absorb microwave energy. On account of the dipole–dipole interaction the excitation spreads to all spins in a homogeneous packet of width $\delta = 1/T_2$ and is transferred to the lattice in the process of spin–lattice relaxation. Therefore the spin–lattice relaxation efficiency depends on the number of spins in the homogeneous packet. As the packet width changes, the degree of saturation of the homogeneous packet and therefore the resonance absorption coefficient both change. The shape of the observed signals is described quite well by expression (5) when the dependence of T_2 on B is taken into account. The curve in Fig. 2 shows the computed dependence of the derivative of the absorption as a function of B; the points correspond to the experimental spectrum. In the calculation, the parameters C and D were chosen so as to obtain the best agreement between theory and experiment. Thus, analysis of the shape of the zero-field signals yields a relation between the magnetic-field-independent part of the homogeneous broadening and the contribution of the secular part of the dipole–dipole interactions. Unfortunately, the absolute values of these contributions to the homogeneous width of a spin packet cannot be obtained on the basis of existing experimental data.

Analysis of expression (5) shows that the amplitude of the zero-field signals should be proportional to $(B_1)^4$, i.e., to the squared intensity of the microwave radiation. An experimental check confirmed this dependence. Figure 3 displays the experimental

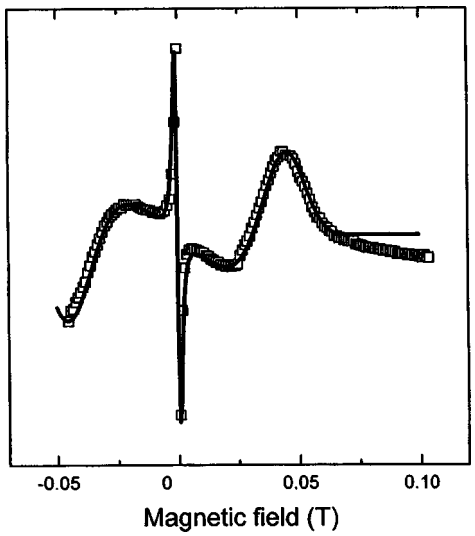

FIG. 2. Comparison of the experimental zero-field spectrum of a resonance signal at 96.5 GHz (squares) with the calculation (line).

dependences of the amplitudes of ordinary EPR signals (squares) and the zero-field signal (circles) versus the intensity of the microwave radiation. The lines correspond to linear and quadratic dependences. An explanation of the orientational dependence of the signal amplitude is obtained in this model. In our case of a transition between the states $|\pm 2\rangle$ in a spin system with spin $S=2$, the wave functions of the states in the first approximation have the form[12]

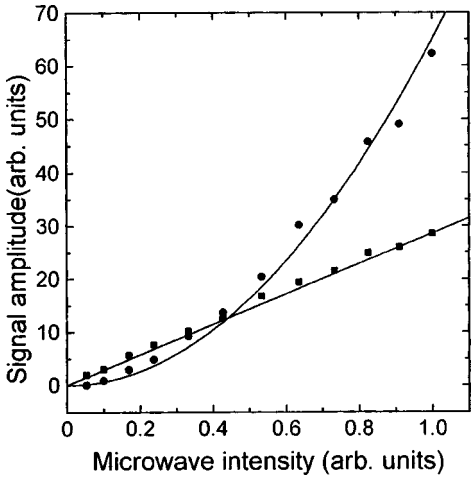

FIG. 3. Amplitudes of ordinary EPR signals (squares) and the zero-field signal (circles) versus the intensity of the microwave radiation; curves — linear and quadratic dependences.

$$\psi_{1,2}=\frac{1}{\sqrt{2}}(a_1|+2\rangle \pm a_2|-2\rangle), \tag{6}$$

where $a_1=a_2$ for $B=0$. For such states only the z component of the magnetic dipole moment operator possesses nonzero matrix elements. For this reason, the probability of magnetic dipole transitions between these states is proportional to $(B_1\cos\theta)^2$, and in Eq. (4) one should use $B_1\cos\theta$ instead of B_1. Thus, when the vector $\mathbf{B}_1$ deviates from the principal axis of the center, the amplitude of the signals should decrease as $(\cos\theta)^4$, as was in fact observed experimentally.

We note that other spectroscopic manifestations of the dependence of μ on B had been observed earlier. In the case that the resonance line is inhomogeneously broadened by the superhyperfine interaction, the linewidth was observed to decrease in weak magnetic fields.[13] The effect that we observed is due to a different manifestation of this dependence, specifically, narrowing of a homogeneous spin packet inside an inhomogeneously broadened EPR line. Its presence indicates that the broadening of resonance transitions is inhomogeneous and that the dipole–dipole interactions make the dominant contribution to the width of a homogeneous packet. Since in our case no decrease was observed in the zero-field inhomogeneous line width, it is obvious that for the given center inhomogeneous broadening is due to the variance of the local crystal fields.

On the whole, wideband EPR spectroscopy in weak magnetic fields yields additional information about the line shape and nature of the broadening of resonance transitions that is lost in stationary methods when working in high magnetic fields. These data are especially valuable for the submillimeter frequency range, where there are no pulsed spectrometers.

I thank K. M. Salikhov for helpful discussions. This work was supported by a Grant from the Academy of Sciences of Tatarstan.

[a)]e-mail: tarasov@dionis.kfti.kcn.ru

[1] E. A. Vinogradov, N. A. Irisova, T. S. Mandel'shtam, and T. A. Shmaonov, Prib. Tekh. Éksp., No. 5, 192 (1967).
[2] J. Magarino, J. Tuchendler, J. P. D'Haenens, and A. Linz, Phys. Rev. B **13**, 2805 (1976).
[3] M. Motokawa, H. Ohta, and N. Maki, Int. J. Infrared Millim. Waves **12**, 149 (1991).
[4] V. F. Tarasov and G. S. Shakurov, Appl. Magn. Reson. **2**, 571 (1991).
[5] R. Bramley, Int. Rev. Phys. Chem. **5**, 211 (1986).
[6] G. S. Shakurov and V. F. Tarasov, Proc. Soc. Photo-Opt. Instrum. Eng. **3176**, 25 (1977).
[7] V. F. Tarasov and Sh. S. Shakurov, Opt. Spektrosk. **81**, 962 (1996) [Opt. Spectrosc. **81**, 880 (1996)].
[8] A. M. Portis, Phys. Rev. **91**, 1071 (1953).
[9] T. G. Castner Jr., Phys. Rev. **115**, 1506 (1959).
[10] S. A. Al'tshuler and B. M. Kozyrev, *Electronic Paramagnetic Resonance of Compounds of Intermediate-Group Elements* [in Russian], Nauka, Moscow, 1972.
[11] K. I. Zamaraev, Yu. N. Molin, K. M. Salikhov, *Spin Exchange. Theory and Physicochemical Applications* [in Russian], Nauka, Novosibirsk, 1977.
[12] A. Abragam and B. Bleaney, *Electron Paramagnetic Resonance of Transition Ions*, Clarendon Press, Oxford, 1970 [Russian translation, Mir, Moscow, 1972].
[13] R. Bramley and S. J. Strach, J. Magn. Reson. **61**, 245 (1985).

Translated by M. E. Alferieff

Polariton enhancement of the Faraday magnetooptic effect

V. E. Kochergin,[a] A. Yu. Toporov, and M. V. Valeĭko
Institute of General Physics, Russian Academy of Sciences, 117942 Moscow, Russia

(Submitted 28 July 1998)
Pis'ma Zh. Éksp. Teor. Fiz. **68**, No. 5, 376–379 (10 September 1998)

Enhancement of the Faraday magnetooptic effect by the excitation of surface polariton on an interface between an iron garnet and silver is observed. The main contribution to this effect is due to the rotation of the polarization of a surface polariton as the polariton propagates along the interface. © *1998 American Institute of Physics.* [S0021-3640(98)00517-9]

PACS numbers: 78.20.Ls, 71.38+i

Surface polaritons (SPs) in combination with the action of different types of influences on surfaces and on thin-film structures are of great interest from both the fundamental and applied standpoints.[1,2] Specifically, SPs can enhance magnetooptic effects. Existing data show enhancement of the Kerr magnetooptic effect (KMOE) by SP excitation on the interface of a magnetic metal film and air, in multilayer structures consisting of a precious metal and a ferromagnetic metal, or in Co–Cu superlattices.[3–5] It has also been suggested that polariton enhancement of the Faraday magnetooptic effect (FMOE) can be obtained in a structure consisting of a bismuth-containing iron garnet (Bi-IG) coated with a metallic film.[6] In the present letter we report the experimental observation of FMOE enhancement by SP excitation in a similar structure with double passage of light through a Bi-IG film, and we analyze the physical mechanisms of this phenomenon.

The experimental arrangement is displayed in Fig. 1. Surface polaritons were excited on the interface between a silver film *3* and a Bi-IG film *2* by means of a diffraction grating. The grating method of SP excitation is the only method that can be used in this configuration because of the high refractive index of Bi-IG in the visible range ($n=2.17$ at wavelength $\lambda=0.63$ μm). The samples were unilateral Bi-IG films, 1.96 μm thick, grown by liquid-phase epitaxy on 300-μm thick gadolinium gallium garnet (111) substrates. The samples possessed easy-plane anisotropy with saturation and anisotropy fields of 0.9 Oe and 2 Oe, respectively. A grating with period $T=0.7$ μm and depth $h=0.3$ μm was prepared on the Bi-IG surface by a holographic method with a photoresist illuminated by He–Cd laser radiation ($\lambda=0.44$ μm), followed by ion etching. The lattice vector was parallel to one of the easy axes of the Bi-IG film. A 60-nm thick silver film and a 20-nm thick protective gold layer were deposited on the grating by electron-beam evaporation at 10^{-6} torr.

The structure prepared in this manner was placed between two crossed pairs of coils, which produced magnetic fields up to 20 Oe, sufficient to saturate the Bi-IG film. The

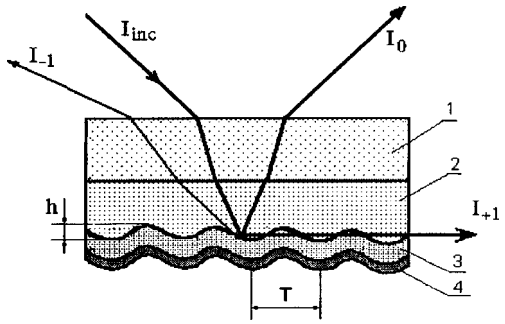

FIG. 1. Optical scheme of the measurements: *1* — gallium–gadolinium garnet substrate; *2* — Bi-containing iron-garnet film; *3* — silver film; *4* — gold film.

field was directed along a lattice vector in the Bi-IG film plane. A single-mode He–Ne laser with wavelength $\lambda = 0.63$ μm and 1 mrad divergence was used as the source of radiation. The angle of incidence of the radiation on the structure was set to within 0.5 min. Radiation in the $(+1)$st diffraction order was used to excite SPs. For the geometry used in the experiment, it was convenient to detect the FMOE for radiation diffracted in the (-1)st order. Moreover, this made it possible to avoid the influence of the KMOE associated with the specular reflection from the Bi-IG film–substrate interface. The measurements were performed in an ac magnetic field with a differential (balance) polarimeter.[7,8] The incident radiation was linearly polarized at a angle of 45° with respect to the plane of incidence.

The amplitudes S_{sum} and S_{dif} of the sum and difference signals of the balance polarimeter were measured as functions of the angle of incidence of the light on the structure. The amplitude S_{sum} is the proportional to the total intensity of the radiation diffracted in (-1)st order, while S_{dif} is proportional to the product of the total intensity of the radiation in the (-1)st diffraction order and the angle of rotation of the plane of polarization. The angular dependence of S_{sum} is displayed in Fig. 2. One can see a minimum corresponding to SP excitation. Since, in additon to Faraday rotation of the polarization there is also energy transfer from the radiation to the SPs, which is manifested differently for the *p*- and *s*-polarized components of the radiation, hysteresis appears in S_{sum} as a function of the applied magnetic field. The dependence of the amplitude of the hysteresis loop on the angle of incidence has a resonance maximum whose position and shape is the same as that of the minimum in Fig. 2. For the same reason, hysteresis as a function of the magnetic field is also observed for S_{dif}. The angular dependence of the ratio $S_{\text{dif}}/S_{\text{sum}}$ characterizes the angle of rotation the plane of polarization of the light as it interacts with the structure and is presented in Fig. 3 (curve *1*). One can see that this ratio increases for angles corresponding to the excitation of SPs and that the angular positions of the FMOE maximum and reflection minimum are the same.

The rotation of the plane of polarization of the light as it interacts with the structure under study can be due to three effects: 1) Faraday rotation accompanying double passage through the Bi–IG film; 2) change in the polarization of the light caused by the fact that the action of the magnetic field on the magnetooptic material (Bi-IG) influences the difference of the amplitudes and phases of the reflection (reradiation) coefficients of the

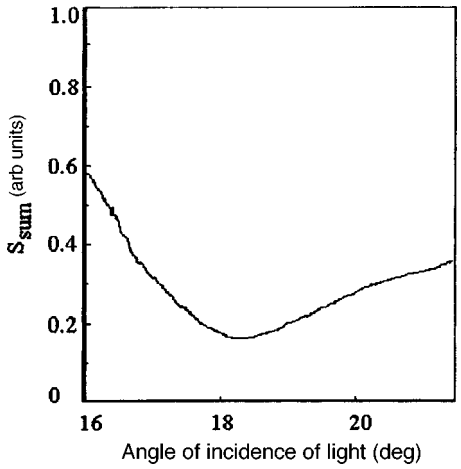

FIG. 2. Angular dependence of the total signal S_{sum}.

p and *s* components from the Bi-IG–silver interface; and, 3) rotation of the plane of polarization of a SP propagating along the Bi-IG–silver interface. The influence of the first effect has been well studied and is described in the literature.[9] The second effect intensifies under conditions when SPs are excited, and its contribution likewise can be calculated by well-known methods.[10] The total contribution of effects 1 and 2, calculated on the basis of the experimental curves of S_{sum} and S_{dif} and the amplitudes of the hysteresis loops, is presented for the same structure in Fig. 3 (curve *2*). Thus, the difference of curves *1* and *2* in Fig. 3 should be attributed to the third effect. One can see that it enhances the FMOE by approximately a factor of 5.

The calculation of the third effect is a complicated problem, which falls outside the scope of the present letter, since an adequate physical model describing the behavior of

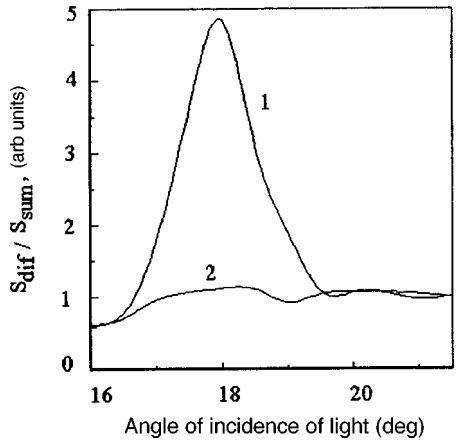

FIG. 3. Angular dependence of the signal ratio S_{dif}/S_{sum}: *1* — experimental curve under SP excitation conditions; *2* — computed curve, in which the rotation of the polarization of the SP is excluded.

SPs in gyrotropic media does not yet exist. The problem is that, on the one hand, according to Maxwell's equations, SPs in isotropic media can exist only in the form of a *p*-polarized wave, and any rotation of the plane of polarization of this wave will lead to additional dissipation of energy. On the other hand, in the Faraday-effect geometry SPs can exist in the form of a two-wave solution of Maxwell's equations, thereby admitting the existence of a *s*-polarized component of the SP.[2] Qualitatively, the conclusion that the third effect plays a dominant role agrees with the fact that the distance traveled by SPs in the structure studied is approximately an order of magnitude greater than the thickness of the Bi-IG film, and the main rotation of the plane of polarization in the observed FMOE occurs over this distance.

In summary, we observed experimentally the enhancement of the FMOE by excitation of surface polaritons. Rotation of the polarization of SPs propagating along the interface between the metal and the gyrotropic medium makes the main contribution to the effect. The coefficient of enhancement can be increased by optimizing the parameters of the structure in which the SP is excited and by fabricating a structure in which the excitation of far-ranging SPs can occur.

We thank the staff of the laboratory of Professor V. A. Sychugov for preparing the gratings and A. A. Beloglazov for helpful discussions. This work was supported by the Russian Fund for Fundamental Research, Grant 98-02-17421.

[a)]e-mail: kocherg@kapella.gpi.ru

---

[1] V. M. Agranovich and D. L. Mills (eds.), *Surface Polaritons*, North-Holland, Amsterdam, 1982 [Russian translation, Nauka, Moscow, 1985].
[2] A. D. Boardman, *Electromagnetic Surface Modes*, Wiley, New York, 1982.
[3] P. E. Ferguson, O. M. Stafsudd, and R. F. Wallis, Physica B **89**, 91 (1977).
[4] V. I. Safarov, V. A. Kosobukin, and C. Hermann, Phys. Rev. Lett. **73**, 3584 (1994).
[5] V. A. Kosobukin, Fiz. Tverd. Tela (St. Petersburg) **38**, 3461 (1996) [Phys. Solid State **38**, 1888 (1996)].
[6] D. Boardman, A. I. Voronko, A. Yu. Toporov *et al.*, J. Appl. Phys. **75**, 6804 (1994).
[7] V. S. Zapasskiĭ, Zh. Prikl. Spektrosk. **37**, 181 (1982).
[8] P. M. Vetoshko, V. B. Volkovoy, A. Yu. Toporov *et al.*, J. Appl. Phys. **70**, 6298 (1991).
[9] A. K. Zvezdin and V. A. Kotov, *Magnetooptics of Thin Films* [in Russian], Nauka, Moscow, 1988.
[10] V. E. Kochergin, A. A. Beloglazov, M. V. Valeĭko *et al.*, Kvantovaya Élektron. (Moscow) **25**, 457 (1998).

Translated by M. E. Alferieff

Field-asymmetric transverse magnetoresistance in a nonmagnetic quantum-size structure

A. A. Gorbatsevich, Yu. V. Kopaev, I. V. Kucherenko, O. E. Omel'yanovskiĭ, and V. I. Tsebro[a)]
P. N. Lebedev Physics Institute, Russian Academy of Sciences, 117924 Moscow, Russia

V. V. Kapaev
Moscow Institute of Electronics, 103498 Moscow, Russia

(Submitted 15 July 1998)
Pis'ma Zh. Éksp. Teor. Fiz. **68**, No. 5, 380–385 (10 September 1998)

A new phenomenon is observed experimentally in a heavily doped asymmetric quantum-size structure in a magnetic field parallel to the quantum-well layers — a transverse magnetoresistance which is asymmetric in the field (there can even be a channge in sign) and is observed in the case that the structure has a built-in lateral electric field. A model of the effect is proposed. The observed asymmetry of the magnetoresistance is attributed to an additional current contribution that arises under nonequilibrium conditions and that is linear in the gradient of the electrochemical potential and proportional to the parameter characterizing the asymmetry of the spectrum with respect to the quasimomentum. © *1998 American Institute of Physics.*
[S0021-3640(98)00617-3]

PACS numbers: 72.15.Gd, 72.20.My, 73.20.Dx

1. An artificially grown asymmetric quantum-size structure in a magnetic field oriented parallel to the quantum-well layers is a system with broken fundamental symmetries with respect to inversion of the coordinates and to time reversal. These symmetry breakings lead to unusual macroscopic properties. Specifically, it has been shown theoretically[1,2] that such a system can possess anomalously large photogalvanic and magnetoelectric effects. The large values of the photogalvanic effect were confirmed experimentally in Refs. 3 and 4.

In the present letter we report the observation of a fundamentally new phenomenon — a transverse magnetoresistance which is asymmetric with respect to the sign of the field — arising in an asymmetric quantum-size structure. The effect is observed in the case when a built-in lateral electric field exists in the structure. This usually happens in a small region near the fused-in metal contact.

2. Our experimental GaAs/$Al_xGa_{1-x}As$ ($x=0.34$) nanostructure is a heavily doped single *i*-GaAs quantum well having average width (300 Å) and bounded on both sides by $\sim$300 Å wide $Al_xGa_{1-x}As$ barrier layers, uniformly doped with silicon to volume density $c_{Si}\sim 10^{18}$ cm^{-3}. The well is separated from the doped barrier regions by *i*-$Al_xGa_{1-x}As$ spacer layers $\sim$100 Å wide.

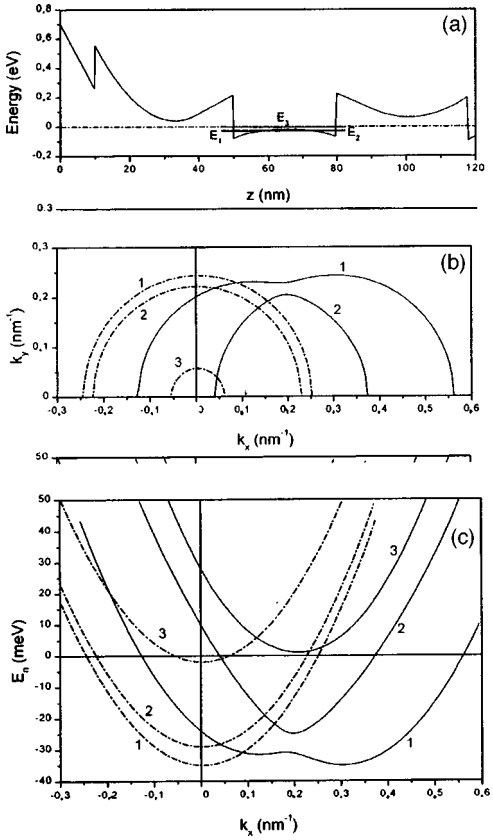

FIG. 1. Computed potential profile (a) of the conduction band bottom in the direction of the growth axis of the nanostructure; Fermi contours (b) and dispersion curves (c) for the three bottom subbands in 1 kOe (dot-and-dash curves) and 70 kOe (solid curves) magnetic fields.

A quantum-mechanical calculation of the space-quantization energy levels in this geometry showed that there are three levels below the Fermi level E_F: E_1, E_2, and E_3, such that $E_F-E_1\approx 32$ meV, $E_2-E_1\approx 5$–6 meV, and $E_F-E_3\approx 1$–5 meV. The levels E_1 and E_2 are located slightly below the convex bottom of the quantum well, so that this structure can be viewed as a bilayer two-dimensional electronic system (see Fig. 1).

The electronic parameters of the system were determined from measurements of the Hall effect and Shubnikov–de Haas oscillations with the magnetic field oriented in a direction normal to the plane of the nanostructure. The experimental value of the Fermi energy is $E_F=(\hbar e/m^*c)(1/\Delta(1/H))\approx 32$ meV (at $m^*=0.067m_e$), and the two-dimensional charge-carrier density $n=(e/\pi\hbar c)(1/\Delta(1/H))\approx 0.9\times 10^{12}$ cm^{-2} was found to be approximately two times smaller than the carrier density determined from the Hall constant R_H in weak magnetic fields $n=1/ecR_H\approx 1.9\times 10^{12}$ cm^{-2}. These data show that in accordance with the model calculation the carrier densities in the two bottom subbands are approximately equal, and the population of the third subband is extremely small because of the closeness of the bottom of this subband to the Fermi level.

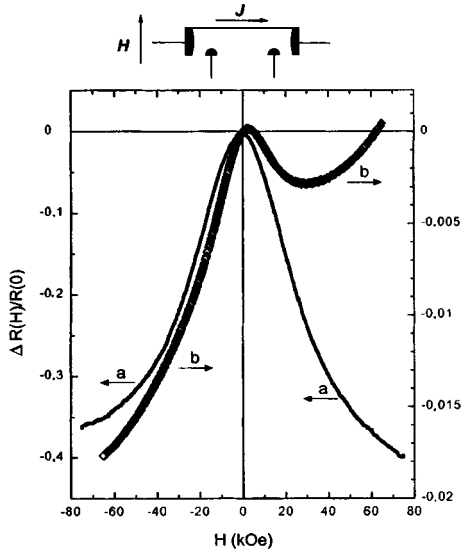

FIG. 2. Curves of the transverse magnetoresistance at liquid-helium (a) and room (b) temperatures for opposite orientations of the magnetic field. The geometry of the contacts is shown in the top portion of the figure.

The degree of asymmetry of the nanostructure can be judged according to the variation of the dispersion curves (Fig. 1c) and the shape of the Fermi contours (Fig. 1b) as a function of the magnetic field for each filled subband (charge-carrier motion is confined to the $x-y$ plane, and the magnetic field is directed along the y axis). One can see that despite the very small difference of the potential energy profile of the nanostructure to the left and right of the interfaces (~ 20 meV), the magnetic field distorts the charge-carrier spectrum very strongly, deforming the Fermi contour along the x axis and leading to a very strong asymmetry of the dispersion curves $E(k_x)$.

3. The magnetoresistance measurements were performed by the standard four-contact method with dc current. The potential contacts were of two types: a) fused-in metallic (indium) contacts (in this case the sections of the near-contact region of the nanostructure with a built-in lateral electric field contribute to the measured electrical resistance), and b) lithographically prepared lateral contacts through etched-out extensions of the nanostructure itself (in this case the near-contact region with the built-in electric field does not make a contribution).

a) Fused-in indium potential contacts. In this configuration the samples had a rectangular shape with the dimensions $\sim 2\times 8$ mm and two current contacts fused in along the entire width of the sample and two ~ 0.5 mm fused-in potential contacts along one side of the sample, as shown in the upper part of Fig. 2.

Figure 2 shows the measurements of the transverse magnetoresistance at liquid-helium (curve a) and room (curve b) temperatures for both directions of the magnetic field. One can see that at liquid-helium temperature there is a strong negative transverse magnetoresistance ($\Delta R(H)/R(0)\sim -0.4$ at $H=75$ kOe), which differs by $\sim 10\%$ for opposite orientations of the magnetic field, i.e., asymmetrically with respect to the direction of H. At room temperature the magnetoresistance decreases strongly in absolute

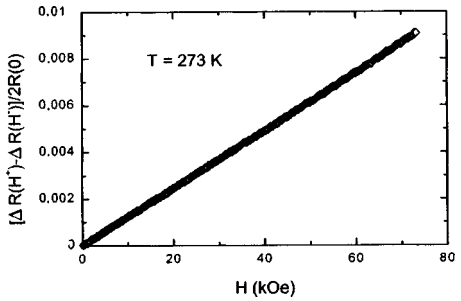

FIG. 3. Difference between the curves of the room-temperature transverse magnetoresistance measured for opposite directions of the magnetic field, plotted versus the absolute magnitude of the field.

magnitude to ~ 0.01 in strong magnetic fields, and it becomes asymmetric in H with respect to not only the magnitude but also the shape of the curves $\Delta R(H)/R(0)$ (curve b).

It should be emphasized particularly that neither the magnitude nor the sign of the asymmetry of the transverse magnetoresistance depends on the direction of the measuring current J through the sample for a fixed direction of the magnetic field, i.e., they are determined not by the relative orientation of the vectors **H** and **J** (provided that $\mathbf{H} \perp \mathbf{J}$) but by the relative orientation of the vector **H** and the vector **l** in the direction of the growth axis ($\mathbf{H} \perp \mathbf{l}$).

If the field dependence of the transverse magnetoresistance, measured for one direction of **H** is subtracted from the corresponding dependence measured for the opposite direction, then in all cases there is a strictly linear dependence of the difference obtained on the absolute magnitude of H. This fact is illustrated especially well by the data obtained at room temperature, where the magnetoresistance is small and the dependence $\Delta R(H)/R(0)$ has a pronounced nonmonotonic character (Fig. 3).

We note that when the sample is rotated so that the vector **H** is parallel to the current vector **J** (the case of longitudinal magnetoresistance), the magnitude, and at high temperatures even the sign of the magnetoresistance change, but the important fact is that the asymmetry of the $\Delta R(H)/R(0)$ curves vanishes completely (Fig. 4).

b) Combined fused-in and lithographic potential contacts. The region of the nanostructure near the fused-in metallic contact is a region with the built-in lateral electric field.[b)] This electric field ($\mathbf{E}_0$), as will be noted below, confers to this region a nontrivial symmetry, as a result of which there arises a correction to the conductivity (or current) that is linear in the magnetic field. Since the observed asymmetry of the magnetoresistance is proportional to the magnitude and direction of $\mathbf{E}_0$, it is obvious that the magnetoresistance asymmetry measured and described above is a difference effect, which is observable to the extent that the oppositely directed built-in electric fields $\mathbf{E}_0^1$ and $\mathbf{E}_0^2$ in the near-contact regions of the first and second potential contacts are unequal. For this reason, it was of interest to perform measurements of the transverse magnetoresistance on samples where only one fused-in potential contact is present on one side of the sample, since in this case an appreciable enhancement of the asymmetry effect should be expected.

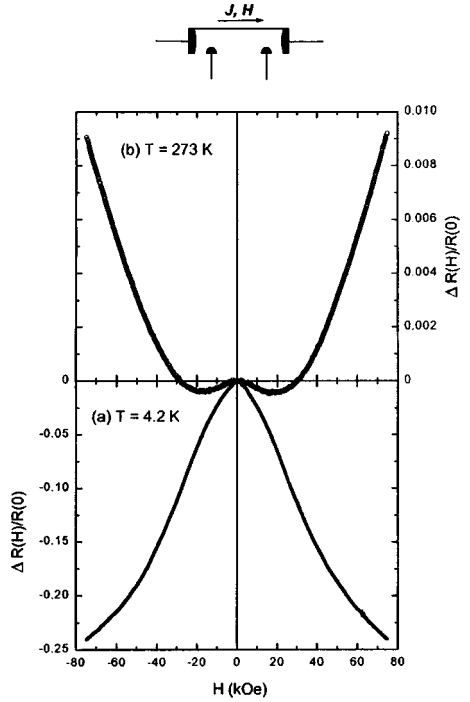

FIG. 4. Curves of the longitudinal magnetoresistance at liquid-helium (a) and room (b) temperatures for opposite orientations of the magnetic field.

The results of such measurements at liquid-helium and room temperatures are shown in Fig. 5. Three potential contacts were used (see top part of Fig. 5): one fused-in indium contact *1* and two lateral lithographic contacts *2* and *3*, one of which was located close to the fused-in contact *1* so as to increase appreciably the contribution of the near-contact region of the fused-in contact *1* to the total measured magnetoresistance in measurements of the potential difference with contacts *1–2*. The distance between contacts *1* and *2* was ~ 0.3 mm and the distance between contacts *2* and *3* was ~ 6 mm.

As one can see from the data presented in Fig. 5a, in the case of the potential contacts *1–2* the asymmetry of the transverse magnetoresistance at $T = 4.2$ K increased appreciably and reached $\sim 50\%$ (curve *1*a). In the case of the potential contacts *1–3* the asymmetry was $\sim 2\%$, in accordance with the ratio of the distances between the contacts *1–2* and *1–3* (curve *2*a). Finally, in the case of the potential contacts *2–3* the magnetoresistance curves are completely symmetric (curve *3*a).

We note that the room temperature magnetoresistance (Fig. 5b) in the case of potential contacts *1–2* does not simply become even more asymmetric. It even becomes opposite in sign: positive for one direction of the magnetic field and negative for the other (see curve *1*b).

4. The macroscopic symmetry of the asymmetric system of quantum wells in a magnetic field parallel to the layers is characterized by a *t*-odd polar vector[1,2]

$$\mathbf{T} \propto \mathbf{H} \times \mathbf{P}, \tag{1}$$

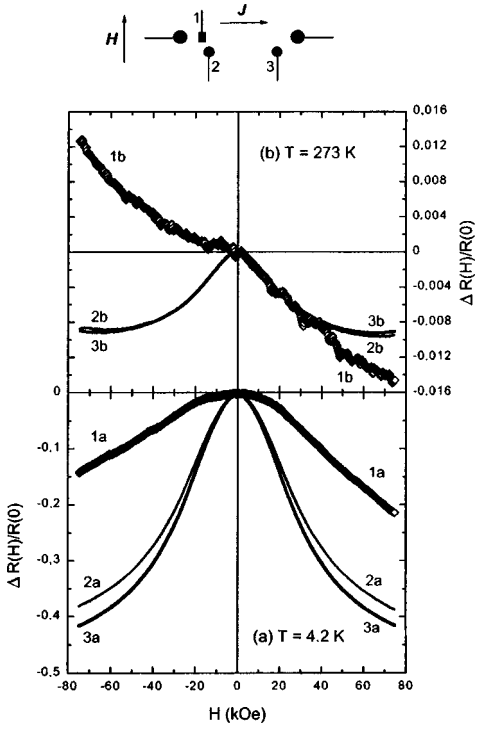

FIG. 5. Curves of the transverse magnetoresistance at liquid-helium (a) and room (b) temperatures in the case of combined potential contacts. Curves *1*a and *1*b were obtained with potential contacts *1–2*; curves *2*a, *2*b and *3*a, *3*b were obtained with contacts *1–3* and *2–3*, respectively.

where **H** is the external magnetic field, and **P** is a polar vector characterizing the spatial asymmetry of the system and is directed perpendicular to the plane of the quantum wells. Physically, the vector **T** is the toroidal moment density.[5,6]

Since **T** and the quasimomentum **k** have the same transformation properties, the product of **T** by **k** is an invariant, and the energy spectrum, which can contain all possible invariants, is asymmetric in the quasimomentum: $E(\mathbf{k}) \neq E(-\mathbf{k})$.

It is also known (see Refs. 1 and 2) on the basis of symmetry considerations that under nonequilibrium conditions there can exist a macroscopic current

$$\mathbf{j} = \beta \mathbf{T}, \tag{2}$$

where the coefficient β is due to the departure from equilibrium. If the source of disequilibrium is photoexcitation, the above-mentioned anomalously large photogalvanic effect is observed.[3,4] However, a relation between **j** and **T** similar to Eq. (2) can exist if the nonequilibrium is produced by an ordinary dissipative (Ohmic) current passed through the system. In this case, there exists in the system a gradient of the electrochemical potential, and the dissipative coefficient β is linear in the electric field **E**: $\beta \propto \alpha \mathbf{L} \cdot \mathbf{E}$, where α is a scalar and **L** is a polar vector. In the samples investigated the vector **L** is determined by the built-in electrostatic field in the near-contact space-charge region. The expression for the current (2) in this case can be rewritten in the form

$$\mathbf{j}=\alpha(\mathbf{P}\times\mathbf{H})(\mathbf{L}\cdot\mathbf{E}). \tag{3}$$

In a macroscopically nonuniform system $\mathbf{E}$ is the gradient of the electrochemical potential. The current contribution (3) leads in an obvious manner to an anomalous contribution to the electrical conductivity, one which is asymmetric with respect to the magnetic field.

In the microscopic description of the effect, one must substitute into the general expression for the current density (where $E(\mathbf{k})$ is the energy spectrum and D is the $\mathbf{k}$-space dimension)

$$\mathbf{j}=\int \frac{\partial E(\mathbf{k})}{\partial \mathbf{k}} f(\mathbf{k}) \frac{d^D\mathbf{k}}{(2\pi)^D} \tag{4}$$

the distribution function $f(\mathbf{k})$ found from the kinetic equation

$$\left(\mathbf{v}\cdot\frac{\partial}{\partial \mathbf{r}}-\frac{e}{\hbar}\left(\mathbf{E}+\frac{1}{c}\mathbf{v}\times\mathbf{H}\right)\cdot\frac{\partial}{\partial \mathbf{k}}\right) f(\mathbf{k},\mathbf{r})=-\frac{f(\mathbf{k},\mathbf{r})-f^0(\mathbf{k},\mathbf{r})}{\tau}, \tag{5}$$

where τ is the corresponding relaxation time, $f^0(\mathbf{k},\mathbf{r})$ is the equilibrium distribution function, $\mathbf{E}=-\nabla\varphi(\mathbf{r})$ is the electric field, and $\mathbf{v}=\partial E(\mathbf{k})/\partial\mathbf{k}$ is the velocity of carriers with the spectrum $E(\mathbf{k})$ obtained by solving the Schrödinger equation.

For an asymmetric structure, similar to the one investigated in the present work, the quasiclassical energy spectrum to be substituted into Eq. (4) has the form

$$E(k_x,k_y)=E_n(k_x,k_y)+\varphi(x)=\frac{\hbar^2k_y^2}{2m}+E_n(k_x)+\varphi(x)\,, \tag{6}$$

where $E_n(k_x)$ is the size-quantized and magnetic-field-quantized energy spectrum, which in the general case can be easily obtained numerically (see Fig. 1c).

In a system with a built-in potential neither term on the left-hand side of Eq. (5) is small, generally speaking, and at equilibrium they exactly compensate one another. If the deviation from equilibrium is small, the current $j=n\mu\nabla F$ (where F is the electrochemical potential) flowing in the system can be taken as the corresponding small parameter. In this case the kinetic equation (5) can be solved by the perturbation method. It can be shown that the first-order correction to the distribution functions does not give a contribution to the electrical conductivity that is asymmetric with respect to the magnetic field. In the case of nondegenerate charge-carrier statistics, we have for the second-order correction introduced in the distribution function by the effect under study

$$f^{(2)}=-\frac{e^2\tau^2}{\hbar T}f^{(0)}\left(\mathbf{E}_0\cdot\frac{\partial}{\partial\mathbf{k}}\right)\left(\mathbf{v}\cdot\frac{\partial}{\partial\mathbf{r}}\right)F\,. \tag{7}$$

In this equation $\mathbf{E}_0=-\nabla\varphi_0$ is the electric field vector of the built-in field in our system (near the metallic contact). Upon substitution of expression (7) into Eq. (4), the corresponding contribution to the current is different from zero only if the spectrum (6) is asymmetric with respect to the quasimomentum. The expression obtained in this manner for the current has the same form as expression (3), where the built-in field $\mathbf{E}_0$ enters as the vector $\mathbf{L}$.

[a)]e-mail: tsebro@sci.lebedev.ru

[b)]Simply depositing indium on the sample surface decreases the surface barrier (see Fig. 1) to ~ 0.5 V. This results in electron enrichment of the quantum well beneath the contact. On the other hand, when a metallic indium contact is fused in to some depth, the potential barrier approaches the quantum well, as a result of which the region beneath and in direct proximity to the contact becomes depleted of carriers. This depleted near-contact region possesses a very high resistivity, and for this reason, despite its small size (estimated as $\sim 1-10$ μm), its field-asymmetric contribution to the magnetoresistance turns out to be very considerable and determines the asymmetry of the transverse magnetoresistance of the sample as a whole.

[1] A. A. Gorbatsevich, V. V. Kapaev, and Yu. V. Kopaev, JETP Lett. **57**, 580 (1993).
[2] A. A. Gorbatsevich, V. V. Kapaev, and Yu. V. Kopaev, Ferroelectrics **161**, 303 (1994).
[3] Yu. A. Aleshchenko, I. D. Voronova, S. P. Grishechkina *et al.*, JETP Lett. **58**, 384 (1993).
[4] O. E. Omel'yanovskiĭ, V. I. Tsebro, and V. I. Kadushkin, JETP Lett. **63**, 209 (1996).
[5] V. L. Ginzburg, A. A. Gorbatsevich, Yu. V. Kopaev, and B. A. Volkov, Solid State Commun. **50**, 339 (1984).
[6] A. A. Gorbatsevich, Zh. Éksp. Teor. Fiz. **95**, 1467 (1989) [Sov. Phys. JETP **68**, 847 (1989)].

Translated by M. E. Alferieff

On the splitting of the lower band of charged elementary excitations of a two-dimensional antiferromagnet

A. F. Barabanov, O. V. Urazaev, and A. A. Kovalev
Institute of High-Pressure Physics, Russian Academy of Sciences, 142092 Troitsk, Moscow Region, Russia

L. A. Maksimov
Kurchatov Institute Russian Science Center, Institute of Superconductivity and Solid-State Physics, 123182 Moscow, Russia

(Submitted 27 July 1998)
Pis'ma Zh. Éksp. Teor. Fiz. **68**, No. 5, 386–391 (10 September 1998)

A spin-polaron approach is developed on the basis of a generalized Kondo lattice model for a two-dimensional antiferromagnet (CuO_2 plane model). This approach makes it possible to describe the splitting of polaron bands of carriers both in the presence of long-range magnetic order ($T=0$) and for a finite spin-correlation length ($T\neq 0$) and also can account for the strong deviation from the Luttinger theorem and the shadow-bands effect at both zero and finite temperatures. © *1998 American Institute of Physics.* [S0021-3640(98)00717-8]

PACS numbers: 75.50.Ee, 74.20.Mn, 71.38.+i, 75.30.Mb

It is well known that in high-T_c superconductors the motion of holes in the CuO_2 planes occurs against the background of an antiferromagnetic (AFM) spin substrate and can be interpreted as a correlated motion of a hole paired with spin excitations (a spin polaron).[1,2] Ordinarily, spin polarons are investigated in the t-J model[1] and the three-band Hubbard model.[3–5] Recently it was shown explicitly that in order to describe the hole spectral function correctly, it is important to treat elementary excitations on the basis of the concept of a small-radius spin polaron.[6] In Ref. 6 the spectral function of a hole was calculated in a self-consistent Born approximation using phenomenological screening of the vertex close to the antiferromagnetic vector $\mathbf{Q}=(\pi,\pi)$, which describes scattering of a spin polaron by spin waves of the Bose condensate. As was shown by Schrieffer,[7] in the zeroth approximation it is important to take into account the pairing of fermions with the spin Bose condensate. This procedure requires constructing a superposition of a local polaron and an infinite-radius polaron at $T=0$. This construction is nontrivial if the spin AFM substrate is treated in a spherically symmetric state (a state of the RVB type), and for $T=0$ it has been developed for the model of a two-dimensional Kondo lattice and for the Emery model.[8,9]

In the present work, a spin polaron, consisting of a superposition of a local polaron, an intermediate-radius polaron, and an infinite-radius polaron is studied on the basis of a generalized Hamiltonian of a Kondo lattice with hops to first-, second-, and third-nearest neighbors (such a Hamiltonian is adequate for the Emery model[10]). This makes it pos-

sible to describe at both $T=0$ and $T\neq 0$ the properties of the spectrum of elementary excitations that are due to the splitting of the lower band — strong violation of the Luttinger theorem and the shadow bands[11,12] — and to describe the continuous variation of the spectral density of charge carriers accompanying loss of long-range order.

The Hamiltonian of the Kondo lattice has the form

$$\hat{H}=\hat{J}+\hat{T}+\hat{I}, \quad \hat{J}=J\sum_{\mathbf{r}} \mathbf{a}_{\mathbf{r}}^{+}\tilde{\mathbf{S}}_{\mathbf{r}}\mathbf{a}_{\mathbf{r}},$$
$$\hat{T}=\tau_g\sum_{\mathbf{r,g}} a_{\mathbf{r}+\mathbf{g}}^{+}a_{\mathbf{r}}+\tau_d\sum_{\mathbf{r,d}} a_{\mathbf{r}+\mathbf{d}}^{+}a_{\mathbf{r}}+\tau_{2g}\sum_{\mathbf{r,g}} a_{\mathbf{r}+2\mathbf{g}}^{+}a_{\mathbf{r}}, \quad \hat{I}=\frac{I}{2}\sum_{\mathbf{r,g}} \hat{\mathbf{S}}_{\mathbf{r}}\cdot\hat{\mathbf{S}}_{\mathbf{r}+\mathbf{g}}. \tag{1}$$

Here $\mathbf{g}=\pm\mathbf{g}_x\pm\mathbf{g}_y$ is the vector of nearest neighbors; $\mathbf{d}$ and $2\mathbf{g}=2\mathbf{g}$ are vectors of the second- and third-nearest neighbors. The Fermi operator $a_{\mathbf{r},\sigma}^{+}$ creates a hole with spin $S=1/2$ and spin projection $\sigma/2$ ($\sigma=\pm 1$). The notation $\tilde{S}_r=S_r^{\alpha}\sigma^{\alpha}$ is used in the Kondo interaction Hamiltonian $\hat{J}$.

To study elementary excitations on the basis of the spin-polaron approach, we introduce the following basis of site operators:

$$A_{\mathbf{r},1}=a_{\mathbf{r}}, \quad A_{\mathbf{r},2}=\tilde{S}_{\mathbf{r}}a_{\mathbf{r}}. \tag{2}$$

To take into account an infinite-radius polaron at $T=0$, we also include the operators

$$A_{\mathbf{r},j}=\tilde{Q}_{\mathbf{r}}A_{\mathbf{r},i}, \quad \tilde{Q}_{\mathbf{r}}=N^{-1}\sum_{\boldsymbol{\rho}} e^{i\mathbf{Q}\cdot(\mathbf{r}+\boldsymbol{\rho})}\tilde{S}_{\mathbf{r}+\boldsymbol{\rho}}, \quad j=i+2,\ i=(1-2), \tag{3}$$

which describe pairing of local polarons with spin excitations with long-range order. We note that for $M=0$ the contribution from these operators vanishes. Finally, we introduce the operators

$$A_{\mathbf{r},j}=\tilde{Q}_{\mathbf{r}}^{(1)}A_{\mathbf{r},i}, \quad \tilde{Q}_{\mathbf{r}}^{(1)}=N^{-1}\sum_{\boldsymbol{\rho},\mathbf{q}\in\Omega} e^{i\mathbf{q}\cdot(\mathbf{r}+\boldsymbol{\rho})}\tilde{S}_{\mathbf{r}+\boldsymbol{\rho}}, \quad j=i+4,\ i=(1-2). \tag{4}$$

Here Ω is a small region of the Brillouin zone near the point (π,π), presented below in Fig. 3. The summation does not include $\mathbf{q}=\mathbf{Q}$.

The operators $A_{\mathbf{r},5}$ and $A_{\mathbf{r},6}$ describe an intermediate-radius polaron, i.e., the coupling of a local polaron with spin waves, whose momentum belongs to square regions around $\mathbf{Q}$ with linear dimensions L.

To determine the spin-polaron spectrum $\varepsilon_i(\mathbf{k})$ (here i is the band number) we shall employ the matrix of two-time retarded Green's functions $G_{i,j}(t,\mathbf{k})$ for the operators $A_{\mathbf{k},\sigma,i}$.

We shall solve the system of equations of motion for $G_{i,j}(\omega,\mathbf{k})$, using the standard Mori–Zwanzig projection method[13] and we shall confine ourselves to the previously chosen basis of operators $\{A_{\mathbf{k},\sigma,i}\}$. At $T=0$ (case 1) we study a basis consisting of six operators $i=1-6$. At finite temperature (case 2) the operators $A_{\mathbf{k},\sigma,3}$ and $A_{\mathbf{k},\sigma,4}$ are absent in the set of operators, since they describe an infinite-radius polaron, which exists only in the presence of long-range order.

As a result, the Green's function has the form

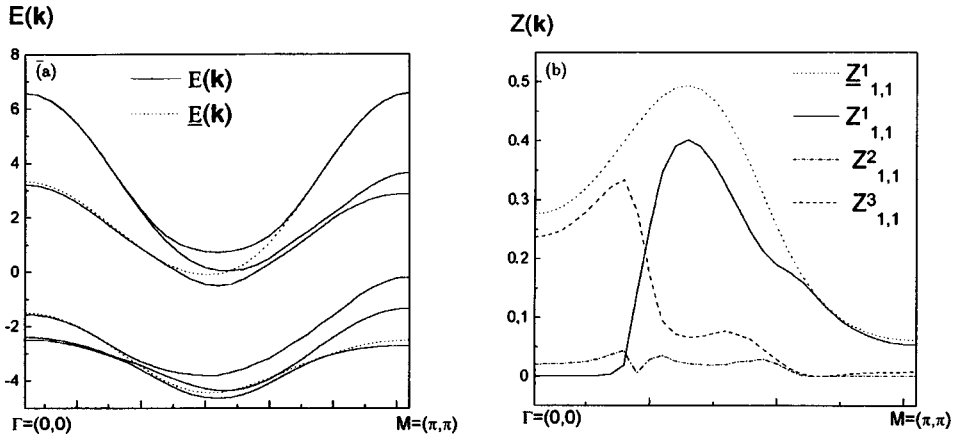

FIG. 1. a: Spectrum $E^{i}(k)$ of quasiparticle excitations at $T=0$ along the symmetric direction $k=k_x=k_y$. $E^{(i)}(k)$ is the local-polaron approximation. b: Residues $Z^{(i)}_{1,1}(k)$ of the electronic Green's function $\langle\langle a_{k\sigma}|a^{+}_{k\sigma}\rangle\rangle$ which correspond to poles of $E^{(i)}(k)$. The residue $Z^{(1)}_{1,1}(k)$ of the Green's function corresponds to the band $E^{(1)}(k)$ in the local-polaron approximation.

$$G_{i,j}(\omega,\mathbf{k})=\sum_{l=1}^{12}\frac{Z^{(l)}_{(i,j)}(\mathbf{k})}{\omega-\varepsilon_l(\mathbf{k})}. \tag{5}$$

Specifically, the quantity $Z^{(l)}_{(1,1)}(\mathbf{k})$ refers to the number of bare holes with fixed spin σ and momentum $\mathbf{k}$ in the state $|\mathbf{k},\sigma\rangle$ of the quasiparticle band $\varepsilon_l(\mathbf{k})$. We note that the spectral weights (residues) $Z_{(i,j)}(\mathbf{k})$ satisfy the sum role $\Sigma_s Z^{(s)}_{(1,1)}(\mathbf{k})=1$.

We note that the dependence of the spin-polaron excitations spectrum ϵ_l on the correlation function $M=\langle\mathbf{S_Q}\cdot\mathbf{S_Q}\rangle$ is manifested only when the Q-polaron states $A_{\mathbf{r},3}$ and $A_{\mathbf{r},4}$ are taken into account. To determine the spectrum $\varepsilon(\mathbf{k})$ it is necessary to know the spin correlation functions $\langle\mathbf{S}_{\mathbf{R}_1}\cdot\mathbf{S}_{\mathbf{R}_2}\rangle$. We calculated them in the same manner as in Ref. 14. Specifically, the following numerical values of the spin correlation function were obtained at $T=0$: $\langle\mathbf{S_R}\cdot\mathbf{S_{R+g}}\rangle=-0.332$, $\langle\mathbf{S_R}\cdot\mathbf{S_{R+g}}\rangle=-0.145+M$, and $\langle\mathbf{S_R}\cdot\mathbf{S_{R+g}}\rangle=-0.144+M$, where $M=0.0577$. The following values of the model parameters were used: $\tau=1$, $\tau_{2g}=0.5\tau$, $\tau_d=\tau_{2g}$, $\tau_g=-\tau_{2g}$, $J=5\tau_{2g}$, and $I=0.5\tau_{2g}$, which were chosen so that the minimum of the lower band would lie near the point $(\pi/2,\pi/2)$. The value of the parameter L, which gives for the operators $A_{\mathbf{q},5(6)}$ the region Ω, was chosen by a variational method for each $\mathbf{k}$ in the Brillouin zone. It was found that the region Ω depends strongly on $\mathbf{k}$. For example, $L(0,0)=0.05\pi$ and $L(\pi,\pi)=0.35\pi$. The calculations were performed in the light-doping limit, $n\ll 1$, n being the total number of carriers per cell. Case 2 is represented by the temperature $T=0.1I$, which corresponds to a correlation length $\xi=40$ lattice constants.

The results for the most interesting lower bands $\varepsilon_l(\mathbf{k})$ for $\mathbf{k}$ along the symmetry direction from $\Gamma=(0,0)$ to $M=(\pi,\pi)$ are presented in Figs. 1 and 2, respectively, for cases 1 and 2. Figure 3 displays the constant-energy surfaces of the first band. As one can see from Figs. 1a and 2a, the minimum of the lower band in both cases lies near the point $(\pi/2,\pi/2)$, which is characteristic for the Emery model, and corresponds to the experi-

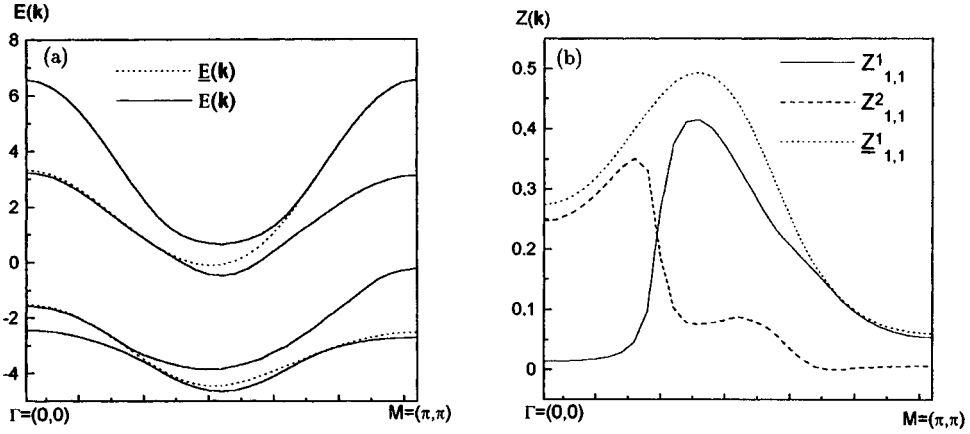

FIG. 2. a: Spectrum $E^{i}(k)$ of quasiparticle excitations at $T=0.1I$ along the symmetric direction $k=k_x=k_y$. $E^{(i)}(k)$ is the local-polaron approximation. b) Residues $Z^{(i)}_{1,1}(k)$ of the electronic Green's function $\langle\langle a_{k\sigma}|a^{+}_{k\sigma}\rangle\rangle$ which correspond to poles of $E^{(i)}(k)$. The residue $Z^{(1)}_{1,1}(k)$ of the Green's function corresponds to the band $E^{(1)}(k)$ in the local-polaron approximation.

mentally observed spectrum.[15] As one can see from these figures, the cases $T=0$ and $T\neq 0$ are similar, with the exception of the vanishing of the second band in case 2, where there is no long-range order.

Figures 1b and 2b display the number bare-carrier occupation numbers as a function of **k** for the cases $T=0$ and $T\neq 0$, respectively. The second band for the case $T=0$ has negligible residues, and except for its presence the figures are similar. Therefore the set of operators $A_{1,2,3,4}$ at $T=0$ can be adequately replaced by the set of operators $A_{1,2,5,6}$ when long-range order vanishes.

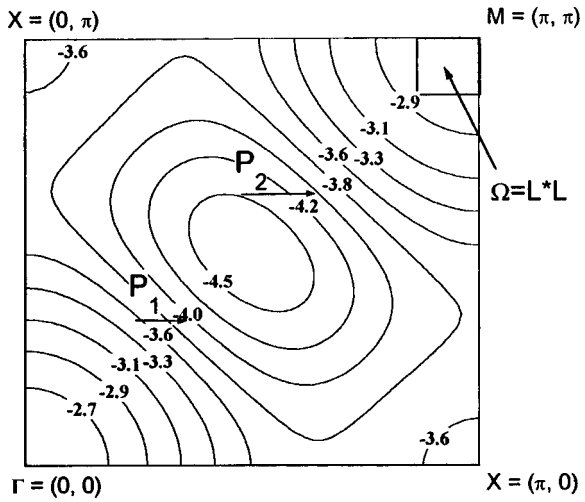

FIG. 3. Constant-energy surfaces of the lower band $E^{(1)}(\mathbf{k})$ at $T=0.1I$.

We call attention to the fact that the results of our calculations on the basis of the Mori–Zwanzig method for the lower band are qualitatively identical to the computational results for the coherent part of the spectral function $A(\mathbf{q},\omega) = -(\mathbf{1}/\pi)\cdot \mathrm{Im}\ \mathbf{G}_{11}$ by the self-consistent Born approximation method.[16] Specifically, both methods describe the ''shadow-band'' effect.[11,12] According to this effect, if the motion of the electron occurs against the background of a Néel state with a doubled lattice period, then each coherent peak of the spectral function will have a corresponding peak with the same energy but with wave vector $\mathbf{q}+\mathbf{Q}$. In the case of a spherically symmetric spin state, the distance between the two peaks is only approximately equal to $\mathbf{Q}$, and, most importantly, the heights of the peaks (i.e., the corresponding residues) differ in magnitude (in Fig. 3 the residue at the point P_1 is 0.4, while the residue at the point P_2 is 0.2. It is important that the shadow-band effect does not vanish at $T \neq 0$.

We also note that the differences of the residues of the lower band in Figs. 1b and 2b from 1 have the effect that the Luttinger theorem is sharply violated. For example, if in our model there are 0.16 states below the Fermi level $\varepsilon = -4.0$ (see Fig. 3), then for the case of the same one-electron spectrum in the tight-binding model there are 0.50 states.

It is interesting that, as our calculations show, the form of the bands remains qualitatively the same right up to temperatures at which the spin correlation length ξ decreases to 3–6 lattice constants.

This work was supported by the International Association for the Promotion of Co-operation with Scientists from the New Independent States of the Former Soviet Union (INTAS) and the Russian Fund for Fundamental Research (Grants INTAS-RFBR 95-0591; RFFI 98-02-1787, 96-15-906708, and 98-02-16730) and the Russian National Superconductivity Program (Grant 93080).

[1] E. Dagotto, Rev. Mod. Phys. **66**, 763 (1994).
[2] W. Brenig, Phys. Rep. **251**, 4 (1995).
[3] V. J. Emery, Phys. Rev. Lett. **58**, 2794 (1987).
[4] F. C. Zhang and T. M. Rice, Phys. Rev. B **37**, 3759 (1988).
[5] A. F. Barabanov, L. A. Maksimov, and G. V. Uimin, JETP Lett. **47**, 622 (1988); Zh. Éksp. Teor. Fiz. **96**, 655 (1989) [Sov. Phys. JETP **69**, 371 (1989)]; A. F. Barabanov, R. O. Kuzian, and L. A. Maksimov, J. Phys. Condens. Matter **3**, 9129 (1991).
[6] A. F. Barabanov, R. O. Kuzian, and L. A. Maksimov, Zh. Éksp. Teor. Fiz. **111**, 1758 (1988) [*sic*]; Phys. Rev. B **55**, 4015 (1997).
[7] J. R. Schrieffer, J. Low Temp. Phys. **99**, 397 (1995).
[8] A. F. Barabanov, E. Zasinas, O. V. Urazaev, and L. A. Maksimov, JETP Lett. **66**, 182 (1997).
[9] L. A. Maksimov, A. F. Barabanov, and R. O. Kuzian, Phys. Lett. A **232**, 286 (1997); L. A. Maksimov, R. Hain, and A. F. Barabanov, Phys. Lett. A **238**, 288 (1998).
[10] P. Prelovshek, Phys. Lett. A **126**, 287 (1988); A. Ramsak and P. Prelovshek, Phys. Rev. B **42**, 10415 (1990).
[11] A. P. Kampf and J. R. Schrieffer, Phys. Rev. B **42**, 7967 (1990).
[12] P. Aebi, J. Osterwalder, P. Schwaller *et al.*, Phys. Rev. Lett. **74**, 1885 (1995).
[13] H. Mori, Prog. Theor. Phys. **33**, 423 (1965).
[14] A. F. Barabanov and O. A. Starykh, J. Phys. Soc. Jpn. **61**, 704 (1992); A. Barabanov and V. M. Berezovsky, Zh. Éksp. Teor. Fiz. **106**, 1156 (1994) [JETP **79**, 627 (1994)]; J. Phys. Soc. Jpn. **63**, 3974 (1994); Phys. Lett. A **186**, 175 (1994).
[15] B. O. Wells, Z.-X. Shen, A. Matsuura *et al.*, Phys. Rev. Lett. **74**, 964 (1995).
[16] R. O. Kuzian, A. F. Barabanov, and L. A. Maksimov, Phys. Rev. B, 1998, to be published.

Translated by M. E. Alferieff

Intraband population inversion and amplification of IR radiation through charge-carrier injection into quantum wells and quantum dots

L. E. Vorob'ev[a)]
St. Petersburg State Technical University, 195251 St. Petersburg, Russia

(Submitted 27 July 1998)
Pis'ma Zh. Éksp. Teor. Fiz. **68**, No. 5, 392–399 (10 September 1998)

A mechanism is proposed for obtaining intraband population inversion of electrons in size-quantization levels through the injection of electron–hole pairs into the *i* region of a heterostructure with quantum wells or quantum dots. Key elements of the mechanism are the simultaneous generation of interband ($h\nu \approx E_g$) near-IR radiation and the presence of a ''metastable'' level. In quantum wells such a level can be produced by making use of the weak overlap of the wave functions of electrons in the levels of a quantum well of complicated configuration and exploiting the characteristic features of the interaction of electrons with optical phonons in polar semiconductors. In quantum dots such a level forms as a result of the phonon bottleneck effect. Estimates are made of the gain for mid-IR radiation in intraband optical transitions of electrons. © *1998 American Institute of Physics.*
[S0021-3640(98)00817-2]

PACS numbers: 73.20.Dx, 42.50.Gy, 33.80.Be

1. INTRODUCTION

An active search is underway for phenomena and for types of quantum-well (QW) structures in which it is possible to obtain a population inversion between size-quantization levels of electrons in the QWs (intraband population inversion). This is of interest because of the need for mid-IR (MIR, $\lambda \approx 4-15$ μm) and far-IR (FIR, $\lambda > 15$ μm) lasers. In these regions the development of conventional injection lasers, in which an interband population inversion is obtained by electron–hole pair injection and the emission of radiation is due to interband radiative recombination of electrons and holes, faces fundamental difficulties because of the fact that the Auger-recombination probability increases as the band gap E_g decreases.

Some of the proposed phenomena that give rise to intraband population inversion of electrons in QWs have recently been implemented in lasers operating on intersubband transitions. Foremost among these is electron tunneling in a system of QWs in a transverse electric field,[1] which is embodied in a modified form in the quantum cascade laser.[2] Another phenomenon used in the development of an optically pumped ''fountain'' laser[3] are electron transitions between size-quantization levels in asymmetric QWs accompanied by the emission of an optical phonon in the presence of interlevel optical pumping.

The characteristic features of the probability of electron transitions between different levels in tunneling-coupled asymmetric QWs with the emission of optical phonons have been successfully used to obtain population inversion and generation of MIR radiation.

However, the fabrication of quantum cascade lasers is a complicated technological problem, and the use of optical pumping decreases interest in ''fountain'' lasers.

In the present letter the mechanism of population inversion of electrons in quantum wells and quantum dots (QDs) through the injection of electrons into the *i* region of a heterostructure is examined. The phenomena described below opens up the possibility of producing new MIR lasers operating on interlevel optical transitions of electrons.

For both QWs and QDs an important condition for obtaining population inversion is the generation of near-IR (NIR) radiation ($h\nu \approx E_g$) and simultaneously the presence of a ''metastable'' level. In QWs such a level can be produced by adjusting the well parameters and using a special well configuration (for example, in the form of a rectangular funnel). An important role here is played by the dependence of the probability of interlevel electron transitions with the emission of polarized optical phonons on the degree of overlap of the wave functions of different levels and on the wave vector of the emitted phonon. In QDs the metastable level is formed on account of the so-called phonon bottleneck effect.

Although the analysis is made for specific heterostructures, the principle for obtaining a population inversion is general and can be used to produce population inversion in other types of heterostructures with QWs.

2. INTRABAND POPULATION INVERSION IN QUANTUM WELLS

As an example, we shall consider a specific n^+-i-p^+ heterostructure with an undoped *i* layer of $Ga_{1-x}Al_xAs$, containing a funnel-shaped $Ga_{1-x}Al_xAs/GaAs$ quantum well at the center (Fig. 1a). The composition *x* to the left and right of the QW increases continuously within the layer from $x=0.3$ to 0.8. The narrow part of the QW consists of a GaAs layer with thickness $L_N=110$ Å and the wide part is formed by two $Ga_{0.75}Al_{0.25}As$ layers 55 Å thick, so that the total width of the top part of the QW is $L_W=220$ Å. Next, there are two $Ga_{0.7}Al_{0.3}As$ layers, having a total width of approximately $L=1000$ Å, to the left and right of the QW, and these layers are followed by $Ga_{1-x}Al_xAs$ layers with a total thickness of 3 μm and composition varying from $x=0.3$ to $x=0.8$, forming a waveguide in the *i* layer for both MIR and NIR radiation.

According to the calculations, such a complicated QW contains three size-quantization levels with energies $E_1=28$, $E_2=106$, and $E_3=206$ meV (Fig. 1a). A slight increase in the height of a step in the QW (increasing the composition to $x>0.3$) results in the appearance of another level in the QW, so that a quantum well with the chosen parameters is close to being resonant. We note that quasidiscrete levels with quantization energy and interlevel splitting of approximately 1 meV are present in the above-barrier region with $L=1000$ Å.

The electrons injected into the *i* region enter quasidiscrete levels in the above-barrier region and are then trapped in the levels E_1, E_2, and E_3 of the QW as a result of the interaction with optical and acoustic lattice vibrations and elastic scattering by interfacial asperities. We shall assume the temperature to be low enough that thermal ejection of electrons out of the QW levels can be neglected.

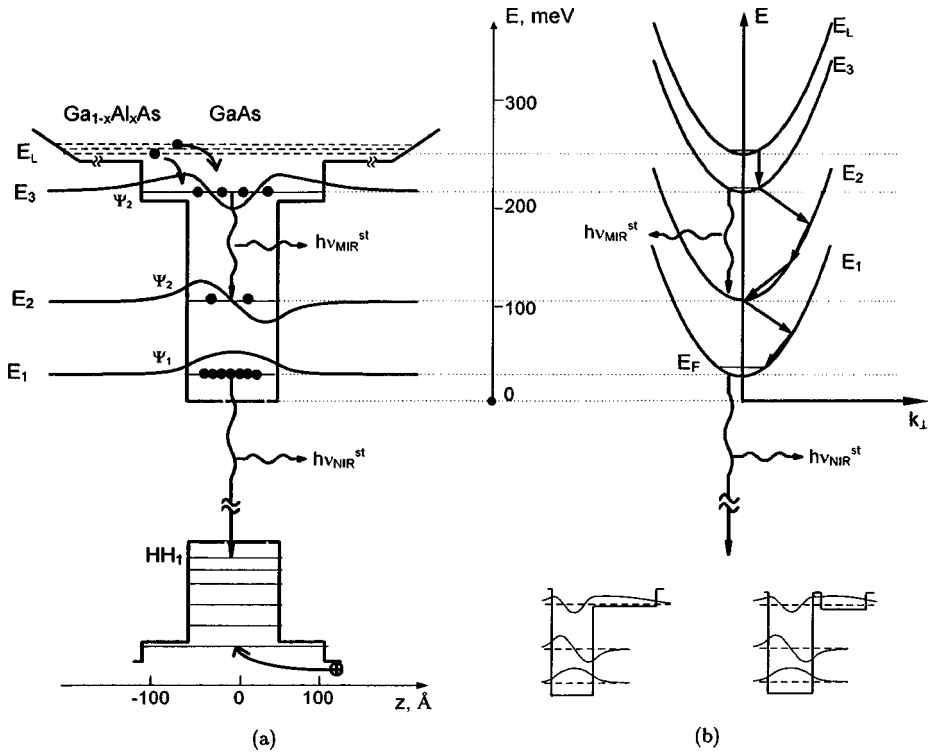

FIG. 1. a) Diagram of transitions in a quantum well in the *i*layer of a n^+-i-p^+ laser heterostructure, position E_i of the size-quantization levels, and the wave functions of the electrons. The solid and wavy arrows show the electron transitions between levels with the emission of a phonon and optical transitions accompanying the generation of near-IR (NIR) and middle (IR) (MIR) radiations. b) Diagram of inter- and intrasubband electron transitions with emission of optical phonons. The main transitions are shown. The vertical arrows show optical transitions accompanying stimulated emission of MIR and NIR light. The configurations of the quantum wells which give the smallest overlap of the electron wave functions in the upper and two lower levels are shown at the bottom.

Under stationary (but nonequilibrium) conditions the density of electrons in the levels can be found from the following system of equations, which take only the basic processes into account:

$$\eta JA_3 - N_3W_{23} - N_3W_{13} - N_3(\tau_{\nu 3}^{\mathrm{sp}})^{-1} = 0, \tag{1}$$

$$\eta JA_2 + N_3W_{23} - N_2W_{12} - N_2(\tau_{\nu 2}^{\mathrm{sp}})^{-1} = 0, \tag{2}$$

$$\eta JA_1 + N_3W_{13} + N_2W_{12} - N_1(\tau_{\nu 1}^{\mathrm{sp}})^{-1} - B_1^{\mathrm{st}}N_\nu = 0. \tag{3}$$

Here N_1, N_2, and N_3 are the surface electron densities in the levels 1, 2, and 3; $\tau_{\nu i}^{\mathrm{sp}}$ is the lifetime in the level E_i with respect to interband radiative recombination accompanying spontaneous transitions in the QW: an electron in the conduction band $\rightarrow$ hole in the valence band; N_ν is the photon density and B_1^{st} is a proportionality coefficient. The last term in Eq. (3) describes the emptying of level 1 as a result of stimulated emission of NIR. It is important in the presence of a current J above the threshold current J_{th} for

generation of NIR radiation. As follows from the experimental data, $N_\nu \sim (J/J_{\rm th}-1)$ for $J>J_{\rm th}$. The coefficient η takes account of the fraction of electrons reaching the region of the quantum well; A_1, A_2, and A_3 are coefficients determining the electron fluxes into the levels E_1,E_2, and E_3. Obviously, $A_1+A_2+A_3 \simeq 1$, and the ratio of the coefficients A_i is determined by the probabilities that electrons from above-barrier quasidiscrete levels are trapped in the QW levels; W_{ij} is the probability of a transition from the level i into the level j accompanying an interaction with optical and acoustic phonons and interfacial asperities. It is known that in GaAs/AlGaAs QWs scattering by interfacial asperities is important only for QWs with sizes $L_W<70$ Å.[4] For this reason, we shall neglect this form of scattering in our QW. The calculations show that in our QW the probabilities W_{ij} of intersubband transitions (like the probability W_{ii} of intraband scattering) with the participation of acoustic phonons is much smaller (by more than an order of magnitude) than the probabilities of scattering with emission of polarized optical (PO) phonons. For this reason, in what follows we shall take into account only processes accompanied by the emission of PO phonons, making the assumption that $k_BT \ll \hbar\omega_0$ ($\hbar\omega_0$ is the PO phonon energy).

The probability of a transition from the state $E_i(\mathbf{k}_{\perp i})$ into the state $E_j(\mathbf{k}_{\perp j})$ ($\mathbf{k}_\perp$ is the wave vector of an electron in a direction perpendicular to the growth axis of the structure) with emission of a PO phonon with energy $\hbar\omega_0$ equals

$$w_{ji}(\mathbf{k}_{\perp i},\mathbf{k}_{\perp j}) = \frac{2\pi}{\hbar}|M_{ji}^{\rm PO}|^2 \delta[E_i(\mathbf{k}_{\perp i}) - E_j(\mathbf{k}_{\perp j}) - \hbar\omega_0], \tag{4}$$

where $M_{ji}^{\rm PO}$ is the matrix element of the interaction with polarized optical lattice vibrations, and

$$E_{i,j}(\mathbf{k}_{\perp i,j}) = E_{i,j} + \hbar^2\mathbf{k}_{\perp i,j}^2/2m_e .$$

The total probability of a transition from the state $E_i(\mathbf{k}_{\perp i})$ to the subband E_j equals

$$W_{ji}(\mathbf{k}_{\perp i}) = \frac{2\pi}{\hbar}\sum_{\mathbf{k}_{\perp j}}\sum_{q_z}|C_q|^2|J_{ji}(q_z)|^2\delta_{\mathbf{q}_\perp,\mathbf{k}_{\perp j}-\mathbf{k}_{\perp i}}\delta\left[E_i+\frac{\hbar^2\mathbf{k}_{\perp i}^2}{2m_e}-E_j-\frac{\hbar^2\mathbf{k}_{\perp j}^2}{2m_e}-\hbar\omega_0\right]. \tag{5}$$

Here C_q determines the electron–phonon interaction energy:

$$|C_q|^2 = \frac{2\pi e^2\hbar\omega_0}{V(q_\perp^2+q_z^2)\epsilon^*}, \quad \frac{1}{\epsilon^*} = \frac{1}{\epsilon_\infty}-\frac{1}{\epsilon_0}, \tag{6}$$

where V is the normalization volume; $\mathbf{q}_\perp$ and $\mathbf{q}_z$ are the components of the phonon wave vector along and perpendicular to the layer; ϵ_∞ and ϵ_0 are the high- and low-frequency permittivities of the polar crystal; and, J_{ji} equals

$$J_{ji}(q_z) = \int \Psi_j^*(z)e^{-iq_zz}\Psi_i(z)dz \tag{7}$$

and is determined by the overlap of the wave functions of the levels i and j.

As one can see from Eq. (5), the probability of scattering from subband E_i into subband E_j is all the greater the smaller the value of $q_\perp$ (i.e., the smaller the energy splitting between the levels i and j) and the greater the overlap of the wave functions of levels i and j, and that the probability W_{ii} of intraband transitions with phonon emission is greater than the probability W_{ji} of intersubband transitions. For this reason, an electron which has entered band 2 as a result of scattering from band 3 (Fig. 1) ends up at the bottom of band 2 after two intraband scatterings and then passes from states near the bottom of subband 2 into subband 1, where it rapidly drops to the band bottom, emitting an optical phonon.

A calculation of the probabilities according to Eq. (5) for our QW (Fig. 1a) gives $W_{12}=2\times10^{12}$, $W_{23}=4\times10^{11}$, $W_{13}=2\times10^{11}$ s^{-1}, $A_1=0.054$, $A_2=0.086$, and $A_3=0.86$. Moreover, $W_{ii}\gg W_{ij}$; W_{13}, $W_{23}\ll W_{12}$; and, A_1, $A_2\ll A_3$, which according to Eqs. (5) and (7) is due to the small overlap of the wave functions of electrons in the levels E_1 and E_3, E_2 and E_3, E_L and E_1, and E_L and E_2 as compared with those for the electrons in levels E_1 and E_2 and E_L and E_3, and also, according to Eqs. (5) and (6), to the lower values of the phonon wave vector $q_\perp$ for the transitions $E_2\to E_1$ and $E_L\to E_3$ as compared with the values of $q_\perp$ for the transitions $E_3\to E_1$, $E_3\to E_2$, $E_L\to E_1$, and $E_L\to E_2$ (Figs. 1a and 1b). For this reason, it can be said that the level E_3 is ''metastable.''

The picture of electron motion along the levels is as follows. After emitting an optical phonon, an electron is trapped in level E_3 of the QW (Fig. 1). Next, after emitting a PO phonon, the electron ends up in the band E_2, and after two intraband phonon emissions it rapidly drops to the bottom of the subband E_2. Rapidly emitting a PO phonon, the electron passes into the band E_1 and, emitting another phonon, drops to the bottom of the band E_1 into a state near the Fermi quasilevel E_F.

Summing Eqs. (1), (2), and (3) we obtain

$$\eta J\cong N_3(\tau_{\nu3}^{\rm sp})^{-1}+N_2(\tau_{\nu2}^{\rm sp})^{-1}+N_1(\tau_{\nu1}^{\rm sp})^{-1}+B_1^{\rm st}N_\nu; \tag{8}$$

$\tau_{\nu3}^{\rm sp}$, $\tau_{\nu2}^{\rm sp}$, $\tau_{\nu1}^{\rm sp}$ are approximately equal to one another, and near the threshold ($J<J_{\rm th}$) one has N_3, $N_2\ll N_1$, and the last term can be neglected. Then $J_{\rm th}\cong\eta^{-1}\cdot N_{1\rm th}(\tau_{\nu1}^{\rm sp})^{-1}$.

Ordinarily, at injection levels the prevailing form of recombination in GaAs/AlGaAs heterolasers near the lasing threshold is radiative recombination, and $\tau_{\nu i}^{\rm sp}\simeq10^{-8}-10^{-9}$ s. Let us assume that the radiation losses are such that the electron density required for lasing equals $N_{1\rm th}=5.5\times10^{11}$ cm^{-2} (the volume density equals 0.5×10^{18} cm^{-3}), while the losses $\eta=0.5$. Then from Eq. (8) the threshold current is approximately $J_{\rm th}=180$ A/cm^2, which corresponds to the experimentally observed values of $J_{\rm th}$ in lasers with QWs.

For $J>J_{\rm th}$ the main term in Eq. (8) is the last term. As already mentioned, $N_\nu\sim(J/J_{\rm th}-1)$, and it can be assumed approximately that $B_1^{\rm st}\sim N_1$ (Ref. 5). Then in the case $J\gg J_{\rm th}$ we find from Eq. (8) that N_1 does not change as the current increases. This is a well-known fact: After lasing starts, the probability of stimulated emission grows with the current because N_ν increases, as a result of which the electron density remains close to the threshold value, despite the fact that the number of injected electron–hole pairs increases with J.

Solving the system of equations (1) and (2) we obtain

$$N_3 - N_2 = \eta J\left(A_3 \frac{W_{12} - W_{23}}{W_{12}(W_{13} + W_{23})} - A_2 W_{12} \right). \tag{9}$$

Hence it follows that population inversion appears if $W_{12} > W_{23}$ and $A_3 > A_2$, which holds well for the QW with the configuration chosen.

Substituting into Eq. (9) the numerical values presented above for the probabilities and the coefficients A_i, we obtain $N_3 - N_2 = 6 \times 10^8 \cdot J/J_{\text{th}}$ cm^{-2}.

We note that an important condition for achieving population inversion is generation of NIR radiation. Stimulated NIR emission ''dumps'' electrons from the level E_1, and as the current J increases, it maintains a constant electron density in the level E_1: $N_1 \cong N_{1\text{th}}$ (for $N_{1\text{th}} = 5.5 \times 10^{11}$ cm^{-2} the Fermi level $E_F \approx 20$ meV). If the stimulated NIR emission were absent, then even for $J/J_{\text{th}} = 10$ the density would become so high that its interaction would decrease the population inversion. Aside from this, because the the Fermi level increases to values $E_F > E_2 - E_1$, the electrons would end up in the band E_2.

The lifetime of electrons in the level E_3 can be increased by decreasing even more the overlap of the wave functions of electrons in the level E_3 with levels E_2 and E_1. Asymmetric QWs can be used for this purpose (Fig. 1b).

3. AMPLIFICATION OF MIR RADIATION IN QUANTUM WELLS

Following Ref. 6, we find the gain in the presence of direct optical transitions between levels 3 and 2 can be expressed as

$$\alpha_{32} = \frac{4\pi e^2 (N_3 - N_2)\cos^2\theta}{cnL_W} \omega_{32} |Z_{32}|^2 \frac{\Gamma}{\Gamma^2 + (\hbar\omega - \hbar\omega_{32})^2}, \tag{10}$$

where $Z_{32} = \int \Psi_3^* z \Psi_2 dz$, θ is the angle between the z axis and the polarization vector e_ω of the wave, Γ is the broadening, and n is the refractive index. Calculations for Z_{32} give $Z_{32} = 23$ Å.

For $\omega = \omega_{32}$, $J/J_{\text{th}} \approx 15$, $\cos\theta = 1$, and $\Gamma \approx 1$ meV we obtain for α the value $\alpha_{\max} = 6 \times 10^2$ cm^{-1}. This gain is sufficient for generating MIR radiation. Optical confinement for both MIR and NIR radiation can be accomplished by varying continuously the composition in the i layer (and therefore also the refractive index) from $x = 0.31$ to $x = 0.8$ over a thickness of 1.5 μm to the left and right of the QW.

4. INTRABAND POPULATION INVERSION OF ELECTRONS AND AMPLIFICATION OF MIR RADIATION IN QUANTUM DOTS

Consider a layer of InGaAs/GaAlAs quantum dots with surface density N. Let the composition and parameters of the QDs be such that there exist two levels E_1 and E_2. For certain dimensions of self-organizing InAs/GaAs QDs, for example, such a situation can be realized for holes.[7] In what follows, however, we shall talk about electrons in QDs.

Electrons and holes injected from the n^+ and p^+ regions into the i region with QD layers rapidly enter the so-called wetting layer[7] (WL) and are then captured in levels of quantum dots (Fig. 2) in a time of approximately 10^{-12} s (Ref. 8). An electron can reside in the level E_2 for quite a long time, approximately several tens of picoseconds[8] on account of the phonon bottleneck effect. For this reason, at high injection levels (for currents above the threshold current J_{th}) a population inversion of electrons can be

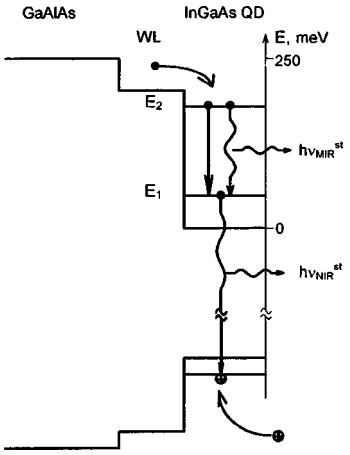

FIG. 2. Diagram of transitions and position of the levels in a quantum dot in the i layer of a n^+-i-p^+ laser heterostructure. WL is the wetting layer. The nonradiative transitions are shown by the solid line, transitions with photon emission are shown by a wavy line.

produced between the levels E_2 and E_1 provided that the level E_1 is actively emptied by stimulated NIR emission ($h\nu \approx E_g$) accompanying interband radiative recombination of electrons and holes in the QDs.

The system of equations describing the filling of the levels of ten QD layers in a stationary state is

$$\left[n_2(\tau_{\nu 2}^{\mathrm{sp}})^{-1} + n_2\left(1 - \frac{n_1}{m_1 N}\right)(\tau_{21})^{-1} \right] \times 10 = \eta J A_2 \left(1 - \frac{n_2}{m_2 N}\right), \tag{11}$$

$$\left[n_1(\tau_{\nu 1}^{\mathrm{sp}})^{-1} + B_1^{\mathrm{st}} N_\nu - n_2\left(1 - \frac{n_1}{m_1 N}\right)(\tau_{21})^{-1} \right] \times 10 = \eta J A_1 \left(1 - \frac{n_1}{m_1 N}\right), \tag{12}$$

where N is the QD density in one layer; n_1 and n_2 are the electron densities in the second and first QD levels; m_1 and m_2 are the numbers of the states in the first and second levels of the QD; η is a coefficient describing losses due to recombination outside the QDs; τ_{21} is the lifetime of an electron in the level E_2 with respect to a nonradiative transition to the level E_1; $\tau_{\nu 2}^{\mathrm{sp}}$ and $\tau_{\nu 1}^{\mathrm{sp}}$ are the interband radiative recombination times for spontaneous (sp) transitions from the levels E_2 and E_1, respectively; the coefficients A_2 and A_1 are proportional to the probabilities of capture of electrons in the levels E_2 and E_1 ($A_2 + A_1 \approx 1$). The second term on the left-hand side in Eq. (12) governs the emptying of the level E_1 as a result of stimulated NIR emission. Just as in the case of QWs, we shall assume that the number of NIR photons increases linearly with increasing current: $N_\nu \propto (J/J_{\mathrm{th}} - 1)$, while $B_1^{\mathrm{st}} \propto n_1$. For $J > J_{\mathrm{th}}$ the second term in Eq. (12) dominates over the first term and can be satisfactorily approximated as $(\tau_{\nu 1}^{\mathrm{sp}})^{-1} n_1 (J/J_{\mathrm{th}} - 1)$. Such an approximation for $J > J_{\mathrm{th}}$, according to Eqs. (11) and (12), makes n_1 independent of J, just as in QWs. It can be assumed with justification that $A_1 \ll A_2$ and $\tau_{21} \ll \tau_{\nu 2}^{\mathrm{sp}}$, $\tau_{\nu 1}^{\mathrm{sp}}$. According to Ref. 9, $m_1 = 2$ and $m_2 = 4$, while the density of self-organizing QDs is

approximately $N=4\times10^{10}$ cm^{-2} (Ref. 10). For a system with ten QD layers $\eta J=\eta J_{\rm th}=100$ A/cm^2 (Ref. 8), and from Eqs. (11) and (12) for $J<J_{\rm th}$ we obtain $\tau_{\nu1}^{\rm sp}\approx1.8\times10^{-9}$ s, which is close to the data presented in the literature.

Now it is not difficult to use Eqs. (11) and (12) to determine n_2 as a function of current. Let us find the current at which a population inversion and amplification of MIR radiation in electron transitions $E_2\rightarrow E_1$ appear. The gain equals

$$\alpha_{2\rightarrow1}=\sigma_{12}\frac{N}{L}\left[\frac{n_2}{N}\left(1-\frac{n_1}{m_1N}\right)-\frac{n_1}{N}\left(1-\frac{n_2}{m_2N}\right)\right], \tag{13}$$

where L is the thickness of the QD layer, while the absorption cross section $\sigma_{12}=1.6\times10^{-15}$ cm^2 (Ref. 10). Let the losses of NIR radiation be such that lasing starts when 2/3 of all states in the E_1 level are filled, i.e., $n_1/m_1N=2/3$ (to obtain interband population inversion and amplification of NIR radiation it is sufficient to have $n_1/m_1N>1/2$). Then it follows from Eq. (13) that $\alpha_{2\rightarrow1}>0$ for $n_2/m_2N=1/2$, which holds for a current 25 times higher than the threshold value. For $J/J_{\rm th}=100$ the ratio $n_2/m_2N=2/3$ and the gain for $L=100$ Å, according to Eq. (13), will equal 30 cm^{-1}. The situation improves significantly if the QD contains three levels. Then a current only six times greater than the threshold value is required to achieve the same gain ($\alpha_{3\rightarrow2}=30$ cm^{-1}) in transitions between levels 3 and 2.

Auger processes can decrease the population of level E_2. However, by adjusting the parameters of the QDs, the wetting layer, and the GaAlAs layer, this process can be considerably weakened.[11]

In Ref. 12 spontaneous MIR emission ($\lambda\approx10$–20 μm) from laser structures with InGaAs/GaAlAs quantum dots and a waveguide at 0.9 μm was observed. The MIR radiation appeared after NIR lasing started ($\lambda\approx0.9$ μm) and increased with current. Spontaneous MIR emission from similar structures but with QWs (having, according to the calculations, two electron and two hole levels) was an order of magnitude weaker and did not have a current threshold. These facts agree with the bottle described above.

I thank D. A. Firsov for assisting in separate numerical calculations and S. A. Gurevich, G. G. Zegrya, N. N. Ledentsov, and R. A. Suris for a discussion of the results obtained in this work.

This work was supported in part by the Russian Fund for Fundamental Research, Grant 96-02-17404), INTAS-RFBR (Grant 00615i96), the Ministry of Science and Technology program ''Physics of Solid-State Nanostructures'' (Grant 96-1029), and the Federal Target Program ''Integration'' (Project No. 75).

[a)]e-mail: LVor@phsc2.stu.neva.ru

[1] R. F. Kazarinov and R. A. Suris, Fiz. Tekh. Poluprovodn. **5**, 797 (1971); **6**, 148 (1972) [Sov. Phys. Semicond. **5**, 707 (1971); **6**, 120 (1972)].
[2] J. Faist, F. Capasso, D. L. Sivco *et al.*, Science **264**, 553 (1994).
[3] O. Gauthier-Lafaye, S. Savage, P. Boucaud *et al.*, Appl. Phys. Lett. **70**, 1 (1997).
[4] H. Sakaki, T. Noda, K. Hirakawa *et al.*, Appl. Phys. Lett. **51**, 1 (1997).
[5] W. Tsang (ed.), *Semiconductor Injection Lasers*, Academic Press, New York, 1985, Chap. 2 [Russian translation, Radio i Svyaz', Moscow, 1990].
[6] T. Ando, A. Fowler, and F. Stern, Rev. Mod. Phys. **54**(2), 437–672 (1982).

[7] M. Grundmann, O. Stier, and D. Bimberg, Phys. Rev. B **52**, 11969 (1995).
[8] N. N. Ledentsov, in *The Physics of Semiconductors*, edited by M. Sheffler and R. Zimmerman, World Scientific, Singapore, 1997, Vol. 1, p. 19.
[9] B. T. Miller, W. Hansen, S. Manus *et al.*, Phys. Rev. B **56**, 6764 (1997).
[10] S. Sauvage, P. Boucaud, F. H. Julien *et al.*, Appl. Phys. Lett. **71**, 2785 (1997).
[11] G. G. Zegrya and A. S. Polkovnikov, Zh. Eksp. Teor. Fiz. **113**, 1491 (1998) [JETP **86**, 815 (1998)].
[12] L. E. Vorob'ev, D. A. Firsov, V. A. Shalygin *et al.*, JETP Lett. **67**, 275 (1998).

Translated by M. E. Alferieff

Electron paramagnetic resonance in a subsystem of structural defects as a factor in the plasticization of NaCl crystals

Yu. I. Golovin, R. B. Morgunov, V. E. Ivanov, S. E. Zhulikov, and A. A. Dmitrievskiĭ
G. R. Derzhavin Tambov State University, 392622 Tambov, Russia

(Submitted 27 July 1998)
Pis'ma Zh. Éksp. Teor. Fiz. **68**, No. 5, 400–405 (10 September 1998)

A change in the macroplastic deformation rate and an increase in the travel distances of edge dislocations are observed in NaCl single crystals placed in crossed dc and rf magnetic fields. The magnetic-field frequencies at which softening maxima are observed correspond to the resonance frequencies of transitions between Zeeman sublevels in paramagnetic complexes of structural defects. © *1998 American Institute of Physics.* [S0021-3640(98)00917-7]

PACS numbers: 76.30.−v, 33.35.+r, 62.20.Fe, 81.40.Lm

Electronic magnetic effects in the physics of plasticity are observed, as a rule, under very specific conditions: at low temperatures or in high magnetic fields.[1,2] These are not necessary conditions for observing magnetic resonance in a pair of particles which have unpaired spins, if the lifetime of the pair (from the moment of creation up to formation of a stable covalent bond) is shorter than the spin–lattice relaxation time.[3] In this case, at high temperatures even very weak magnetic fields can mix singlet and triplet states of a pair at the moment it is formed and thereby change the concentration of the final product of the reaction.[4] The recently discovered effect whereby a weak magnetic field with induction $B \sim 1$ T influences the mobility of dislocations in ionic crystals[5] and the results of a detailed study of this effect[6,7] suggest that such conditions can be satisfied in pairs formed by a dislocation and a point defect. For this reason, the combined action of a weak dc and microwave magnetic fields can, in principle, lead to magnetic resonance in nonequilibrium complexes of defects and influence the production efficiency of secondary reaction products and thereby affect dislocation mobility.[8]

Our objective in the present work was to investigate the mobility of individual edge dislocations and macroplastic flow of crystals under conditions of simultaneous action of crossed dc and rf magnetic fields.

We investigated the plasticity of crystals in external magnetic fields by two standard procedures: 1) measuring the travel distances of individual dislocations, and 2) registering the change in the macrodeformation diagram of crystals at the moment the microwave field is switched on. In the experiments, we used NaCl single crystals doped with divalent metals (mainly Ca) at a level of 0.01 at.% (in investigations of microplasticity) and 0.1 at.% (in experiments with macrodeformation) and annealed at 700 K and cooled

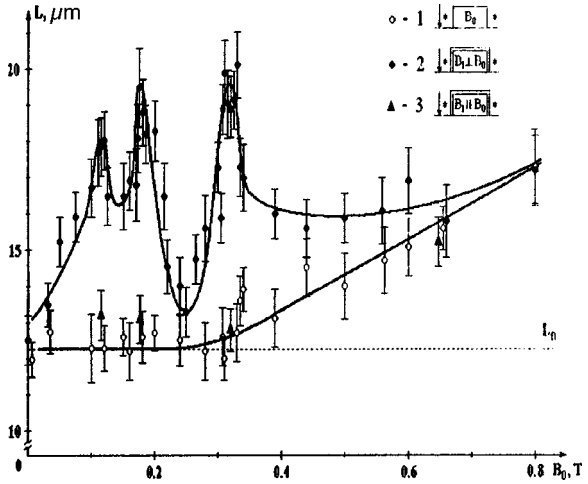

FIG. 1. Average dislocation travel distance L versus the induction B_0 of a dc magnetic field applied for 15 min: *1* — in the absence of a microwave field; *2* — with simultaneous application of a microwave field in the configuration $\mathbf{B}_1 \perp \mathbf{B}_0$, where $\mathbf{B}_1$ is the magnetic induction of the microwave field; *3* — with simultaneous application of a microwave magnetic field in the configuration $\mathbf{B}_1 \parallel \mathbf{B}_0$. The dislocation travel distance L_0 due to the action of an etchant in the absence of external magnetic fields is shown by the dotted line.

to 293 K in 10 h. The samples were placed inside a H_{10} waveguide, connected to a klystron operating at frequency $\nu = 9.5$ GHz and generating a flux of electromagnetic field through the crystal with a power ~ 10 mW. The waveguide was placed between the poles of an electromagnet which produced a dc magnetic field with induction $B_0 = 0 - 0.8$ T at the location of the crystal. In all experiments the vector $\mathbf{B}_0$ was directed along [001].

In the first series of experiments we investigated the effect of dc and microwave fields on the mobility of individual edge dislocations. Their travels, initiated by external magnetic fields, were measured by the standard method of double chemical etching. Each point in the plots in this series of experiments (Fig. 1) is the result of averaging 100–400 runs of individual dislocations measured under identical conditions, while the total number of individual measurements of travel distances exceeds 5×10^3.

Double etching of the samples in the absence of external perturbations gave an average dislocation displacement $L_0 = 12 \pm 1$ μm. This displacement is due to the action of internal mechanical stresses and the etching out of obstacles near the surface.[9] The displacement of dislocations in crystals exposed for 15 min to microwaves in the absence of the dc magnetic field was of the same magnitude, i.e., treatment of the crystals in an ac magnetic field alone had no effect on dislocation mobility (Fig. 1).

The exposure of crystals to a dc magnetic field with induction $B_0 < 0.35$ T for 15 min in the absence of microwaves did not produce an increase in the average travel distance L as compared with L_0 (Fig. 1). An increase in dislocation travel distances under the influence of a dc magnetic field alone occurred only for $B_0 > 0.35$ T. The threshold value $B_0 \approx 0.35$ T at which the travel distances in crystals exposed to a dc magnetic field first exceeded L_0 was close to that obtained in Ref. 10.

Simultaneous exposure of crystals to a dc magnetic field and microwave radiation for 15 min (in the configuration $\mathbf{B}_1 \perp \mathbf{B}_0$, where $\mathbf{B}_1$ is the induction of the microwave field) resulted in a qualitative change in the dependence $L(B_0)$, which became nonmonotonic in crossed fields — it acquired three peaks: at $B_0 = B_{\text{res1}} = 0.12 \pm 0.02$ T, $B_0 = B_{\text{res2}} = 0.18 \pm 0.02$ T, and $B_0 = B_{\text{res3}} = 0.32 \pm 0.03$ T (Fig. 1). Measurements were performed with special care near the peaks: with a smaller step in B_0 and a larger statistical sample (up to 500 measurements per point).

When the dc and microwave fields were applied in the configuration $\mathbf{B}_1 \parallel \mathbf{B}_0$, the peaks in the function $L(B_0)$ vanished and the dependence itself became virtually the same as in the absence of a microwave field (Fig. 1).

A similar result was obtained at microwave frequency $\nu = 152$ MHz, at which a weaker but nonetheless easily distinguishable increase in the dislocation travel distances is also observed in a field $B_{\text{res3}} = 0.005$ T. Therefore peaks in the dependence $L(B_0)$ can be observed in a wide range of microwave frequencies by varying the induction of the dc magnetic field.

It was established that when the crystals are exposed to microwave and dc magnetic fields simultaneously and when they are exposed to a dc magnetic field without a microwave field, the individual dislocations are equally likely, on average over the crystal, to move in the crystallographic directions [110], [111], [$\bar{1}$10], and [1$\bar{1}$0] on all faces of the sample. Therefore the role of external fields in our experiments reduced to the depinning of dislocations from obstacles, and the motion of the dislocations occurred under the influence of random internal mechanical stresses.

In the second series of experiments we investigated the effect of the simultaneous action of a dc magnetic field and a microwave field with frequency $\nu = 9.5$ GHz, applied in the configuration $\mathbf{B}_1 \parallel \mathbf{B}_0$, on the macroplastic flow rate of the crystals. Macroplastic deformation of the crystals was carried out in a ''soft'' machine with quartz rods. The machine produced a mechanical compressive stress which increased linearly with time, $\sigma = st$, where $s = \text{const}$.[11] An induction sensor was used for continuous recording of the length of the sample to within ± 0.1 μm. This made it possible to construct the loading diagram, i.e., the dependence of the strain ϵ on σ or on the running time t elapsed since the start of loading, on a X–Y plotter.

When the microwave field was switched on in the absence of a dc magnetic field no changes occurred in the strain rate $d\epsilon/dt$ (Fig. 2). This showed that any changes arising in the strain diagram when a microwave field is switched on in the presence of a dc magnetic field can be interpreted as being due to the combined effect of dc and ac magnetic fields. Next, each sample was deformed to a plastic strain $\epsilon = 0.5\%$ in 10–15 min with the magnetic field switched on. The microwave field was switched on for 20–30 s during the deformation process. The combined effect of the fields on the macroplasticity was investigated in a comparatively narrow range of strains ($0.1\% < \epsilon < 0.5\%$) at the easy-glide stage.

It was established that the switching on of a microwave field below the yield stress did not produce any changes in the diagram $\epsilon(t)$ (Fig. 2). Above the yield stress the microwave field changed the slope of the strain curve $d\epsilon/dt$. To investigate the dependence of the softening effect on B_0 we measured the ratio of the plastic flow rate $(d\epsilon/dt)_2$ after the microwave field was switched on to the plastic flow rate $(d\epsilon/dt)_1$

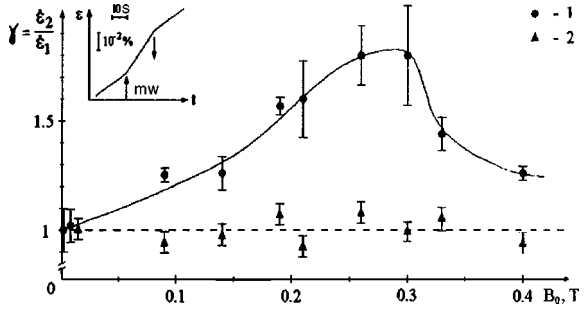

FIG. 2. The dependence of the softening γ of the crystals (ratio of the plastic flow rate $(d\epsilon/dt)_2$ after the microwave field is switched on to the plastic flow rate $(d\epsilon/dt)_1$ before the microwave field is switched on) versus the induction B_0 of the dc magnetic field in which the straining is performed: *1* — above the yield stress in the strain range $0.1\% < \epsilon < 0.5\%$, *2* — below the yield stress at strains $\epsilon < 0.03\%$. Inset: Typical fragment of the dependence of the strain ϵ on deformation time t at the times when the microwave field is switched on and off.

before the field was switched on (see inset in Fig. 2). The ratio $\gamma = (d\epsilon/dt)_2/(d\epsilon/dt)_1$ was taken as a measure of the combined effect of crossed fields on the plasticity. Each point on the plots in the second series of experiments is the result of 10 individual measurements of γ performed under identical conditions.

It was established that the dependence $\gamma(B_0)$ is nonmonotonic. It has a maximum at $B_0 \approx 0.3$ T and possibly also at $B_0 \approx 0.2$ T (this is indicated by the asymmetry of the peak recorded at 0.3 T); see Fig. 2. As a rule, switching off the microwave field restored the plastic flow rate (see inset in Fig. 2). In a small number of cases the strain rate $d\epsilon/dt$ was not restored after the microwave field was switched off. Therefore the combined effect of microwave and dc magnetic fields on macroplastic flow is also of a resonant character, the positions of the maxima of the softening effect being close to those observed in the investigations of the travel distances of individual dislocations.

In both series of experiments described above, the arrangement and the results of the experiment were similar to the conventional conditions under which an EPR signal is observed, with the exception of the fact that the response consisted not of absorption of an electromagnetic wave but rather of a change in the characteristics of the plasticity of the crystal. Without going into the specific mechanisms of depinning of dislocations from obstacles, we shall discuss first the general conclusions following from the results obtained. The values $B_{\text{res1}} = 0.12 \pm 0.02$ T, $B_{\text{res2}} = 0.18 \pm 0.02$ T, and $B_{\text{res3}} = 0.32 \pm 0.03$ T found experimentally in the first series of experiments correspond to the field $B_{th} = h\nu/\mu_B g$ at which, at the microwave frequency employed, $\nu = 9.5$ GHz, resonance transitions occur between the spin sublevels (split in the dc magnetic field) of electrons with Landé factors $g_1 = 5.7 \pm 0.7$, $g_2 = 3.8 \pm 0.3$, and $g_3 = 2.1 \pm 0.2$, respectively. The observed increase in dislocation mobility at frequency $\nu = 152$ GHz in a field $B_0 = 0.005$ T is additional evidence for the resonance nature of the phenomenon observed.

The positions of the peaks in the dependence $\gamma(B_0)$ in experiments with macroplastic deformation (Fig. 2) are determined to lower accuracy. Within the limits of the measurement error this dependence agrees with that obtained in measurements of the

mobility of individual dislocations in the first series of experiments. The low accuracy of the measurements of the positions of the peaks in the second series of experiments could be due to both the irregularity of the macroplastic deformation and the variance in the plastic flow rate in the experimental range of strains as well as to the wider spectrum of electronic processes accompanying macroplastic deformation than in the case of the motion of individual dislocations.

Both series of experiments attest to the fact that the softening of the crystals in crossed dc and microwave fields is due to electron paramagnetic resonance in the subsystem of structural defects of the crystal. In addition, the closeness of g_3 to the Landé factor of a free electron shows that in a magnetic field spin degrees of freedom are active in the subsystem of structural defects. It is significant that the dc and ac magnetic fields employed in our experiments are too weak to change the state of thermalized paramagnetic centers or of an established covalent bond between defects, since the energy imparted to these centers in a 1 T magnetic field is $\sim \mu_B g B \sim 10^{-4}$ eV, which is two orders of magnitude smaller than the average energy $kT \sim 10^{-2}$ eV of thermal fluctuations which mix electronic states. A method of explaining such unexpected results is now known. According to Ref. 3, an energetically weak magnetic field is capable of influencing not the equilibrium state of paramagnetic defects but rather their evolution during spin-dependent relaxation processes. This is confirmed by the enormous quantity of experimental data on the influence of weak magnetic fields on the kinetics and yield of chemical reactions.[3,4]

It is well known that F-like, V_k, and other paramagnetic centers and their metastable complexes arise during deformation and fracture of ionic crystals.[12–14] Defects of this kind could have formed in our experiments during the nucleation and motion of dislocations. The relaxation of these metastable defects and the process of interaction of dislocations with them, like most other solid-phase chemical reactions, proceed in several stages, one of which could be too short to be influenced by thermal fluctuations. Apparently, magnetic fields interfere in the process of the evolution of structural defects during this brief stage. Additional investigations are required to identify this stage and to establish the reactants that make up the complexes of paramagnetic defects involved in the spin-dependent reaction in our experiments.

We note that an investigation of the crystals which we employed in our experiments in the EPR spectrometer did not show resonance absorption of microwave power at the values of B_0 indicated above. This fact and the need for prolonged exposure of the crystals in crossed magnetic fields in order to observe resonances in the dislocation mobility show that only a small number of pairs of defects which enter into a reaction are present simultaneously in the crystal, and their appearance is a rare event that cannot be detected with an EPR spectrometer.

In summary, we have established experimentally that the spin-dependent magnetically sensitive reactions in the subsystem of paramagnetic structural defects in NaCl crystals make an appreciable contribution to the plastic properties of the crystals and that the kinetics of these reactions can be effectively regulated with a weak dc magnetic field and its combined action with a microwave field. It was shown that the dislocation mobility can be used as an indicator of spin resonance in nonthermalized short-lived complexes of paramagnetic defects. The results obtained can serve as a basis for a new and highly sensitive method of investigating paramagnetic structural defects in crystals, mak-

ing it possible to establish directly the interrelationship of the plastic properties of crystals and the electronic state of defects.

We thank V. V. Kveder and A. I. Shalynin for assisting in some of the experiments performed on the EPR spectrometer.

This work was supported by the Russian Fund for Fundamental Research (Grant 97-02-16074).

[1] M. I. Kaganov, V. Ya. Kravchenko, and V. D. Natsik, Usp. Fiz. Nauk **111**, 655 (1973) [Sov. Phys. Usp. **16**, 878 (1974)].
[2] V. V. Kveder, Yu. A. Osip'yan, and A. I. Shalynin, Zh. Éksp. Teor. Fiz. **83**, 699 (1982) [Sov. Phys. JETP **56**, 389 (1982)].
[3] A. L. Buchachenko, R. Z. Sagdeev, and K. Z. Salikhov, *Magnetic and Spin Effects in Chemical Reactions* [in Russian], Nauka, Novosibirsk, 1978.
[4] Ya. L. Zel'dovich, A. L. Buchachenko, and E. L. Frankevich, Usp. Fiz. Nauk **155**, 3 (1988) [Sov. Phys. Usp. **31**, 385 (1988)].
[5] V. I. Al'shits, E. V. Darinskaya, T. M. Perekalina, and A. A. Urusovskaya, Fiz. Tverd. Tela (Leningrad) **29**, 467 (1987) [Sov. Phys. Solid State **29**, 265 (1987)].
[6] V. I. Al'shits, E. V. Darinskaya, and O. L. Kazakova, Zh. Éksp. Teor. Fiz. **111**, 615 (1997) [JETP **84**, 338 (1997)].
[7] Yu. I. Golovin and R. B. Morgunov, Chem. Rev. **24**, 1 (1998).
[8] M. Molotskii and V. Fleurov, Philos. Mag. Lett. **73**, 11 (1996).
[9] V. B. Pariĭskiĭ, A. I. Landau, and V. I. Startsev, Fiz. Tverd. Tela (Leningrad) **5**, 1377 (1963) [Sov. Phys. Solid State **5**, 1002 (1963)].
[10] V. I. Al'shits, E. V. Darinskaya, and O. L. Kazakova, Fiz. Tverd. Tela (St. Petersburg) **40**, 81 (1998) [Phys. Solid State **40**, 70 (1998)].
[11] Yu. I. Golovin and R. B. Morgunov, JETP Lett. **61**, 596 (1995).
[12] K. Hoffman and E. Linke, Phys. Status Solidi A **32**, K67 (1975).
[13] J. Wollbrant, U. Bruckner, and E. Linke, Phys. Status Solidi A **77**, 545 (1983).
[14] V. A. Zakrevskiĭ and A. V. Shul'diner, Fiz. Tverd. Tela (Leningrad) **27**, 3042 (1985) [Sov. Phys. Solid State **27**, 1826 (1985)].

Translated by M. E. Alferieff

Anomalous millimeter-wave absorption in the superconducting phase of $La_{2-x}Sr_xCuO_4$

A. V. Pronin, B. P. Gorshunov, and A. A. Volkov
Institute of General Physics, Russian Academy of Sciences, 117942 Moscow, Russia

H. S. Somal, D. van der Marel, and B. J. Feenstra
University of Groningen, NL-9747 AG Groningen, The Netherlands

Y. Jaccard and J.-P. Locquet
IBM Research Division, Zurich Research Laboratory, CH-8803 Rüschlikon, Switzerland

(Submitted 2 February 1998; resubmitted 27 July 1998)
Pis'ma Zh. Éksp. Teor. Fiz. **68**, No. 5, 406–409 (10 September 1998)

Direct measurements of the complex conductivity spectra of thin-film $La_{2-x}Sr_xCuO_4$ are made at frequencies of $5-40\ cm^{-1}$. Narrow, intense Drude-type excitation is observed in the superconducting phase.
 [S0021-3640(98)01017-2]

PACS numbers: 74.25.Fy, 74.72.Dn, 74.76.Bz

Measurements of the complex dynamic conductivity $\sigma=\sigma_1+i\sigma_2$ of high-temperature superconductors (HTSCs) yield important information about the nature of pairing, the quasiparticle density of states, and the charge-carrier scattering mechanisms.[1,2] In pure samples of the cuprate $YBa_2Cu_3O_{7-\delta}$, which is the best-studied cuprate to date, the linear temperature dependence[1,3] of the penetration depth in the limit $T\rightarrow 0$ and the intense absorption band in the millimeter (MM) and submillimeter (SBMM) conductivity spectra σ_1 at temperatures $T<T_c$,[4,5] which leads to a peak in the temperature dependence $\sigma_1(T)$,[4,6,7] are currently viewed as evidence of *d*-type pairing or, at least, the presence of zeros of the order parameter on the Fermi surface.[8–10] In this connection, the problem of expanding the experimental data for other HTSCs is topical. In the present work, we performed measurements of the complex conductivity spectra of another superconducting cuprate $La_{2-x}Sr_xCuO_4$ in the millimeter and submillimeter ranges ($5-40\ cm^{-1}$).

We investigated a high-quality $La_{1.84}Sr_{0.16}CuO_4$ (LSCO) film 59 nm thick, deposited by molecular epitaxy on a plane-parallel, isotropic $SrLaAlO_4$ substrate approximately 1 mm thick. The *c* axis of the film was oriented perpendicular to the plane of the substrate. The method of synthesis and the structure and electrophysical properties of the film are described in Ref. 11. The superconducting transition temperature $T_c=38.5$ K, with a transition width of 1.5 K, which is comparable to the parameters of the best bulk samples.

The energy transmittance spectra $\mathrm{Tr}(\nu)$ and the phase spectra $\varphi(\nu)$ of a wave transmitted through a film–substrate sandwich were measured on a laboratory BWT spectrometer (which utilizes a backward wave tube as the radiation source).[12] The optical constants of the film were calculated directly from these spectra (without using the

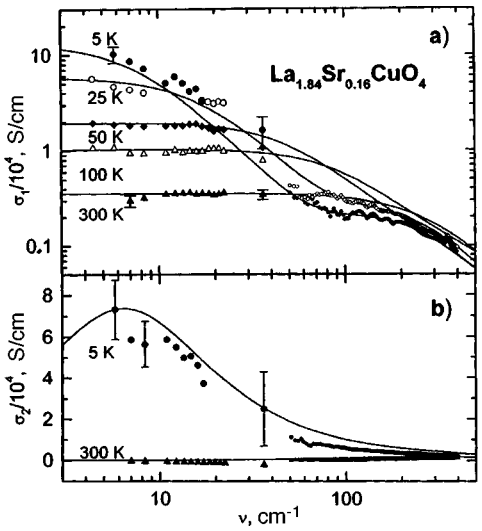

FIG. 1. Spectra of the real (a) and imaginary (b) parts of the conductivity of LSCO in the normal and superconducting phases. Solid lines — least-squares result for the model (1) described in the text.

Kramers–Kronig relations) using general formulas for the complex transmittance of a bilayer system.[13] The optical parameters of the substrate were measured in advance. A detailed description of this method for measuring the MM–SBMM spectra of superconducting films on dielectric substrates is given in Ref. 14.

Figure 1 displays the wide-range ($5-400\ \mathrm{cm}^{-1}$) spectra of the real $\sigma_1(\nu)$ and imaginary $\sigma_2(\nu)$ parts of the complex conductivity of LSCO. To complete the picture, the original MM–SBMM data ($5-40\ \mathrm{cm}^{-1}$) are supplemented by higher frequency IR spectra ($50-400\ \mathrm{cm}^{-1}$), obtained from measurements of the reflectance of a LSCO single crystal.[15] The well-known decrease[2,16] in the real part of the conductivity with decreasing temperature in the superconducting (SC) phase is observed above $30\ \mathrm{cm}^{-1}$.

The main result of the present work is the observation of an intense absorption band in the σ_1 spectra in the superconducting phase of LSCO in the MM–SBMM region and is demonstrated in Fig. 1a. As the temperature decreases from 50 to 5 K the MM–SBMM conductivity increases severalfold; the dispersion-free behavior of σ_1 in the normal phase is replaced at temperatures $T<T_c$ by Drude-type dispersion in the spectra[17] — σ_1 decreases as the frequency increases. This absorption band becomes narrower and more intense as the temperature decreases. The temperature evolution of the band leads to the appearance of a wide maximum in the dependence $\sigma_1(T)$ below T_c (Fig. 2).

We note that the MM–SBMM absorption band observed in the superconducting phase of LSCO (like the analogous band in YBCO at these frequencies[4]) agrees qualitatively with models in which the energy gap has zeroes on the Fermi surface; these give rise to a narrow absorption peak at low frequencies.[9,10]

To obtain quantitative estimates of the parameters of the observed absorption band, the experimental spectra were analyzed using a phenomenological model for the complex conductivity.[6] To describe the MM–SBMM section of the spectrum we used the Drude

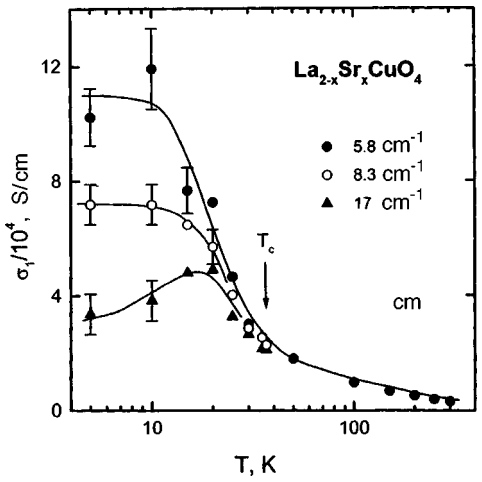

FIG. 2. Temperature dependence of the real part of the conductivity of LSCO for three fixed frequencies.

model and the δ function at zero frequency in the spectrum of $\sigma_1(\nu)$, which is responsible for dc superconductivity (with allowance for its contribution to $\sigma_2(\nu) \propto 1/\nu$), and the absorption band in the IR region was modeled by a Lorentzian whose parameters were found to be practically temperature-independent:

$$\sigma^*(\omega) = \sigma_1(\omega) + i\sigma_2(\omega) = \frac{n_n e^2}{m} \frac{1}{(\gamma - i\omega)} + \frac{n_s e^2}{m}\left[\frac{\pi}{2}\delta(0) + i\frac{1}{\omega}\right] + \text{``IR Lorentzian.''} \tag{1}$$

Here n_s and n_n are the densities of the paired and unpaired carriers, respectively, and γ is the relaxation rate of the unpaired carriers. The spectra were analyzed by the least-squares method under the condition that the following sum rule is satisfied: $n_s + n_n = n_0 = \text{const}(T)$.[18]

The presence of substantial dispersion in the MM–SBMM spectra of σ_1 and σ_2 in the superconducting phase made it possible to determine positively the temperature dependence of the relaxation rate γ (Fig. 3) and to estimate the plasma frequencies of the paired, $(\omega_{pl}^s)^2 = 4\pi n_s e^2/m$, and unpaired, $(\omega_{pl}^n)^2 = 4\pi n_n e^2/m$, electrons. At $T = 5$ K one has $\omega_{pl}^s/2\pi = 3900 \pm 800$ cm^{-1} and $\omega_{pl}^n/2\pi = 7800 \pm 1500$ cm^{-1}. Hence we find for the ''total'' plasma frequency $\omega_{pl}^0/2\pi = \sqrt{(\omega_{pl}^s)^2 + (\omega_{pl}^n)^2}/2\pi = 8700 \pm 1700$ cm^{-1}, which agrees with the estimate[16] obtained from IR measurements on LSCO: $\omega_{pl}^0/2\pi = 6300$ cm^{-1}. For the individual densities of the paired ($x_s = n_s/n_0$) and unpaired ($x_n = n_n/n_0$) electrons we obtain $x_s = (\omega_{pl}^s/\omega_{pl}^0)^2 \approx 20\%$ and $x_n = (\omega_{pl}^n/\omega_{pl}^0)^2 \approx 80\%$, i.e., even at the lowest temperatures most of the electrons in LSCO remain unpaired. For the London penetration depth we have $\lambda_L = c/\omega_{pl}^s = 0.4$ μm, which agrees well with the data from kinetic (0.4 μm),[19] microwave (0.4 μm),[20] IR (0.43 μm),[15] and μSR (0.3 μm)[21] measurements.

In summary, we measured the complex conductivity spectra of $La_{2-x}Sr_xCuO_4$ in the millimeter and submillimeter regions of the spectrum (5–40 cm^{-1}). Strong anomalous absorption in the superconducting phase was observed in the spectra of the real part of

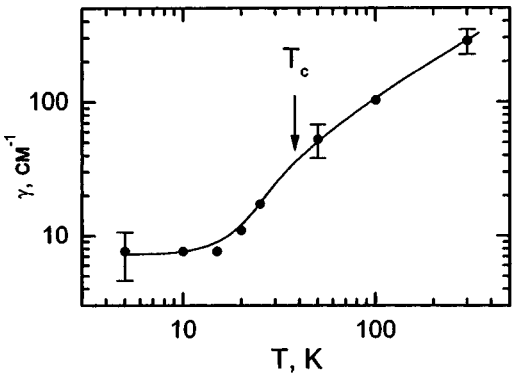

FIG. 3. Temperature dependence of the relaxation rate γ obtained by analyzing the spectra of σ_1 and σ_2. The large decrease in γ in the superconducting phase is responsible for the wide maximum in the temperature dependence of σ_1 (Fig. 2).

the conductivity at these frequencies. From the experimental data obtained we determined the plasma frequency of $La_{2-x}Sr_xCuO_4$ and the temperature dependence of the relaxation rate of the unpaired carriers that give rise to the observed absorption.

This work was performed with the support of the Russian Fund for Fundamental Research (Grant 96-02-17645) and the Russian Ministry of Science and Technology Policy (Grant 3.2 — Microwave Physics) and as part of the Joint Russian–Dutch Project NWO 047-005-12-96.

[1] D. A. Bonn and W. N. Hardy, in *Physical Properties of High Temperature Superconductors*, edited by D. M. Ginsberg, World Scientific, Singapore, 1996, Vol. 5.
[2] D. B. Tanner and T. Timusk, in *Physical Properties of High Temperature Superconductors*, edited by D. M. Ginsberg, World Scientific, Singapore, 1992, Vol. 3.
[3] W. N. Hardy, D. A. Bonn, D. C. Morgan *et al.*, Phys. Rev. Lett. **70**, 3999 (1993).
[4] M. C. Nuss, P. M. Mankievich, M. L. O'Malley *et al.*, Phys. Rev. Lett. **66**, 3305 (1991); A. A. Volkov, B. P. Gorshunov, G. V. Kozlov *et al.*, Zh. Éksp. Teor. Fiz. **95**, 261 (1989) [Sov. Phys. JETP **68**, 148 (1989)].
[5] P. G. Quincey, P. B. Whibberley, and J. R. Birch, Solid State Commun. **76**, 1281 (1991).
[6] D. A. Bonn, P. Dosanjh, R. Liang, and W. N. Hardy, Phys. Rev. Lett. **68**, 2390 (1992); D. A. Bonn, R. Liang, T. M. Riseman *et al.*, Phys. Rev. B **47**, 11314 (1993).
[7] A. Frenkel, F. Gao, Y. Liu *et al.*, Phys. Rev. B **54**, 1355 (1996).
[8] D. J. Scalapino, Phys. Rep. **250**, 329 (1995); K. Maki and H. Won, Ann. Phys. (Leipzig) **5**, 320 (1996).
[9] S. M. Quinlan, P. J. Hirschfeld, and D. J. Scalapino, Phys. Rev. B **53**, 8575 (1996).
[10] J. P. Carbotte, C. Jiang, D. N. Basov *et al.*, Phys. Rev. B **51**, 11798 (1995); H. Yamagata and H. Fukuyama, J. Phys. Soc. Jpn. **65**, 2204 (1996).
[11] J.-P. Locquet, A. Catana, E. Machler *et al.*, Appl. Phys. Lett. **64**, 372 (1994); J.-P. Locquet and E. Machler, MRS Bull. **19**, 39 (1994).
[12] A. A. Volkov, Yu. G. Goncharov, G. V. Kozlov *et al.*, Infrared Phys. **25**, 369 (1985); A. A. Volkov, G. V. Kozlov and A. M. Prokhorov, Infrared Phys. **29**, 747 (1989).
[13] M. Born and E. Wolf, *Principles of Optics*, Pergamon Press, Oxford, 1980, 4th edition [Russian translation, Nauka, Moscow, 1970].
[14] B. P. Gorshunov, G. V. Kozlov, A. A. Volkov *et al.*, Int. J. Infrared Millim. Waves **14**, 683 (1993).
[15] H. S. Somal, B. J. Feenstra, J. Schutzmann *et al.*, Phys. Rev. Lett. **76**, 1525 (1996).
[16] F. Gao, D. B. Romero, D. B. Tanner *et al.*, Phys. Rev. B **47**, 1036 (1993).
[17] A. V. Sokolov, *Optical Properties of Metals*, American Elsevier, New York, 1967 [Russian translation, Fizmatgiz, Moscow, 1961].
[18] R. A. Ferrel and R. E. Glover, Phys. Rev. **109**, 1398 (1958).
[19] J.-P. Locquet, Y. Jaccard, A. Cretton *et al.*, Phys. Rev. B **54**, 7481 (1996).

[20] T. Scibauchi, H. Kitano, K. Uchinokura *et al.*, Phys. Rev. Lett. **72**, 2263 (1994).
[21] Y. J. Uemura, G. M. Luke, B. J. Sternleib *et al.*, Phys. Rev. Lett. **62**, 2317 (1989).

Translated by M. E. Alferieff

On the mechanism of light-induced orientation of molecules in absorbing nematic liquid crystals

A. S. Zolot'ko[a)]
P. N. Lebedev Physics Institute, Russian Academy of Sciences, 117924 Moscow, Russia

(Submitted 28 July 1998)
Pis'ma Zh. Éksp. Teor. Fiz. **68**, No. 5, 410–414 (10 September 1998)

A new mechanism is proposed for the collective light-induced rotation of orientationally ordered molecules of absorbing nematic liquid crystals. The mechanism derives from the noncentral character of the light-induced change in the interaction potential of the excited and unexcited molecules and also from the anisotropy of their correlation function. Rotation is produced by the difference of the torques exerted by the intermolecular forces orienting the ensembles of excited and unexcited molecules. © *1998 American Institute of Physics.*
[S0021-3640(98)01117-7]

PACS numbers: 61.30.Gd, 78.20.Wc

1. Nematic liquid crystals (NLCs) are extremely susceptible to external perturbations, specifically, the influence of a light field, because of the combination of the orientational ordering and mobility of their constituent molecules.[1–4] The ''giant'' orientational nonlinearity of transparent NLCs is nine orders of magnitude greater than the Kerr nonlinearity of ordinary liquids.[1] The light-induced reorientation of the director **n** of a transparent NLC is due to the torque exerted by the light field **E** on the molecular dipoles induced by this field.

However, it was discovered comparatively recently that light-induced reorientation of the director (LRD) can be even more effective in NLCs containing traces of light-absorbing dye molecules[5,6] or consisting completely of absorbing molecules.[7] For example, the threshold of the light-induced Fréedricksz transition in NLCs doped with traces ($\sim 1\%$) of anthraquinone dye is $P_{\text{th}} \sim 1$ mW for a focused light beam.[5] This is two orders of magnitude lower than the threshold for transparent NLCs, $P_{\text{th}} \sim 100$ mW.[2] Moreover, in contrast to the case of transparent NLCs, for which the LRD is always positive (**n** is oriented parallel to **E**), for absorbing NLCs the LRD can also be negative (**n** is oriented perpendicular to **E**).

In Ref. 6 it was suggested that in absorbing NLCs the LRD is due to the interaction of an ensemble of excited dye molecules, which is characterized by an orientational distribution that is asymmetric relative to the director, with the molecules of the nematic matrix. Calculations of the torque acting on the director, which are in quantitative agreement with experiment, were performed in Refs. 7–10, where the appearance of the torque was attributed to the change in the average interaction potential of an excited dye molecule with the director[7–9] or with a molecule of the nematic matrix.[10] However, for the

potentials used in Refs. 7–10 the torque acting on an excited molecule should be compensated by the torque exerted by the excited molecule on the nematic matrix. In Refs. 8 and 10 this difficulty was overcome by introducing the torque exerted on the director as a result of the orientational relaxation of excited dye molecules.

In the present letter a direct calculation of the torque acting on the director is performed. The main idea of the calculation is to take into account the noncentrality of the light-induced change of the interaction potential between an excited dye molecule and a molecule of the nematic matrix and also the anisotropy of the short-range order (i.e., the dependence of the pair distribution function of the molecules on the unit vector **m**, parallel to the line connecting their centers). These factors acting together cause the orienting torques exerted on the matrix by the intermolecular forces to be different from the torques acting on the ensemble of excited molecules. This difference is the reason for the rotation of the director.

2. Let $\mathbf{r}_d$ and $\mathbf{r}_m$ be the radius vectors of the centers of a dye molecule and a molecule of the nematic matrix, and let $\mathbf{l}^{(d)}$ and $\mathbf{l}^{(m)}$ be the unit vectors parallel to the long axes of these molecules. The pair interaction potential $U^{(d,m)}$ of two molecules, which depends on $\mathbf{l}^{(d)}$, $\mathbf{l}^{(m)}$, and $\mathbf{R}=\mathbf{r}_m-\mathbf{r}_d$ is generally speaking noncentral $[(\mathbf{R}\times\partial U^{(d,m)}/\partial\mathbf{R}]\neq 0)$.[11] A matrix molecule exerts on a dye molecule a torque $\mathbf{M}_{dm}=-[\mathbf{l}^{(d)}\times\partial U^{(d,m)}/\partial\mathbf{l}^{(d)}]$. Similarly, a dye molecule exerts a torque $\mathbf{M}_{md}=-[\mathbf{l}^{(m)}\times\partial U^{(m,d)}/\partial\mathbf{l}^{(m)}]$ on a matrix molecule. It follows from conservation of angular momentum that

$$\mathbf{M}_{dm}+\mathbf{M}_{md}-\left[\mathbf{R}\times\frac{\partial U^{(d,m)}}{\partial\mathbf{R}}\right]=0, \tag{1}$$

which signifies that for a noncentral potential the net torque $\mathbf{M}^{(d,m)}=\mathbf{M}_{dm}+\mathbf{M}_{md}$ acting on the two molecules is different from zero.

If a dye molecule is in an excited state, then the potential $U^{(d,m)}$ changes by an amount $\Delta U^{(d,m)}(\mathbf{R},\mathbf{l}^{(d)},\mathbf{l}^{(m)})$. In consequence, the torque $\mathbf{M}^{(d,m)}$ also changes:

$$\Delta\mathbf{M}^{(d,m)}=\left[\mathbf{R}\times\frac{\partial\Delta U^{(d,m)}}{\partial\mathbf{R}}\right]. \tag{2}$$

To determine the density of the net torque exerted on the director of an absorbing NLC as a result of the excitation of a portion of the dye molecules, one must sum Eq. (2) over all pairs consisting of an excited dye molecule (i) and a matrix molecule (j), and then divide the sum obtained by the volume V:

$$\Gamma_{\text{abs}}=\frac{1}{V}\sum_{i,j}\Delta\mathbf{M}^{(i,j)}. \tag{3}$$

In Eq. (3) the contribution introduced by the change in the interaction of the excited and unexcited dye molecules is neglected. This is justified if the concentration c_d of dye molecules is low, which corresponds to the experimental situation ($c_d\leqslant 1\%$). We shall express the sum (3) in terms of the pair distribution function of the dye and nematic molecules $F_2(R,\mathbf{m},\mathbf{l}^{(d)},\mathbf{l}^{(m)},\mathbf{n})$ and the probability $w(\mathbf{l}^{(d)})$ of finding a dye molecule with orientation $\mathbf{l}^{(d)}$ in the excited state:

$$\Gamma_{\rm abs}=c_d c_m\int\frac{d\mathbf{l}^{(d)}}{4\pi}w(\mathbf{l}^{(d)})\int\frac{d\mathbf{l}^{(m)}}{4\pi}\int d\mathbf{m}\int_0^\infty dRR^2F_2$$
$$\times(R,\mathbf{m},\mathbf{l}^{(d)},\mathbf{l}^{(m)},\mathbf{n})\Delta\mathbf{M}^{(d,m)}(R,\mathbf{m},\mathbf{l}^{(d)},\mathbf{l}^{(m)}). \quad (4)$$

Here $R=|\mathbf{R}|$, $\mathbf{m}=\mathbf{R}/R$, and c_m is the concentration of molecules of the nematic matrix. The distribution function $F_2(R,\mathbf{m},\mathbf{l}^{(d)},\mathbf{l}^{(m)},\mathbf{n})$ is normalized by the condition $F_2=1$, if R is greater than a few times the molecular size.

3. To calculate the torque density $\Gamma_{\rm abc}$ it is necessary to have explicit expressions for the functions $w(\mathbf{l}^{(d)})$, $U^{(d,m)}(\mathbf{R},\mathbf{m},\mathbf{l}^{(d)},\mathbf{l}^{(m)})$, and $F_2(R,\mathbf{m},\mathbf{l}^{(d)},\mathbf{l}^{(m)},\mathbf{n})$.

The probability $w(\mathbf{l}^{(d)})$ can be estimated as follows:

$$w(\mathbf{l}^{(d)})=w_\perp+\Delta w(\mathbf{e}\cdot\mathbf{l}^{(d)})^2, \quad (5)$$

where

$$w_\perp=\frac{S_p\tau^*}{3\hbar\omega c_d}\left(\alpha_\parallel+2\alpha_\perp-\frac{\Delta\alpha}{S_{2d}}\right),\quad \Delta w=\frac{S_p\tau^*}{\hbar\omega c_d}\frac{\Delta\alpha}{S_{2d}},\quad S_p=\frac{cn}{8\pi}|A|^2$$

is the magnitude of the Poynting vector; $\mathbf{e}$, $\mathbf{A}$, and ω are, respectively, the polarization unit vector, the complex amplitude, and the frequency of the light field; c is the speed of light in vacuum; n is the index of refraction of the NLC; $\Delta\alpha=\alpha_\parallel-\alpha_\perp$, where $\alpha_\parallel$ and $\alpha_\perp$ are the coefficients of absorption of the extraordinary and ordinary light waves; $\tau^*=\min(\tau_e,\tau_D)$, where τ_e is the lifetime of a dye molecule in the excited state and τ_D is the rotational diffusion time; and, S_{2d} is the order parameter of the dye molecules.

We shall assume that the change in the potential $\Delta U^{(d,m)}(R,\mathbf{m},\mathbf{l}^{(d)},\mathbf{l}^{(m)})$ accompanying the excitation of a dye molecule is due to the change in the dipole–dipole dispersion forces.[12] The interaction energy of a dye molecule in the state $|\gamma\rangle$ and a matrix molecule in the ground state $|0\rangle$ equals

$$\mathcal{U}(\gamma,0)=-\frac{1}{R^6}\sum_{\substack{\lambda=l,t\\ \delta=l,t}}B_{\lambda\delta}(\gamma,0)u_{\lambda\delta}, \quad (6)$$

where the coefficients $B_{\lambda\delta}$ depend on the energy spectrum and state of the molecules and characterize the interaction between longitudinal (l) and transverse (t) fluctuation dipole moments of the dye molecules (λ) and the molecules of the nematic matrix (δ); $u_{ll}=(\mathbf{l}^{(d)}\cdot\mathbf{l}^{(m)})^2-6(\mathbf{l}^{(d)}\cdot\mathbf{l}^{(m)})(\mathbf{m}\cdot\mathbf{l}^{(d)})(\mathbf{m}\cdot\mathbf{l}^{(m)})+9(\mathbf{m}\cdot\mathbf{l}^{(d)})^2(\mathbf{m}\cdot\mathbf{l}^{(m)})^2$, $u_{lt}=1+3(\mathbf{m}\cdot\mathbf{l}^{(d)})^2-u_{ll}$, $u_{tl}=1+3(\mathbf{m}\cdot\mathbf{l}^{(m)})^2-u_{ll}$, $u_{tt}=4-3(\mathbf{m}\cdot\mathbf{l}^{(d)})^2-3(\mathbf{m}\cdot\mathbf{l}^{(m)})^2+u_{ll}$.

In a NLC the pair distribution function $F_2(R,\mathbf{m},\mathbf{l}^{(d)},\mathbf{l}^{(m)},\mathbf{n})$ depends on R and five scalar parameters ξ_i: $(\xi_1=\mathbf{m}\cdot\mathbf{l}^{(d)})$, $\xi_2=(\mathbf{m}\cdot\mathbf{l}^{(m)})$, $\xi_3=(\mathbf{n}\cdot\mathbf{l}^{(d)})$, $\xi_4=(\mathbf{n}\cdot\mathbf{l}^{(m)})$, and $\xi_5=(\mathbf{l}^{(d)}\cdot\mathbf{l}^{(m)})$. We shall represent the function F_2 as an expansion in the arguments ξ_i and limit the expansion to terms up to fourth order inclusive:

$$F_2(R,\xi_1,\xi_2,\xi_3,\xi_4,\xi_5)=f_0+\sum_{i=1}^5 f_i(R)\xi_i+\sum_{i,j=1}^5 f_{ij}(R)\xi_i\xi_j$$
$$+\sum_{i,j,k=1}^5 f_{ijk}(R)\xi_i\xi_j\xi_j+\sum_{i,j,k,l=1}^5 f_{ijkl}(R)\xi_i\xi_j\xi_j\xi_j. \quad (7)$$

4. Setting $\Delta U=\mathcal{U}(\gamma,0)-\mathcal{U}(0,0)$, we find from Eqs. (2), (4), (5), and (7)

$$\Gamma_{\rm abs}=\frac{\Delta\epsilon_{\rm eff}|A|^2}{8\pi}(\mathbf{n}\cdot\mathbf{e})[\mathbf{n}\times\mathbf{e}], \tag{8}$$

where

$$\Delta\epsilon_{\rm eff}=-\frac{16\pi c c_m n\tau^*\Delta\alpha}{675\hbar\omega v_m S_{2d}}\sum_{\substack{\lambda=l,t\\ \delta=l,t}}\Delta B_{\lambda\delta}\left(\gamma_{\lambda\delta}^{dd}\nu_{1144}+\gamma_{\lambda\delta}^{mm}\nu_{2244}+\frac{5}{2}\gamma_{\lambda\delta}^{md}\nu_{1234}\right),$$

$$\nu_{ijkl}=3v_m\int_0^\infty\frac{f_{ijkl}(R)}{R^4}dR,\quad v_m=\left(3\int_0^\infty\frac{f_0(R)}{R^4}\right)^{-1},\quad \Delta B_{\lambda\delta}=B_{\lambda\delta}(\gamma,0)-B_{\lambda\delta}(0,0),$$

$$\gamma_{ll}^{dd}=-\gamma_{lt}^{dd}=-\gamma_{ll}^{mm}=\gamma_{tl}^{mm}=-\frac{8}{35},\quad \gamma_{tl}^{dd}=-\gamma_{tt}^{dd}=-\gamma_{lt}^{mm}=\gamma_{tt}^{mm}=-\frac{4}{7},$$

$$\gamma_{lt}^{dm}=-\gamma_{lt}^{dm}=\frac{2}{5},\quad \gamma_{ll}^{dm}=\gamma_{tt}^{dm}=0. \tag{9}$$

Expression (8) has the same form as the expression for the density of the torque acting on the director of a transparent NLC, differing only in that the optical anisotropy $\Delta\epsilon$ is replaced by the effective value $\Delta\epsilon_{\rm eff}$.

We note that if the pair distribution function F_2 is isotropic (i.e., does not depend on the vector **m**), then the torque $\Gamma_{\rm abs}$ vanishes.

This analysis can be extended to the case of NLCs consisting of identical absorbing molecules. In this case the first two terms in the right-hand side of Eq. (9) compensate one another (since $\nu_{1144}=\nu_{2244}$), but the third term, which is proportional to ν_{1234}, introduces a nonzero contribution to the torque $\Gamma_{\rm abs}$.

Let us now make a numerical estimate of $\Delta\epsilon_{\rm eff}$. Using the Maier–Saupe theory, one can estimate $B_{\lambda\delta}$ as $B_{\lambda\delta}(0,0)\sim 15\tilde{U}_0 v_m/8\pi c_m$ ($\tilde{U}_0=4.5k_BT_{NI}$, k_B is Boltzmann's constant, and T_{NI} is the nematic–isotropic phase transition temperature). Assuming that $\Delta B_{\lambda\delta}\sim B_{\lambda\delta}$ in the case of photoexcitation of a molecule, we find

$$\Delta\epsilon_{\rm eff}\sim\frac{6c\tilde{U}_0 n\tau^*\Delta\alpha\gamma_{\lambda\delta}\nu_{ijkl}}{135\hbar\omega S_{2d}}. \tag{10}$$

Since, as follows from Ref. 13, the terms in the expansion of the intermolecular potential $U(R,\xi_1,\xi_2,\xi_3,\xi_4,\xi_5)$, which contain the arguments ξ_1 and ξ_2, are not small compared with the terms which are independent of ξ_1 and ξ_2, it is natural to set $\nu_{ijkl}\sim 0.1-1$. Substituting into Eq. (10) the characteristic values $\tilde{U}_0\sim 1.9\times10^{-13}$ ergs ($T_{NI}\sim 300$ K), $n=1.5$, $\tau^*\sim10^{-8}$ s (Ref. 8), $\Delta\alpha\sim 100$ cm^{-1}, $\gamma_{\lambda\delta}\sim 0.5$, $\omega=3.7\times10^{15}$ s^{-1} ($\lambda=515$ nm), and $S_{2d}\sim 0.8$, we find $\Delta\epsilon_{\rm eff}\sim 6-60$. For transparent NLCs $\Delta\epsilon\approx 0.6$, and therefore $\Delta\epsilon_{\rm eff}/\Delta\epsilon\sim 10-100$. This quantity, characterizing the relative efficiency of LRD in absorbing and transparent NLCs, agrees with the experimental results.[5–7]

It follows from Eq. (9) that the sign of $\Delta\epsilon_{\rm eff}$ depends not only on the character of the change in the interaction potential acting between the dye and matrix molecules accompanying the excitation of the dye molecule but also on the pair distribution function of

these molecules, which is evidently affected by the degree of prolateness of the molecules. This dependence could possibly explain the experimentally observed[14] difference of the signs of LRD in NLCs doped with various anthraquinone dyes.

The light-induced change in the intermolecular forces leads not only to reorientation of the director but also to a change in the order parameter.[15,16] However, this effect can also occur in the presence of an isotropic pair distribution function F_2. A sufficient condition for its appearance is a change in the intermolecular interaction potential. Evidently, a parallel measurement of the nonlinearities of the nematic and isotropic phases could be extremely helpful for investigating intermolecular interactions and molecular ordering.

In summary, in the present letter we examined a new mechanism of collective light-induced rotation of orientationally ordered molecules of NLCs. The mechanism is due to the noncentral character of the change in the interaction potential of the molecules and to the anisotropy of the short-range order. This mechanism is very general and should also occur in other media characterized by an anisotropic orientation of the molecules. Specifically, it could be responsible for the appearance of light-induced anisotropy in Langmuir films and polymers.

I thank M. I. Barnik, E. I. Kats, V. F. Kitaeva, and V. N. Ochkin for helpful discussions.

This work was supported by the Russian Fund for Fundamental Research (Grant 98-03-32226a) and the Interdisciplinary Scientific and Technical Program ''Optics. Laser Physics.''

[a)]e-mail: zolotko@sci.lebedev.ru

---

[1] B. Ya. Zel'dovich, N. F. Pilipetskiĭ, A. V. Sukhov, and N. V. Tabiryan, JETP Lett. **31**, 263 (1980).
[2] A. S. Zolot'ko, V. F. Kitaeva, N. Kroo *et al.*, JETP Lett. **32**, 158 (1980).
[3] B. Ya. Zel'dovich and N. V. Tabiryan, Usp. Fiz. Nauk **147**, 633 (1985) [Sov. Phys. Usp. **28**, 1059 (1985)].
[4] V. F. Kitaeva and A. S. Zolot'ko, Laser Res. USSR **10**, No. 4, 275 (1989).
[5] I. Janossy, A. D. Lloyd, and B. S. Wherrett, Mol. Cryst. Liq. Cryst. **179**, 1 (1990).
[6] I. Janossy, L. Csillag, and A. D. Lloyd, Phys. Rev. A **44**, 8410 (1991).
[7] A. S. Zolot'ko, V. F. Kitaeva, and D. B. Terskov, Zh. Éksp. Teor. Fiz. **106**, 1722 (1994) [JETP **79**, 931 (1994)].
[8] I. Janossy, Phys. Rev. E **49**, 2957 (1994).
[9] E. Santamato, G. Abbate, P. Maddalena *et al.*, Mol. Cryst. Liq. Cryst. **302**, 111 (1997).
[10] L. Marucci and D. Paparo, Phys. Rev. E **56**, 1765 (1997).
[11] I. P. Bazarov and É. V. Gevorkyan, *Statistical Theory of Solid and Liquid Crystals* [in Russian], Moscow State University Press, Moscow, 1983.
[12] Yu. S. Barash, *Van der Waals Forces* [in Russian], Nauka, Moscow, 1988.
[13] Kean Feng and Chia-Wei Woo, Phys. Rev. A **28**, 1587 (1983).
[14] I. Janossy and T. Kosa, Opt. Lett. **17**, 1183 (1992).
[15] D. Paparo, L. Marucci, G. Abbate *et al.*, Phys. Rev. Lett. **78**, 38 (1997).
[16] R. Muenster, M. Jarasch, X. Zhuang and Y. Shen, Phys. Rev. Lett. **78**, 42 (1997).

Translated by M. E. Alferieff

Lack of universal one-parameter scaling in the two-dimensional metallic regime

V. M. Pudalov[a)]
P. N. Lebedev Physics Institute, 117924 Moscow, Russia;
High Pressure Physics Institute, 142092 Troitsk, Moscow Region, Russia

G. Brunthaler, A. Prinz, and G. Bauer
Institut für Halbleiterphysik, Johannes Kepler Universität, A-4040 Linz, Austria

(Submitted 28 July 1998)
Pis'ma Zh. Éksp. Teor. Fiz. **68**, No. 5, 415–419 (10 September 1998)

The two-dimensional metallic state is studied in a number of Si-MOS structures with peak mobilities varying by a factor of 8.5. The data show a density dependence and disorder dependence of the major features of the scaling function and thus reveal the absence of universal one-parameter scaling over wide density range in the metallic regime. © *1998 American Institute of Physics.* [S0021-3640(98)01217-1]

PACS numbers: 72.15.Eb, 71.30.+h

The unexpected appearance of a metal–insulator transition in two-dimensional (2D) Si-MOS structures[1] and its confirmation in other works on different samples[2] and materials[3–6] have generated much excitement because it had been generally believed that all states in 2D are localized. A one-parameter scaling theory (OPST)[7] developed in 1979 for noninteracting particles predicted that no true metallic behavior is possible at $T=0$ in 2D system due to quantum interference. On the other hand, the theory developed by Finkel'stein[8] for strong Coulomb interaction predicted the occurrence of a metallic state in 2D due to divergence of an interaction parameter in the renormalization procedure as $T\to 0$. The new experimental findings have initiated a debate over the nature of the 2D metallic state.[9–11]

Recently, a phenomenological modification of the OPST has been suggested[12] for treating the case of an interacting system, wherein the scaling function in a 2D system, $\beta = d\ \ln G/d\ \ln L$, changes sign at a critical value of the conductivity, G_c. With an eye toward testing the validity of the OPST, we summarize here a number of generic features of the metal–insulator transition in 2D as experimentally observed in different materials and samples:

(i) The resistivity develops exponentially at temperatures below $T_0 \sim 0.3E_F/k$, with E_F the Fermi energy:[1,10]

$$\rho = \begin{cases} \rho_0 + \rho_1\ \exp(-(T_0/T)^p) & \text{at } n > n_c, \\ \rho_1^*\ \exp((T_0/T)^p) & \text{at } n < n_c, \end{cases} \tag{1}$$

where n_c is the critical density, the parameter T_0 is sample and density dependent and $p \approx 1$. The empirical equation (1) was recently supported theoretically.[14,13]

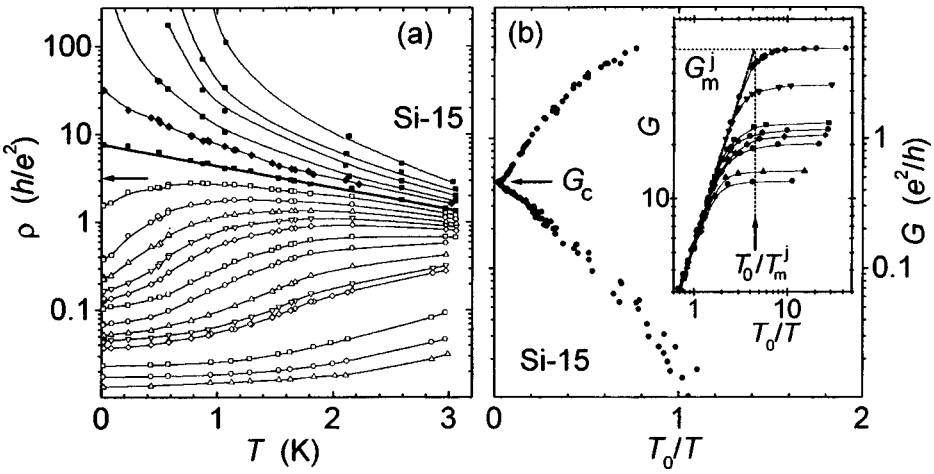

FIG. 1. a: $\rho(T)$ for the sample Si-15 over the range 0.016 to 3 K. Different symbols correspond to n from 0.449 to 0.989 (in steps of 0.054), and further 1.1, 1.2, 1.42, 1.64, 1.74, 2.82, 3.9, $4.98\cdot10^{11}$ cm^{-2}. b: G versus $1/T$ scaled with a single parameter (T_0/T). The inset in part b shows a blowup of the metallic part of the scaling plot in the range of low T. The carrier densities (from top to bottom) are 4.96, 3.1, 1.84, 1.74, 1.63, 1.52, 1.31, and $1.2\cdot10^{11}$ cm^{-2}. The horizontal arrows show the critical values, ρ_c and G_c.

(ii) For lower temperatures, when $\rho_1 \exp(-T_0/T) \ll \rho_0$, the resistivity crosses over to a logarithmic temperature dependence,[14,13] $C \ln T$. The crossover point corresponds to the point of the maximum, $G_m = 1/\rho_0$, of the scaling function $\beta(G)$ (Ref. 13).

(iii) In the region of exponential behavior, according to Eq. (1), the resistivity can be scaled by T/T_0 into a metallic and an insulating branches. The single scaling parameter, $T_0 \propto |n - n_c|^q$, exhibits critical behavior[1–3,6,10] around n_c, and the exponent $q = z\nu \sim 1$ is the product of the dynamic exponent z and the correlation length exponent[15,12] ν.

(iv) The metallic state is destroyed by magnetic fields applied parallel to the 2D plane,[16,2] a fact which points to the importance of spin effects.

In this paper we present experimental data which clearly demonstrate the lack of universality in the modified one-parameter scaling description of the conductivity of the 2D metal. In order to test the role of disorder and interaction, we have performed systematic measurements on a number of Si-MOS samples. Our measurements show that no common scaling function exists, through the following facts: (i) the critical conductivity values G_c for various samples differ from each other and show no tendency to converge towards a limiting value; (ii) the ''crossover'' value of the conductivity, $G_m = \rho_0^{-1}$, is not universal; and (iii) the separatrix dividing the metallic from the insulating phase in the $\rho - T$ plane (Fig. 1a) is ''tilted,'' i.e., temperature (length scale) dependent.

We have performed studies in the metallic regime, i.e., for high conductivities $G > G_c \sim 1$, where G is given in units of e^2/h. We made measurements on a number of Si-MOS samples with peak mobilities[b)] varying by a factor of 8.5: $\mu = 41{,}000$ cm^2 (V·s) (Si-15a), $\mu = 40{,}000$ (Si-5), $\mu = 39{,}000$, $\mu = 36{,}200$ (Si-62), $\mu = 29{,}000$ (Si-22), $\mu = 24{,}200$ (Si-2), $\mu = 19{,}600$ (Si-43), $\mu = 9{,}300$ (NS-2), and $\mu = 4{,}800$ cm^2(V·s) (Si-39). The data were taken by a 4-terminal ac technique in the temperature range from 0.29

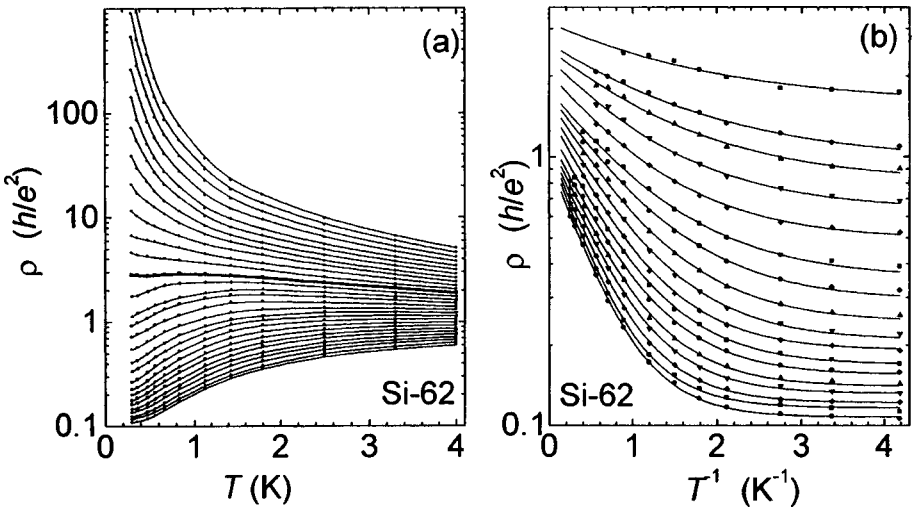

FIG. 2. a: $\rho(T)$ for the sample Si-62 ($n_c=0.956$); b: fit to Eq. (1) with 3 parameters, ρ_0, ρ_1 and T_0 for each density in the metallic range. $n_j=0.978$ to 1.326 in steps of 0.0218 (from top to bottom) and in units of 10^{11} cm^{-2}.

K to 4 K (for all samples), and 0.016 K to 15 K (for a few samples). The resistivity for all samples exhibited a characteristic temperature dependence similar to that shown in Fig. 1, with a critical density n_c separating the metallic ($d\rho/dT>0$, $n>n_c$) from the insulating ($d\rho/dT<0$, $n<n_c$) region, in the limit $T\to 0$.

For samples with lower mobility the magnitude of the drop ρ_1 is less, and the transition is shifted to higher densities. In Si-15a the drop $\rho_1/\rho_0\approx 6$, in Si-62 $\rho_1/\rho_0 \approx 4.5$, whereas for Si-39 the decrease in $\rho(T)$ is within a few percent. By scaling the measured conductivities to the metallic and insulating branches, we examine below the major features of the scaling function, namely: the critical value G_c (at which $\beta(G_c) =0$), the slope $z\nu$ of its steep part in the vicinity of G_c, and the conductivity G_m at which $\beta(G_m)$ reaches maximum.[13] As an example, the rescaled conductivities for Si-15a are shown in Fig. 1b on a T_0/T scale. The scaling procedure is straightforward for medium-mobility samples with a temperature-independent (''horizontal'') line $\rho(n_c)$ and with well-pronounced exponential dependence (1), such as shown in Fig. 2a for the sample Si-62. For the highest-mobility sample Si-15a, where $\rho(n_c)$ is strongly temperature dependent (''tilted''), we limited the scaling analysis to $T\leqslant 0.1E_F/k_B$, in order to decrease the influence of ''tilting.''

In Fig. 3a the values of G_c and $z\nu$ for different samples are summarized and plotted as a function of n_c. The latter is roughly proportional to the concentration of scattering centers at the interface[17] and thus may serve as a measure of the disorder. For the most disordered sample Si-39 the value of $G_c\approx 4$ is not well defined due to the weak change of $\rho(T)$ in the metallic state and is thus not shown in Fig. 3. The values of G_c show a systematic dependence as a function of disorder (i.e., of n_c) and do not exhibit a trend to saturate at a universal value.

Even in within a single sample there is clear evidence for the absence of a universal

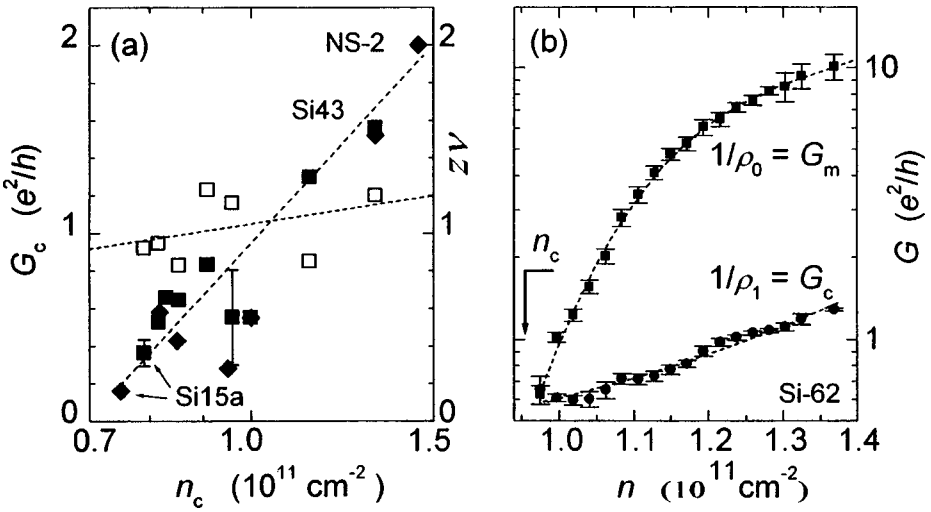

FIG. 3. a: Critical conductivity G_c (closed symbols) and the critical exponent $z\nu$ (open symbols) versus the critical density n_c for different samples. The squares are obtained from temperature scaling, while the diamonds show, for comparison, the onset of the insulating state from non-Ohmic transport measurements.[17] b: G_c versus density, obtained from fitting to Eq. (1). The dashed curves are guides to the eye.

value of G_c. Figure 2b shows a fit of the $\rho(T)$ data for the sample Si-62 using Eq. (1) with ρ_0, ρ_1, and T_0 as fitting parameters, and with $p=1$. The critical conductivity values $G_c=1/\rho_1$ found from this fit for each density are shown in Fig. 3b. Only in a narrow range of densities $n/n_c \leqslant 1.1$ can the G_c be considered constant; above that it increases with density.

The absence of one-parameter scaling can also be seen at higher values of the conductivity (shown in the inset of Fig. 1b), where the individual curves for different electron densities n_j deviate clearly from the common scaling branch. This saturation was found not to be caused by electron overheating[18] and is intrinsic to all the samples studied. Different conductivity curves ''saturate'' at different values $G_m^j=1/\rho_0(n_j)$. The similar result is also demonstrated in Fig. 3b, where the fitting parameter $1/\rho_0$ is plotted as a function of the density. It does not exhibit a tendency to converge to a universal value.

The absence of a universal scaling behavior also follows from the ''tilted'' separatrix $\rho(T)$ (the straight bold line in Fig. 1a). The separatrix corresponds to the density at which the curvature, $d^2\rho/dT^2$ vanishes. This separatrix line is almost horizontal for medium-mobility samples (Si-43, Si-2, Si-22), and it coincides with n_c, in agreement with earlier reports,[1] but is tilted for high-mobility (less-disordered) samples, as is seen in Fig. 1a. Due to the tilting of $\rho_c(T)$, different G_c values may be obtained by performing the scaling analysis in different temperature ranges. The error bar in Fig. 3 for Si-15a reflects the results obtained from scaling over the ranges $T<0.1E_F$ and $T<0.15E_F$ (where $E_F \approx 5.8$ K at $n=n_c$).

The onset of the metallic state occurs, roughly, when the influence of the disordering (localizing) potential is compensated by a corresponding interaction energy, $E_{\rm int}\tau \sim 1$.

Figure 3a demonstrates that higher disorder corresponds to higher n_c and G_c values. Since the ratio E_{ee}/E_F decreases with density as $n^{-1/2}$, this result indicates that there is another mechanism, whose *strength increases with density*, in addition to the pure Coulomb interaction. The correlation between n_c, G_c, and disorder holds also for the *p*-GaAs/AlGaAs system, as follows from comparison of the data in Refs. 5 and 6. Although the sample mobility in Ref. 6 is about 25 times higher, the transition is nevertheless much weaker and its features are more similar to those displayed by our most disordered sample Si-39, where the transition occurs at seven times higher density. This again confirms our conclusion that another mechanism besides the purely Coulomb interaction is involved. We presume, this interaction is caused by spin or exchange effects. Figure 3a shows also the exponents $z\nu$ for different samples. Although these data are scattered and less disorder-dependent than G_c, there is a trend for $z\nu$ to increase from $z\nu \approx 0.9 \pm 0.1$ for the least disordered sample to $z\nu \approx 1.2$ for the sample Si-43.

In summary, we demonstrated that no universality either in G_c, in $z\nu$, or in G_m can be found for the Si-MOS samples, and, hence, no universal one-parameter β function exists. However, due to the rather weak disorder dependence of $z\nu$, the slope of the logarithmic derivative $d \ln G/d \ln T$ does not vary much. This explains why the individual conductivity curves for each sample may be scaled in a limited temperature range, $E_F \gg T > T_0/\ln(\rho_1/\rho_0)$ (where the term ρ_0 in Eq. (1) can be neglected), and in a limited density range in the vicinity of n_c. The conductivity may thus be described in the framework of a particular scaling function[12] $\beta^j = d \ln G/d \ln L$, which should change sign at a certain critical value $G_c^j(n_j)$, where, however, β^j is sample and density dependent.[13]

V. P. acknowledges discussions with M. Baranov, V. Kravtsov, M. Skvortsov, and I. Suslov. This work was supported by RFBR (97-02-17387), by the Programs on ''Physics of Solid-State Nanostructures'' and ''Statistical Physics,'' by INTAS (96-0580, 96-0250), by NWO, and by FWF Vienna, ÖNB (6333) and GME Austria.

[a)]e-mail: pudal@east.ru

[b)]We characterize the samples with peak mobility taken at $T = 20$ to 300 mK, because in the high μ samples the resistivity drops exponentially at $T < 2$ K.

[1] S. V. Kravchenko, G. V. Kravchenko, J. E. Furneaux *et al.*, Phys. Rev. B **50**, 8039 (1994); S. V. Kravchenko, W. E. Mason, G. E. Bowker *et al.*, Phys. Rev. B **51**, 7038 (1995).
[2] D. Popović, A. B. Fowler, and S. Washburn, Phys. Rev. Lett. **79**, 1543 (1997); K. P. Li, D. Popović, and S. Washburn, in *Proceedings EP2DS-12*, Tokyo (1997).
[3] P. T. Coleridge, R. L. Williams, Y. Feng, and P. Zawadzki, Phys. Rev. B **56**, R12764 (1997); M. D'Iorio, D. Brown, and H. Lafontain, http://xxx.lanl.gov/abs/cond-mat/9708201.
[4] K. Ismail, J. O. Chu, D. Popović *et al.*, http://xxx.lanl.gov/abs/cond-mat/9707061.
[5] Y. Hanein, U. Meirav, D. Shahar *et al.*, Phys. Rev. Lett. **80**, 1288 (1998).
[6] M. Y. Simmons, A. R. Hamilton, M. Pepper *et al.*, Phys. Rev. Lett. **80**, 1292 (1998).
[7] E. Abrahams, P. W. Anderson, D. C. Licciardello, and T. V. Ramakrishnan, Phys. Rev. Lett. **42**, 673 (1979).
[8] A. M. Finkel'stein, Z. Phys. B **56**, 189 (1984); Sov. Sci. Reviews/section A- Physics Reviews, edited by I. M. Khalatnikov, **14**, 3 (1990).
[9] P. Phillips and Y. Wan, http://xxx.lanl.gov/abs/cond-mat/9704200; P. Phillips, Y. Wan, I. Martin *et al.*, http://xxx.lanl.gov/abs/cond-mat/9709168; D. Belitz and T. R. Kirkpatrick, http://xxx.lanl.gov/abs/cond-mat/9705023; M. A. Skvortsov, http://xxx.lanl.gov/abs/cond-mat/9712135v2; Y. Lyanda-Geller, Phys. Rev. Lett. **80**, 4273 (1998); S. Chakravarty, S. Kivelson, C. Nayak, and K. Völker, http://xxx.lanl.gov/abs/cond-mat/9805383; S. Cakravarty, L. Yin, and E. Abrahams, http://xxx.lanl.gov/abs/cond-mat/9712217.
[10] V. M. Pudalov, http://xxx.lanl.gov/abs/cond-mat/9707076v2; JETP Lett. **66**, 170 (1997).
[11] Song He and X. C. Xie, http://xxx.lanl.gov/abs/cond-mat/9711195.

[12] V. Dobrosavljević, E. Abrahams, E. Miranda, and S. Chakravarty, Phys. Rev. Lett. **79**, 455 (1997).
[13] V. M. Pudalov, G. Brunthaler, A. Prinz, and G. Bauer, in *Proceedings of the 10th Winter School ''Frontiers in Condensed Matter Physics,''* Mauterndorf, 1998; Physica E 2 Oct. (1998), in press.
[14] V. M. Pudalov, G. Brunthaler, A. Prinz, and G. Bauer, http://xxx.lanl.gov/abs/cond-mat/9801077.
[15] S. V. Kravchenko, D. Simonian, M. P. Sarachik *et al.*, Phys. Rev. Lett. **77**, 4938 (1996).
[16] V. M. Pudalov, G. Brunthaler, A. Prinz, and G. Bauer, JETP Lett. **65** 932 (1997); D. Simonian, S. V. Kravchenko, M. P. Sarachik, and V. M. Pudalov, Phys. Rev. Lett. **79**, 2304 (1997).
[17] V. M. Pudalov, M. D'Iorio, J. W. Campbell, and S. V. Kravchenko, Phys. Rev. Lett. **70**, 1866 (1993).
[18] R. Fletcher, V. M. Pudalov, Y. Feng *et al.*, Phys. Rev. B **56**, 12422 (1997); M. D'Iorio, V. M. Pudalov, and S. G. Semenchinsky, Phys. Rev. B **46**, 15992 (1992).

Published in English in the original Russian journal. Edited by Steve Torstveit.

Effect of a pulsed magnetic field on the transverse resistance of a layered superconductor

V. N. Zavaritskiĭ[a)] and M. Springford

P. L. Kapitsa Institute of Physics Problems, Russian Academy of Sciences, 117334 Moscow, Russia;
Institute of General Physics, Russian Academy of Sciences, 117942 Moscow, Russia;
H. H. Wills Physics Laboratory, University of Bristol, BS8 1TL Bristol, Great Britain

(Submitted 30 July 1998)
Pis'ma Zh. Éksp. Teor. Fiz. **68**, No. 5, 420–425 (10 September 1998)

The field dependences of the transverse resistance of a single crystal of the layered superconductor $Bi_2Sr_2CaCu_2O_y$ (BSCCO-2212) with $T_{c0} \simeq 92$ K are studied in magnetic fields up to 50 T in the perpendicular orientation $H \perp (ab)$. It is established that in the resistive region the resistance is a power-law function of the field, and the temperature dependence of the barrier height for flux creep is obtained. It is found that in a wide temperature range, 50–125 K, the transverse magnetoresistance of the crystal in the normal state and under conditions of superconductivity suppression by a strong magnetic field is negative and can be approximated by a linear law with a temperature-dependent slope. © *1998 American Institute of Physics.*
[S0021-3640(98)01317-6]

PACS numbers: 74.25.Fy, 74.72.Hs, 74.25.Nf

The interrelationship of high-temperature superconductivity and the peculiarities of the normal state of layered cuprate HTSCs has been actively debated ever since these materials were discovered. The anisotropy of the electrical resistance and the qualitatively different character of its temperature dependence, which are a specific feature of the normal state of these compounds, are attracting particular attention.[1] A substantial number of experimental investigations[1] concern the nature of the combination of the quasimetallic temperature behavior of the basal-plane resistivity of BSCCO-2212 ($\rho_{ab} \propto T$) together with quasidielectric behavior in the transverse direction, and attempts have been made to describe them theoretically using both the conventional models of the tunnel effect, hopping conductivity, and the more exotic theories that assume that cuprate superconductors have a non-Fermi-liquid nature.[1,2] Moreover, in a number works (for example, Ref. 3) it has been demonstrated that a modified theory of superconducting fluctuations[4] adequately describes the experimental data[5] in a wide temperature range right up to $4T_c$. Recently, the same transverse resistance was interpreted as a subgap resistance of a superconductor with an exotic pairing mechanism.[6]

Since all the experimental investigations that we know of on this question have been performed in a weak magnetic field, in the present work we studied the transverse resistance of BSCCO-2212 in the normal state and under conditions of superconductivity

suppression by a strong pulsed magnetic field up to 50 T. Strong negative magnetoresistance which, to a first approximation, depends linearly on the magnetic field was observed under these conditions.

Crystals with the nominal composition $Bi_2Sr_2CaCu_2O_y$ (BSCCO-2212) with $T_c > 90$ K were investigated. A high critical temperature was obtained by partial substitution of yttrium impurity for calcium in the lattice.[7] To decrease the overheating effects due to the induction currents induced by the field pulse, we used a small sample cut from a large crystal selected for its macroscopic uniformity of composition and the absence of blocks.[8] The low-resistance electric contacts were prepared by alloying-in a conducting composite in both *ab* planes.[9] The main results of the present work are based on detailed investigations of a crystal with dimensions of $\approx 110 \times 85 \times (4.2 \pm 0.4)\,\mu$m. The character of the temperature dependence and the transverse resistivity $\rho_c(100\ \text{K}) \simeq 15\ \Omega \cdot$ cm attested to the absence of shunting shorts. The critical temperature $T_{c0} \approx 92.2$ K was determined at the level $10^{-4}\rho_c(100\ \text{K})$ from the results of $R(T)$ measurements performed in the laboratory field. A crystal of close to the same size and with $T_{c0} \approx 91.7$ K was used for control measurements.

The pulsed field was produced by discharging capacitors through a solenoid. A container, holding the sample and filled with heat-exchange helium, was positioned at the center of the solenoid with an accuracy of 0.5 mm or better. The signal from a probe coil placed near the sample was used as a position sensor. The orientation $H \perp (ab)$ was set with an accuracy estimated to be not worse than $\approx 5°$. Copper and RuO_2 resistance thermometers, calibrated with CERNOX (Lake Shore) and placed near the sample inside the container, were used to measure the temperature. During calibration, which was performed in the same apparatus, the CERNOX was mounted at the location of the sample. The container holding the thermometers, heater, and sample was connected with a helium bath through a thermal resistance. Active stabilization of the temperature was attained using a standard LTC-21 controller (Neocera). The temperature change in the time of one pulse (≈ 70 ms) was not monitored, but the absence of hysteresis in the field dependence $R(B)$ shows that the effect is negligibly small in a wide temperature range $T > 26$ K. The measurements described were performed at Bristol University on an apparatus for investigating the Shubnikov–de Haas effect. This apparatus was specially adapted for performing potentiometric measurements in the temperature range 4.2–300 K.

The method of Ref. 10 was used to perform the control measurements of the temperature dependences of the transverse resistance $R(T)$ in the laboratory field. The main measurements in pulsed magnetic fields were performed using a 5 μA ac current with frequency $\omega/2\pi = 77.7$ kHz. The signal from the potential contacts to the crystal was recorded with a fast (500 kHz) digital-to-analog converter. The parasitic emf induced by the pulsed field was partially compensated by the signal from a probe coil placed near the sample. The useful signal $V(t)$ at the measuring frequency was determined by fitting the function $\sim V(t)\sin(\omega t + \phi) + A(t)$ to the set of experimental points. Modified standard software for identifying the Shubnikov–de Haas oscillations was used. The shape of the field pulse $B(t)$ was determined by integrating the signal from the probe coil: $B \sim \sin(t/t_0)$ on the rising side of the pulse and $B \sim \exp(-t/\tau)$ on the falling side. Both sides of the pulse were used in the measurements. Since the induction overheating is proportional to the squared rate of change of the field and since the values of $\partial B/\partial t$ on different

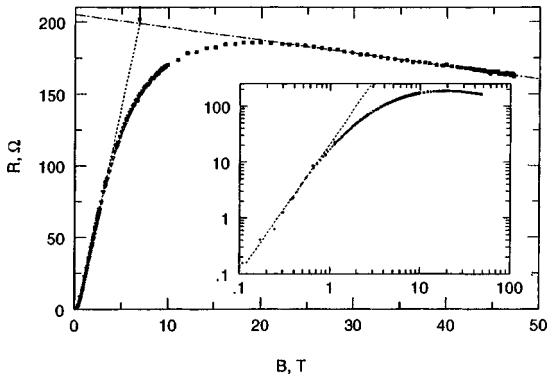

FIG. 1. Typical field dependence of the transverse resistance of a BSCCO crystal at temperatures $T<T_{c0}$. The data presented were obtained at 56.6 K for three field pulses with amplitudes of 2.65, 9.7, and 47.2 T, which are shown by crosses, open triangles, and filled squares, respectively. The dot-and-dash curve shows the approximation used for the negative normal-state magnetoresistance of the crystal; its extrapolation to zero field gives an estimate of the ''normal'' resistance of the crystal, $R_N(0)$, under conditions such that superconductivity is suppressed. Inset: Same data presented in double logarithmic coordinates; dashed curve — approximation of the initial section of the dependence by the law $R(B)\propto B^{\beta}$.

sides of the pulse differ considerably, the absence of hysteresis in the experimental dependences indicated that the temperature of the crystal remained constant during the pulse. The presence of induction overheating was additionally monitored by comparing the dependences $R(B)$ measured at each temperature in a series of pulses with amplitudes differing by a factor of 3–20. It was established that the effects due to induction overheating fall within the limits of the detecting power of the experiment for the temperature range $T\geqslant 25-28$ K (see Fig. 1, which shows a typical result of such an experiment). The linearity of the response of the system was monitored in a series of measurements of the $R(B)$ dependences at two temperatures, 26 and 87 K, for seven current amplitudes in the range $0.1-100\ \mu$A.

To compare the results with the low-frequency measurements and to estimate the frequency dependence of the resistance, series of control measurements of $R(B)$ were performed at two temperatures, 36.2 and 84 K, for five frequencies in the range 11–111 kHz. Identical (to within the random scatter of the points) results were obtained for $T\simeq 84$ K. Some large quantitative discrepancies (not exceeding 12%) with qualitatively identical dependences were recorded at $T\simeq 36.2$ K.

A typical field dependence of the transverse resistance of a BSCCO-2212 crystal is displayed in Fig. 1. The formation of the resistive state is illustrated in the inset, where the same data are plotted in double-logarithmic coordinates. As one can see, the initial segment of the dependence admits an approximation by a simple power law, $R\propto H^{\beta}$. We established that the power-law variation of the resistance as a function of the field holds in a wide temperature range, $0.25\leqslant T/T_c\leqslant 1$, in qualitative agreement with the low-frequency measurements in a dc field.[10] This result attests to the applicability of the theoretical models[11] predicting a logarithmic dependence of the barrier height on the flux creep, $U=U_0\ \log(1/B)$, and accordingly $R\propto\exp(-U/T)B^{U_0/T}$. Figure 2 shows the temperature dependences of the absolute value of U_0, determined both from high-frequency measurements in a pulsed field and from quasistationary measurements in a dc field.[10] As

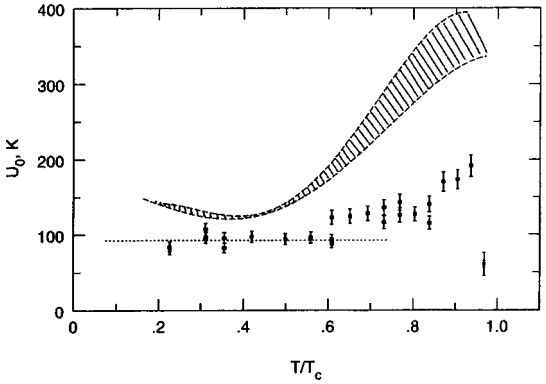

FIG. 2. Temperature dependences of the absolute value of U_0, the parameter in the theoretical dependence $U=U_0 \log(1/B)$ that characterizes the barrier heights for flux creep. The filled squares show $U_0=\beta T$, determined by fitting the relation $R\propto B^{\beta}$ to the data from the region of formation of the resistive state, which were obtained from the high-frequency measurements in a pulsed field. The hatched region corresponds to the results of quasistationary measurements in a dc field.[10]

one can see from Fig. 2, there is a systematic dissimilarity both in the absolute values of U_0, which are determined on substantially different time scales, and in the character of their variation as a function of temperature. This effect could be due to the frequency dependence of the barrier height, but a conclusive answer to this question requires a more detailed investigation.

As one can see from Fig. 1, the field dependences $R(B)$ can be approximated satisfactorily by a power law in the range of resistances right up to $R/R_N\approx 0.05$. As the field increases further, a transition evidently occurs to a regime of flux flow and, in consequence, the dependence flattens out. This dependence can be approximated by a linear function, shown by the dashed line in the main panel. Assuming this interpretation to be correct, it is natural to attribute the section of the curve with a negative magnetoresistance to the normal-state properties of the system and the quantity $R_N(0)$ obtained by extrapolating the asymptotic high-field behavior to zero field can be attributed to the resistance of the system in the absence of superconductivity.

At the same time, a similar dependence is predicted for the resistive state of a layered superconductor with a Josephson link between the layers. Specifically, the initial growth of the resistance is attributed to the suppression of the Josephson critical current as a result of a decrease of the positional correlation between the vortex ''pancakes'' in neighboring planes. The decrease of the resistance with a further increase of the field is attributed in this scenario to the increase in quasiparticle density, which, to a first approximation, is proportional to the field.[12]

An experimental argument in favor of the first explanation is the character of the variation of $R(B)$ with temperature, as is illustrated in Fig. 3, which displays the results, normalized to $R_N(0)$, of measurements performed above and below the superconducting transition temperature. As one can see from the figure, the normal-state transverse magnetoresistance of a BSCCO-2212 crystal at temperatures $T>T_{c0}$ can be approximated satisfactorily by a linear law with a temperature-dependent slope in the entire range of fields up to 50 T. As temperature decreases below T_{c0}, the asymptotic behavior of the

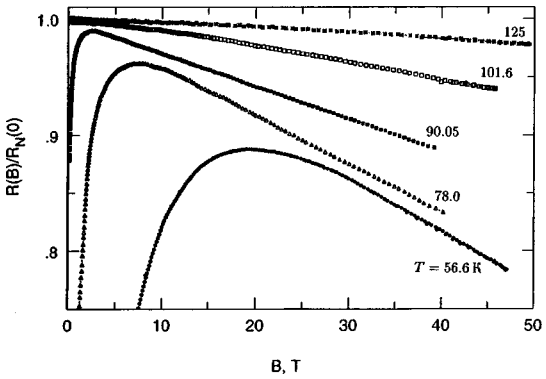

FIG. 3. Temperature evolution of the normalized experimental dependences $R(B)/R_N(0)$ measured both above and below the superconducting transition temperature T_{c0}. The results are presented for $T=56.6$, 78.0, 90.05, 101.6, and 125 K (bottom to top).

strong-field dependences remains unchanged, which shows that a single mechanism is responsible for the phenomenon, and gives a basis for attributing the effect to the normal-state properties and not to superconducting fluctuations, which are probably responsible for the rounding off of the transition, clearly seen in Figs. 1 and 3.

We note that the negative normal-state transverse magnetoresistance of a BSCCO-2212 crystal was observed earlier in Ref. 3, whose authors detected a pronounced quadratic growth of the effect with increasing magnetic field (up to 14 T), in excellent agreement with the predictions of the fluctuation theory.[4] At the same time, although the magnitude of the relative change of the resistance determined in our measurements at 14 T and 100 K agrees, to a high degree of accuracy, with the results presented in Ref. 3, the field dependence obtained can be approximated satisfactorily by a linear dependence, with only a slight flattening out for weak fields. This discrepancy could be due to methodological flaws in our experiments, whose weak point is that the temperature of the sample cannot be measured directly during the field pulse. However, it is obvious that on the rising part of the pulse the temperature of the sample can only increase as a result of Joule heating of the crystal by induction currents, and since $\partial\rho_c/\partial T<0$, this can lead only intensify the negative magnetoresistance, and therefore taking overheating effects into account does not improve the agreement with the data of Ref. 3. In turn, it cannot be asserted that there are no overheating effects in the work cited because the necessary information is lacking.

At the same time, the data presented in Fig. 1 agree qualitatively with the results of an investigation[2] of the transverse magnetoresistance of a crystal of another representative of the family of high-temperature superconductors Bi–Sr–Ca–Cu–O — La-doped $Bi_2Sr_2CuO_y$ (BSCCO-2201)[2] — in the case that its superconductivity is suppressed by a strong field. We note that a positive magnetoresistance was recorded in the *ab* plane of the crystal in the same work. This fact, combined with the positive basal-plane magnetoresistance found[5] in normal-state whiskers with the nominal composition 2212 attests to a similar mechanism of electron transport in the layered superconducting systems Bi–Sr–Ca–Cu–O. Nonetheless, the conclusion that electron transport is of the same

nature in BSCCO cuprates differing by the number of copper–oxygen planes evidently requires more detailed investigation.

Besides the scenarios mentioned above, the observed effect can be interpreted on the basis of a bipolaron model,[13] which predicts a negative transverse magnetoresistance due to a decrease in the polaron gap in the normal-state density of states as a result of spin-splitting of the polaron band. An additional argument in favor of this interpretation is the satisfactory agreement between the temperature dependence of the second critical field of BSCCO-2212, determined from the temperature dependences of the transverse resistance of the crystal and computed in the model mentioned.[14] Assuming the negative magnetoresistance to belong to the normal state of the crystal, to obtain a rough estimate of H_{c2} from measurements performed in a pulsed field it is natural to use the point of intersection of the linear extrapolations of the data from the region of flux flow and the normal state, as shown by the arrow in Fig. 1. It was established that in a wide temperature range, $0.4 \leqslant T/T_c \leqslant 0.97$, the dependence $H_{c2}(T)$ constructed in this manner agrees qualitatively with the results obtained in Ref. 14, demonstrating only negligible quantitative discrepancies. We note that his result attests to the adequacy of the assumptions on which the complicated procedure developed in Ref. 14 to determine H_{c2} is based.

This work was performed as part of projects supported by EPSRC, the Russian Fund for Fundamental Research, and the Council on Superconductivity. The measurements in pulsed magnetic fields were initiated mainly by A. S. Aleksandrov. Their success was ensured, to a large degree, by the hospitality, technical assistance, and moral support of the laboratory staff. We are especially grateful to T. J. B. M. Janssen for adapting the software and A. S. Aleksandrov, A. Varlamov, D. Geshkenbein, and A. Koshelev for helpful discussions.

[a)]e-mail: vlad@kapitza.ras.ru

[1] S. L. Cooper and K. E. Gray, in *Physical Properties of High Temperature Superconductors*, edited by D. M. Ginsberg, World Scientific, Singapore, 1994, Vol. 4, p. 61.
[2] Y. Ando, G. S. Boebinger, A. Passner *et al.*, Phys. Rev. Lett. **77**, 2065 (1996).
[3] Y. F. Yan, P. Matl, J. M. Harris, and N. P. Ong, Phys. Rev. B **52**, R751 (1995).
[4] A. A. Varlamov, Physica C **282–287**, 248 (1997).
[5] Yu. I. Latyshev, O. Labrode, and P. Monceau, Europhys. Lett. **29**(6), 495 (1995).
[6] A. Yurgens, D. Winkler, N. V. Zavaritsky, and T. Claeson, Phys. Rev. Lett. **79**, 5122 (1997).
[7] N. V. Zavaritskiĭ, V. N. Zavaritskiĭ, A. P. McKenzie *et al.*, JETP Lett. **60**, 193 (1994).
[8] V. N. Zavaritsky and W. Y. Liang, J. Low Temp. Phys. **105**, 1273 (1996).
[9] V. N. Zavaritskiĭ, JETP Lett. **63**, 139 (1996).
[10] V. N. Zavaritskiĭ, JETP Lett. **65**, 663 (1997).
[11] G. Blatter, M. V. Feigel'man, V. B. Geshkenbein *et al.*, Rev. Mod. Phys. **66**, 1125 (1994).
[12] A. E. Koshelev, L. I. Glazman, and A. I. Larkin, Phys. Rev. B **53**, 2786 (1996); A. E. Koshelev, Phys. Rev. Lett. **76**, 1340 (1996).
[13] A. S. Alexandrov, V. V. Kabanov, and N. F. Mott, Phys. Rev. Lett. **77**, 4796 (1996).
[14] A. S. Alexandrov, V. N. Zavaritsky, W. Y. Liang, and P. L. Nevsky, Phys. Rev. Lett. **76**, 983 (1996).

Translated by M. E. Alferieff

Subharmonic Shapiro steps and noise in high-T_c superconductor Josephson junctions

M. Tarasov[a)]
Institute of Radio Engineering and Electronics, Russian Academy of Sciences, 103907 Moscow, Russia;
Chalmers University of Technology, Göteborg, S-412 96, Sweden

D. Golubev
Chalmers University of Technology, Göteborg, S-412 96, Sweden;
Physics Institute, Russian Academy of Sciences, 117924 Moscow, Russia

V. Shumeĭko and Z. Ivanov
Chalmers University of Technology, Göteborg, S-412 96, Sweden

E. Stepantsov
Chalmers University of Technology, Göteborg, S-412 96, Sweden;
Institute of Crystallography, Russian Academy of Sciences, 117333 Moscow, Russia

O. Harnak
Chalmers University of Technology, Göteborg, S-412 96, Sweden;
Institute of Thin Film and Ion Technology, Research Center, 52425 Jülich, Germany

T. Claeson
Chalmers University of Technology, Göteborg, S-412 96, Sweden

(Submitted 30 July 1998)
Pis'ma Zh. Éksp. Teor. Fiz. **68**, No. 5, 426–430 (10 September 1998)

An experimental investigation is made of the subharmonic Shapiro steps observed on the I–V curves of high-T_c superconductor Josephson junctions and on the bias-voltage dependences of the rf noise and detector response when the junctions are subjected to external submillimeter radiation. Structures of this type are ordinarily described by a nonsinusoidal current–phase relation, which is why subharmonic steps appear. Numerical modeling of the processes occurring in a Josephson junction by means of a simple current–phase relation, as in the case of an SNS junction, gives good agreement with experiment. The width of the characteristic Josephson generation line of the junction was estimated on the basis of the noise dependences and the selective detector response. The width can be explained by taking into account the shot noise of the tunneling component of the conductivity. A model of the conductivity of a high-T_c superconductor Josephson junction, consisting of a tunnel junction with microshorts possessing metallic conductivity, is discussed. © *1998 American Institute of Physics.*
[S0021-3640(98)01417-0]

PACS numbers: 74.50.+r, 74.25.Fy, 74.72.Bk

Micron-size high-T_c superconductor (HTSC) Josephson junctions on grain boundaries on bicrystalline substrates are ordinarily described well by a simple resistive model of the Josephson junction. On the basis of this model[1–3] the phase difference φ on a junction is described by the Josephson equation

$$\frac{\hbar\dot{\varphi}}{2eR_N}+I_S(\varphi)=I_x+I_0\sin(\omega t), \tag{1}$$

where R_N is the asymptotic resistance of the junction at high voltages, $I_S(\varphi)$ is the dependence of the superconducting current on the phase difference of the wave function across the junction, I_x is the external dc bias current, and I_0 is the amplitude of the external rf current. The external rf current gives rise to Shapiro steps on the current–voltage (I–V) curve of the junction at the voltages

$$V_n=\frac{\hbar\omega}{2e}n. \tag{2}$$

In the general case the steps can arise under the resonance conditions $m\Omega_J=n\Omega$, where $\Omega_J=2eV/\hbar$ and n and m are arbitrary integers. For this reason, the steps can also arise, in principle, at the voltages

$$V_{n,m}=\frac{\hbar\omega}{2e}\frac{n}{m}. \tag{3}$$

It is important to note that in the resistive model (1) no subharmonic steps with $m>1$ appear if the current–phase relation has the standard sinusoidal form (see, for example, Ref. 1):

$$I_S(\varphi)=I_C\sin\varphi. \tag{4}$$

However, in our experiments the subharmonic steps were observed on many junctions. To interpret the experimental data the simple resistive model must be extended to the case of an arbitrary current–phase relation.

In our experiments the I–V curve, the detector response, and the rf noise of YBaCuO Josephson junctions deposited on different bicrystalline MgO and YSZ substrate were measured. The I–V curves of comparatively narrow ($W<2\ \mu$m) and high-resistive junctions were close to the curves calculated in a resistive model. The excess current was low and only weak half-integer subharmonic steps ($m=2$) were observed under the action of submillimeter radiation. The I–V curves of wider junctions ($W=4-8\ \mu$m) differed from the hyperbolic form predicted by the resistive model. A high excess current, up to 50% of the critical current of the junctions, was observed on them. Application of external radiation gave rise to two series of steps (see Fig. 1). The first series appeared at the voltages $V_{1,m}=hf/2em$ and the second series appeared at the voltages

$$V_{m-1,m}=\frac{hf}{2e}\left(1-\frac{1}{m}\right).$$

Subharmonic steps up to sixth order ($m=6$) were observed experimentally. The subharmonic steps were most conspicuous in the rf noise curves measured at a frequency of 1.4 GHz using a cooled amplifier with a cooled rectifier at the input. Such measurements are

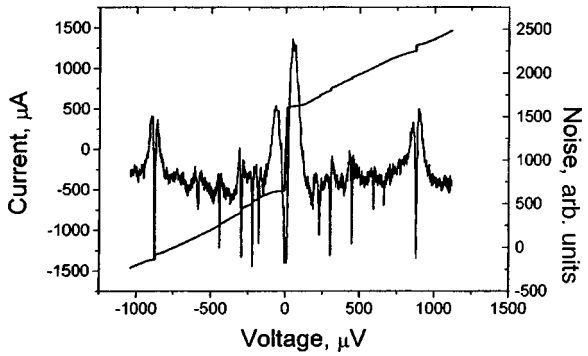

FIG. 1. Experimental I–V curve and noise as a function of the voltage across a junction with a resistance of 1 Ω and a critical current 510 μA, under external irradiation at frequency 400 GHz.

more sensitive than the standard technique of measuring the differential resistance or detector response, and they make it possible to observe higher-order subharmonic steps.

For bridges no more than 2 μm wide the subharmonic steps are hardly perceptible in the I–V curves, but they can be easily observed in the noise dependence at voltages corresponding to 1/2 and 1/3 of a Shapiro step.

To estimate the noise properties we also measured the width of the Josephson generation line at frequencies of 500 and 1000 GHz. The linewidth was determined as the voltage distance between two noise maxima near the voltage corresponding to the frequency of the external radiation. For very small amplitudes of the external microwave radiation this voltage difference equals

$$\Delta V = \pi\sqrt{3}h\Delta f/e.$$

When the signal amplitude is increased, the simple relation between the width of the generation line and the positions of the noise maxima is destroyed, and for this reason the estimates of the width of the generation line were made only according to the response to a weak signal. At 4.2 K the linewidth was 34 GHz on a 20 Ω junction, 28 GHz on a 4 Ω junction, and 4.5 GHz on a junction shunted by an 0.7 Ω external low-inductance shunt.

Several mechanisms could be responsible for the appearance of the subharmonic steps.[4–8]

One such mechanism could be due to the finite capacitance of a junction. In the general case this effect cannot be very strong. Indeed, for zero capacitance there are no subharmonic steps, but they are absent even if the capacitance is large, since the ac voltage across the junction is effectively shunted. As was shown in Ref. 7, subharmonic steps can be observed on the I–V curves in the case $\omega R_N C \sim 1$. For high-T_c superconductor junctions it is quite difficult to estimate the junction capacitance, but it is clear that it is small, since the I–V curve is close to a hyperbolic curve predicted by the resistive model with no capacitance. For this reason the finite small capacitance of a junction can hardly be responsible for the appearance of strong subharmonic steps.

Another possible mechanism is a nonsinusoidal current–phase relation. In the general case the relation between the supercurrent and phase can be written as

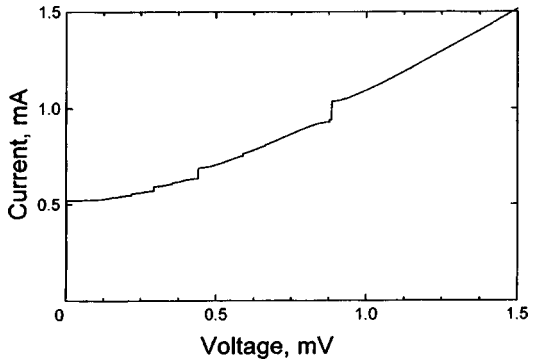

FIG. 2. Numerically computed I–V curve with parameters close to the experimental values.

$$I_s(\varphi)=I_c \sin \varphi+\sum_{m=2}^{+\infty} I_m \sin m\varphi. \tag{5}$$

The higher-order harmonics with $m>1$ lead to the appearance of subharmonic steps.[8] The deviation of the current–phase dependence from a simple sinusoidal curve is not surprising. This type of weak link differs appreciably from the standard link for a tunnel junction, and high-T_c superconductor junctions are ordinarily considered to be close to SNS or more complicated type structures. It is well known that the current–phase relation for a SNS junction at low temperatures and voltages is different from $I_C \sin \varphi$. Subharmonic steps have been observed in classical low-T_c superconductor junctions of the SNS type in many works, specifically in Ref. 9. Another possible reason for the nonsinusoidal relation could be the formation of superconducting microshorts, or Dayem bridges, inside the junction. This type of junction exhibits very strong subharmonic steps[10] and is ordinarily described by a nonsinusoidal $I_S(\varphi)$.[2,3] The dynamics of such junctions, on the whole, is more complicated.[3] In Ref. 5, to explain the experiment of Ref. 4, where half-integer steps were observed in YBaCuO junctions, it was suggested that Dayem microbridges are responsible for the appearance of half-integer Shapiro steps.

Recently,[6] a direct measurement of the current–phase relation was performed, but within the limits of experimental accuracy no deviations from a simple sinusoidal relation were observed. This result shows that the deviation from a sinusoidal relation could be nonsystematic; it could depend on the technological parameters, the structure of the junction, and the presence of defects. We performed numerical modeling using the relation

$$I_S(\varphi)=I_C \sin \varphi \frac{\tanh(a|\cos \varphi|)}{2|\cos \varphi|}. \tag{6}$$

Formally, such a relation corresponds to a single-channel SNS junction with the ratio $\Delta/2T=a$, but this relation reflects the general dependence $I_S(\varphi)$ for many other types of weak links, including multichannel SNS junctions at low temperatures and Dayem bridges. We observed that the experimental I–V curves correspond quite well to the model (see Fig. 2) for $a\cong 10$, despite the fact that the excess current was ignored. This shows that the current–phase relation has a dominating influence.

Another mechanism leading to the appearance of subharmonic steps could be due to the large width of the junction. It is well known from previous experiments that very small point contacts essentially do not exhibit subharmonic steps, but as the pressure on the contact is increased, the contact area increases and ordinarily subharmonic steps appear. A similar trend was observed in Ref. 9, where subharmonic steps were observed in wide Pb–Cu–Pb SNS junctions with $W/\lambda_J = 6.6$, while subharmonic steps were not observed in narrow junctions with $W/\lambda_J = 2$. For our junctions we estimate $\lambda_J \sim 2\ \mu$m, and this mechanism cannot be ruled out for junctions wider than 4 μm. However, numerical modeling of the dynamics of wide junctions in the presence of external microwave generation is much more complicated and definite conclusions cannot be drawn solely from measurements of the I–V curves and the response.

According to the measurements performed, the width of the Josephson generation line is much larger than the computed width. For this reason, we shall endeavor to determine the reason for the broadening of the Shapiro steps. For thermal noise the spectral density of the voltage fluctuations can estimated to high accuracy as

$$S_V(V) = R_d^2(V) S_I \cong \frac{2R_d^2(V) k_B T}{R_0}, \tag{7}$$

where R_0 is the differential resistance in the absence of irradiation. One can see that the maximum of the noise as a function of the voltage is practically identical to the position of the maximum of the differential resistance. The position of the latter can be obtained from the analytical expression for the shape of a step in the presence of thermal noise across a resistance R_0. The broadening of a step is determined by the dimensionless parameter $\gamma = 2ekT/\hbar I_{st}$, where I_{st} is half the step height in the absence of noise. The exact analytical results of Ref. 1 are quite complicated, but approximate values can be used for practical estimates:

$$\Delta V = \begin{cases} 1.92 R_0 \sqrt{2ek_B T I_{st}/\hbar}, & \gamma \lesssim 1, \\ 4\sqrt{3} ek_B T R_0/\hbar, & \gamma \gtrsim 1. \end{cases} \tag{8}$$

For the curve in Fig. 1 we obtain $\gamma = 0.05$ and $\Delta V = 6\ \mu$V at 4.2 K, while the experimental value is 30 μV. For other samples the broadening of a step was 1–3 times greater than that calculated from Eq. (8). The additional broadening of the main Shapiro step can be explained by the shot noise of a junction for quite high bias voltages of 1 or 2 mV. The influence of shot noise can be taken into account in the calculations by simply replacing kT by

$$k_B T_{\text{eff}} = (eV/2)\coth(eV/2k_B T) \tag{9}$$

in expression (7). Then the computed linewidth increases by a factor of 1.5–2 depending on the bias voltage corresponding to the frequency.

We have investigated subharmonic steps in high-T_c superconductor Josephson junctions under the action of submillimeter irradiation. Subharmonic steps up to sixth order were observed on the I–V curve, the detector response, and the bias-voltage dependence of the rf noise. Numerical modeling using a nonsinusoidal current–phase relation gives close agreement with the measured results. Such a dependence $I_S(\varphi)$ could be due to the presence of additional conduction channels in the form of microshorts and defects in the junction in the SNS or Ss′S structures. The width of the Josephson generation line was

found to be several times greater than the value calculated in the simple model of thermal noise. This is explained by the presence of shot noise in the tunneling part of the conductivity of the junction.

We thank the Russian Science and Technology Program ''Topical Problems in Condensed Media Physics,'' the Russian Fund for Fundamental Research, the Ministry of Science of the Russian Federation, and the Swedish Royal Academy of Sciences for financial support.

[a)]e-mail: tarasov@hitech.cplire.ru

---

[1] K. K. Likharev, *Dynamics of Josephson Junctions and Circuits*, Gordon and Breach, New York, 1986.
[2] A. Barone and G. Paterno, *Physics and Applications of the Josephson Effect*, Wiley, New York, 1982.
[3] K. K. Likharev, Rev. Mod. Phys. **51**, 101 (1979).
[4] E. A. Early and A. F. Clark, Appl. Phys. Lett. **62**, 3357 (1993).
[5] L. C. Ku, H. M. Cho, and S. W. Wang, Physica C **243**, 187 (1995).
[6] E. V. Il'ichev, V. M. Zakosarenko, R. P. J. Jisselsteijn *et al.*, Appl. Phys. Lett. **72**, 731 (1998).
[7] C. A. Hamilton and E. G. Johnson, Phys. Lett. A **41**, 393 (1972).
[8] H. Lubbig and H. Luther, Rev. Phys. Appl. **9**, 29 (1974).
[9] J. Clarke, Phys. Rev. B **4**, 2963 (1971).
[10] A. H. Dayem and J. J. Wiegand, Phys. Rev. **155**, 419 (1967).

Translated by M. E. Alferieff

Oscillation phenomena in polyacetylene: $R^1 \times S^1$ Gross–Neveu model with a chemical potential

M. A. Vdovichenko
Moscow Institute of Radio Engineering, Electronics, and Automation, 117454 Moscow, Russia

A. K. Klimenko
Department of Physics, Moscow State University, 117234 Moscow, Russia

(Submitted 9 July 1998)
Pis'ma Zh. Éksp. Teor. Fiz. **68**, No. 5, 431–436 (10 September 1998)

The phase structure of the two-dimensional Gross–Neveu model in a spacetime of the form $R^1 \times S^1$ and in the presence of a chemical potential μ is investigated. The phase portrait of the model is constructed in the parameter plane (μ, λ), where $\lambda = 1/L$ and L is the length of the circle S^1. In the portrait there exist two massive phases, with spontaneously broken chiral invariance, as well as infinitely many massless symmetric phases. Such a vacuum structure leads to oscillations of the critical curve $\mu_c(\lambda)$ of chiral phase transitions. In addition, the particle number density in the vacuum state of the model oscillates if $\mu > \mu_c(\lambda)$. © *1998 American Institute of Physics.*
[S0021-3640(98)01517-5]

PACS numbers: 72.20.Dp, 11.10.Kk, 75.30.Kz, 75.20.Ck

INTRODUCTION

A two-dimensional quantum field theory with a Lagrangian of the form

$$L_\psi = \sum_k \bar{\psi}_k i\hat{\partial}\psi_k + \frac{g}{2N}\left[\sum_k \bar{\psi}_k \psi_k\right]^2 \tag{1}$$

is called a Gross–Neveu (GN) model.[1] In Eq. (1) the ψ_k are two-component Dirac spinors for each fixed value $k = 1, \ldots, N$, and L_ψ is symmetric with respect to a discrete chiral transformation $\psi_k \to \gamma^5 \psi_k$. Instead of Eq. (1), the Lagrangian

$$L_\sigma = \sum_k [\bar{\psi}_k i\hat{\partial}\psi_k + \sigma\bar{\psi}_k\psi_k] - N\sigma^2/2g, \tag{2}$$

which in the equations of motion, where $\sigma = \Sigma\bar{\psi}_k\psi_k$, is equivalent to Eq. (1), is very often studied. Initially, the model was proposed as a simple example demonstrating certain properties of quantum chromodynamics, specifically, asymptotic freedom, spontaneous breaking of chiral invariance, dimensional transmutation, and others. Some of these properties follow from the following expression for the effective model potential obtained in leading order in the $1/N$ expansion:[1]

$$V_0(\sigma)=\frac{N\sigma^2}{2g}+\frac{iN}{(2\pi)^2}\int d^2p\ln(\sigma^2-p^2)=\frac{N\sigma^2}{4\pi}[2\ \ln(\sigma/M)-1]. \quad (3)$$

After renormalization $V_0(\sigma)$ is expressed using only the dimensional parameter M, whose physical meaning is that of a dynamical mass of fermions (dimensional transmutation).

Later, other general theoretical questions, such as the effect of temperature and nonzero particle density,[2–4] nontrivial topology of the space,[5,6] and different fields[7] (including gravitational[8–10]) on the chiral properties of the vacuum were also investigated on the basis of the GN model. Moreover, it was shown in Refs. 11 and 12 that for a variety of quasi-one-dimensional compounds, called Peierls insulators, the microscopic models of the electronic states in the continuous limit are completely analogous to two-dimensional quantum field theories. Specifically, the GN model with $N=2$ was found to be the best theory describing the electrical conductivity of one Peierls insulator, polyacetylene $(CH)_x$. In pure form, with no impurities, polyacetylene, like other Peierls insulators, is an insulator. In the presence of light doping, when the concentration of impurity electrons (holes) does not exceed 6%, it is a conductor with a spinless electric-charge carriers and exhibits diamagnetic properties. However, when the impurity concentration reaches 6% and higher, its magnetic properties change sharply. It becomes a paramagnet by a first-order phase transition. (These and other properties of Peierls insulators can be studied in greater detail in the reviews Refs. 13.)

The aforementioned phase transition in polyacetylene was investigated in a two-dimensional GN model with chemical potential μ in Refs. 14 and 15, where it was shown in leading order in N that at the critical value of the chemical potential $\mu_c=M/\sqrt{2}$ a first-order phase transition occurs in the model from a phase with broken chiral invariance (the phase where fermions possess mass M) to a symmetric phase with massless conduction electrons.[a)] (The model had been used previously for qualitative analysis of the properties of Peierls insulators.[16])

The present letter is also devoted to the investigation of a soliton-metallic phase transition in a Peierls insulator in the two-dimensional model (1) with $\mu\neq 0$ in the case that the spacetime possesses a topology of the form $R^1\times S^1$ (compactified spatial axis, rolled up into a circle S^1 of length L).

In reality, most Peierls insulators are three-dimensional crystals, where on account of the characteristic features of the crystal structure the electron motion is essentially one-dimensional. An external stress can deform the crystal lattice, and then the electron motion becomes curvilinear. Here, studying the limiting case of motion on a circle S^1, we have in mind, of course, the fact that it can be used to describe processes in deformed Peierls insulator crystals with large values of L, i.e., under laboratory conditions. (Looking ahead, we note that this is the region where the conductivity oscillations that we observed and the critical curve of the chiral phase transition show up most clearly.) Moreover, we hope that the results obtained below will be helpful for drawing qualitative analogies when constructing superstring theories, in describing phenomena of the Casimir effect type, and so on, i.e., in the cases where the topology of the spacetime is nontrivial.

1. PHASE STRUCTURE OF THE MODEL

The properties of vacuum are uniquely related with the structure of the global minimum of the effective potential of the model. To leading order in the $1/N$ expansion, for arbitrary values of μ and L, the effective potential has the form[5]

$$V_{\mu L}(\sigma)=V_L(\sigma)-N\lambda\sum_{n=0}^{\infty}\alpha_n\theta(\mu-\sqrt{\sigma^2+(2\pi n\lambda)^2})(\mu-\sqrt{\sigma^2+(2\pi\lambda n)^2}), \tag{4}$$

where $\theta(x)=1$ for $x\geqslant 0$, $\theta(x)=0$ for $x<0$, $\lambda=1/L$, $\alpha_n=2-\delta_{n0}$, and

$$V_L(\sigma)=V_0(\sigma)-\frac{N}{\pi L}\int_{-\infty}^{\infty}dp_0\ \ln[1-\exp(-L\sqrt{\sigma^2+p_0^2})]. \tag{5}$$

The global minimum of the function (5), into which the potential (4) transforms at $\mu=0$, is located at the point $\sigma_0(\lambda)$. In addition, $\sigma_0(\lambda)\to M$ if $\lambda\to 0$ and $\sigma_0(\lambda)\sim\pi\lambda/\ln(\lambda/\lambda_0)$ if $\lambda\to\infty$. Here $4\pi\lambda_0=M\exp(\gamma)$, where $\gamma=0.577\ldots$, is the Euler constant.

Our problem is to investigate the function (4) for an absolute minimum. For it the stationary-state equation is

$$\frac{\sigma}{\pi}\left\{\ln\frac{\lambda}{\lambda_0}+I(\sigma)-\frac{\pi\lambda}{\sigma}+\pi\lambda\sum_{n=0}^{\infty}\alpha_n\frac{\theta(\mu-\sqrt{\sigma^2+(2\pi\lambda n)^2})}{\sqrt{\sigma^2+(2\pi\lambda n)^2}}\right\}=0, \tag{6}$$

where

$$I(\sigma)=\sum_{n=1}^{\infty}\{1/n-[n^2+(\sigma/2\pi\lambda)^2]^{-1/2}\}. \tag{7}$$

The structure of Eq. (6) dictates the following algorithm for obtaining a solution. We divide the parameter plane (μ,λ) into regions ω_k,

$$(\mu,\lambda)=\bigcup_{k=0}^{\infty}\omega_k;\quad \omega_k=\{(\mu,\lambda):2\pi\lambda k\leqslant\mu<2\pi\lambda(k+1)\}, \tag{8}$$

and then investigate this equation in each region ω_k successively.

Let $(\mu,\lambda)\in\omega_0$. Here the stationary-state equation has a simpler form:

$$\frac{\sigma}{\pi}\left\{\ln(\lambda/\lambda_0)+I(\sigma)-\frac{\pi\lambda}{\sigma}[\theta(\mu-\sigma)-1]\right\}=0. \tag{9}$$

Hence it is obvious that for $\lambda>\lambda_0$ Eq. (9) has only two solutions: $\sigma_1=0$ and $\sigma_2=\sigma_0(\lambda)$, each of which is a local minimum for the potential $V_{\mu L}(\sigma)$. In this case it is obvious that the critical values of the chemical potential $\mu_{0c}(\lambda)$, for which the global minimum of the potential $V_{\mu L}(\sigma)$ passes from σ_1 to σ_2 and vice versa, is determined by the equation

$$V_{\mu L}(0)=V_{\mu L}(\sigma_0(\lambda)), \tag{10}$$

which can be solved exactly in the region ω_0:

$$\mu_{0c}(\lambda)=[V_L(0)-V_L(\sigma_0(\lambda))]/(N\lambda). \tag{11}$$

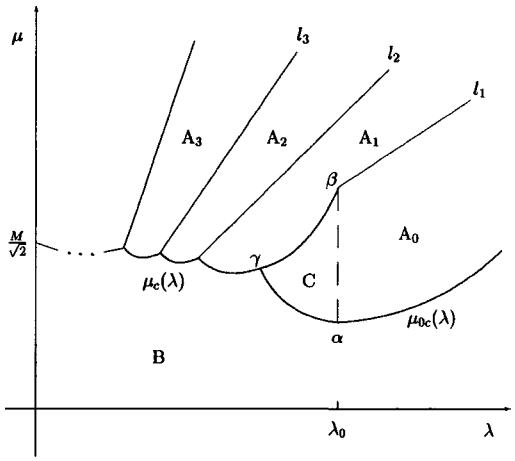

FIG. 1.

For $\mu > \mu_{0c}(\lambda)$ we have a massless symmetric phase of the model (the set A_0 in Fig. 1). If $\mu < \mu_{0c}(\lambda)$, then a phase with spontaneous breaking of chiral invariance, where fermions possess mass $\sigma_0(\lambda)$ (region B in Fig. 1), is realized in the model.

If $\lambda < \lambda_0$, then $\sigma_1 = 0$ will now be the point of local maximum of the potential (4). Instead of it, here $V_{\mu L}(\sigma)$ acquires another local minimum — the point $\sigma_3 = \tilde{\sigma}_0(\lambda) \not\equiv 0$, which for $\lambda = \lambda_0$ becomes zero. The values of the chemical potential $\mu_1(\lambda)$ for which these minima are equivalent are determined by the equation

$$V_{\mu L}(\tilde{\sigma}_0(\lambda)) = V_{\mu L}(\sigma_0(\lambda)). \tag{12}$$

The curve $\mu = \mu_1(\lambda)$ separates the phase B from another massive phase, where the fermion mass equals $\tilde{\sigma}_0(\lambda)$ (the set C in Fig. 1). We also note that transitions between A_0 and B and between B and C are first-order phase transitions. However, the transition from C to A_0 and vice versa is a second-order phase transition. The boundary between the phases C and A_0 is the straight line $\alpha\beta$ (see Fig. 1), where $\alpha = \{(\lambda, \mu): \lambda = \lambda_0,\ \mu = (0.796\ldots)2\pi\lambda_0\}$, $\beta = \{(\lambda, \mu): \lambda = \lambda_0,\ \mu = 2\pi\lambda_0\}$.[b)]

It can be shown similarly, using numerical investigations, that in the region ω_1 there exists a critical curve $\mu_2(\lambda)$ (the curve $\beta\gamma$ in Fig. 1) that satisfies the equation $V_{\mu L}(0) = V_{\mu L}(\tilde{\sigma}_0(\lambda))$ and intersects the curve $\mu_1(\lambda)$ at the point $\gamma = \{(\lambda, \mu): \lambda = (0.841\ldots)\lambda_0,\ \mu = (0.865\ldots)2\pi\lambda_0\}$. The line of first-order phase transitions, $\mu = \mu_c(\lambda)$, on which the symmetry properties of the vacuum model change sharply and which is determined from Eq. (10), starts from this point.

It is known that the value of the effective potential at the point of a global minimum is the thermodynamic potential of the system. For this reason, in the region above the curve $\mu = \mu_c(\lambda)$, the thermodynamic potential $\Omega(\mu, \lambda)$ has the form

$$\Omega(\mu, \lambda) \equiv V_{\mu L}(0) = V_L(0) - N\lambda \sum_{k=0}^{\infty} \alpha_k \theta(\mu - 2\pi k\lambda)(\mu - 2\pi k\lambda). \tag{13}$$

It is easy to see that the first derivative $\partial\Omega/\partial\mu$, i.e., the number density of particles in the ground state of the system, changes value abruptly when each boundary between the regions ω_k (8) is crossed. Therefore we have first-order phase transitions on the lines $l_k=\{(\lambda,\mu):\mu=2\pi k\lambda\}$ and infinitely many massless symmetric phases of the model (the regions A_0, A_1, ... in Fig. 1) above the curve $\mu=\mu_c(\lambda)$ (the curve of chiral phase transitions).

The complete phase portrait of the model is presented in Fig. 1, where the dotted curve is the line of second-order phase transitions and the other curves are lines of first-order phase transitions. We note there exist two tricritical points α, β and infinitely many triple points, where three first-order curves come together (these are the points of intersection of the lines l_k for $k>1$ with the curve $\mu=\mu_c(\lambda)$, and also the point γ).

2. OSCILLATIONS OF THE CRITICAL CURVE $\mu_c(\lambda)$

Direct numerical investigations of the curve $\mu=\mu_c(\lambda)$ show that this curve has characteristic kinks at an infinite number of points where it intersects the lines l_k. In practice, such behavior of any function is usually said to be oscillatory. We shall single out the oscillatory component of the critical curve in explicit form. To this end, we represent Eq. (10), which $\mu_c(\lambda)$ satisfies, in the more detailed form

$$V_L(0)-V_L(\sigma_0(\lambda))=N\lambda\sum_{k=0}^{\infty}\alpha_k\theta(\mu-2\pi k\lambda)(\mu-2\pi k\lambda). \tag{14}$$

We denote the left-hand side of Eq. (14) by $\Delta V(\lambda)$, and we transform the right-hand side using the Poisson summation formula[17]

$$\sum_{k=0}^{\infty}\alpha_k\Phi(k)=2\sum_{k=0}^{\infty}\alpha_k\int_0^{\infty}\Phi(x)\cos(2\pi kx)dx \tag{15}$$

(the coefficients α_k are determined in Eq. (4)). Calculating the integrals in Eq. (15) we obtain for $\mu_c(\lambda)$ the equation

$$\Delta V(\lambda)=\frac{N\mu_c^2(\lambda)}{2\pi}-\frac{2N\lambda^2}{\pi}\sum_{k=1}^{\infty}\frac{\cos(k\mu_c(\lambda)L)-1}{k^2}. \tag{16}$$

From Eqs. (5) and (3) as well as the relation $\sigma_0(\lambda)\to M$ as $\lambda\to 0$ follows $\Delta V(\lambda)=NM^2/4\pi+O(\exp(-M/\lambda))$. With allowance for Eq. (16), this means that $\mu_c(\lambda)\to M/\sqrt{2}$ as $\lambda\to 0$. Moreover, it is now easy to solve Eq. (16) for small λ:

$$\mu_c(\lambda)=\frac{M}{\sqrt{2}}-\frac{2\sqrt{2}\lambda^2\pi^2}{6M}+\frac{2\sqrt{2}\lambda^2}{M}\sum_{k=1}^{\infty}\frac{\cos(kML/\sqrt{2})}{k^2}+o(\lambda^2). \tag{17}$$

Hence one can see that as $L\to\infty$ the function $\mu_c(\lambda)$ oscillates with frequency $M/2\sqrt{2}\pi$.

3. OSCILLATIONS OF THE THERMODYNAMIC POTENTIAL AND PARTICLE NUMBER DENSITY

Let $\mu > M/\sqrt{2}$. Then the state of thermodynamic equilibrium of the system is described by the thermodynamic potential $\Omega(\mu,\lambda)$ (13). It is easy to see that $\Omega(\mu,\lambda)$ also oscillates as L or μ increases. Indeed, let us apply the Poisson summation formula (15) to the infinite sum in Eq. (13). The result is the expression

$$\Omega(\mu,\lambda) = -\frac{N\mu^2}{2\pi} + \frac{2N\lambda^2}{\pi}\sum_{k=1}^{\infty}\frac{\cos(k\mu L)-1}{k^2}, \tag{18}$$

where the oscillatory component is singled out explicitly. The particle number density $n(\mu,\lambda)$ in the ground state is determined by the relation $n(\mu,\lambda) = -\partial\Omega/\partial\mu$. With allowance for Eq. (18), in the present model it has the form

$$n(\mu,\lambda) = \frac{N\mu}{\pi} + \frac{2N\lambda}{\pi}\sum_{k=1}^{\infty}\frac{\sin(k\mu L)}{k}, \tag{19}$$

i.e., for $\mu =$ const and large values of L it oscillates with frequency $\mu/2\pi$. If $L =$ const, then as μ increases, the density oscillates with frequency $L/2\pi$.

CONCLUSIONS

In the present letter the phase structure of the two-dimensional Gross–Neveu model in a $R^1 \times S^1$ space with a chemical potential was investigated in the leading order of the $1/N$ expansion. Two massive phases as well as infinitely many massless phases of the model exist in the phase diagram in Fig. 1. The phases are separated from one another by critical curves of both first and second orders, at the intersections of which lie two tricritical points and infinitely many triple points. A consequence of the phase structure obtained are oscillations of the critical curve of a chiral phase transition, in which the chiral symmetry is restored, as well as oscillations of the particle number density $n(\mu,\lambda)$ in the ground state of the model. (The four-dimensional Nambu–Jona–Lasinio model in a spacetime of the form $R^3 \times S^1$ in the presence of a chemical potential has an even greater diversity of critical properties.[18])

If the GN model is indeed close to reflecting the real properties of polyacetylene or other Peierls insulators, then, as follows from Eq. (17), it could be possible to observe in experiments with these materials oscillations of the critical degree of doping, resulting in a transition from a soliton phase to a metallic phase, depending on the curvature of the experimental sample. Moreover, since the electrical conductivity is proportional to $n(\mu,\lambda)$ (19), in experiments investigating the metallic phase of Peierls insulators their conductivity should also oscillate both as L increases with the impurity electron density held constant (proportional to μ) and with constant curvature L but with increasing degree of doping, i.e., with increasing μ.

[a)]This expression for μ_c was also obtained in Refs. 3 and 4.
[b)]The properties of the model in the region ω_0 are presented in greater detail in Ref. 5.

[1] D. J. Gross, A. Neveu, Phys. Rev. D **10**, 3235 (1974).
[2] L. Jacobs, Phys. Rev. D **10**, 3956 (1974); W. Dittrich and B. G. Englert, Nucl. Phys. B **179**, 85 (1981).
[3] K. G. Klimenko, Teor. Mat. Fiz. **75**, 226 (1988); A. Barducci, R. Casalbuoni, M. Modugno *et al.*, Phys. Rev. D **51**, 3042 (1995).
[4] U. Wolff, Phys. Lett. B **157**, 303 (1985); T. Inagaki, T. Kouno, and T. Muta, Int. J. Mod. Phys. A **10**, 2241 (1995).
[5] A. S. Vshivtsev, K. G. Klimenko, and B. V. Magnitskiĭ, JETP Lett. **61**, 871 (1995).
[6] S. K. Kim, W. Namgung, K. S. Soh, and J. H. Yee, Phys. Rev. D **36**, 3172 (1987); D. Y. Song and J. K. Kim, Phys. Rev. D **41**, 3165 (1990); F. Ravndal and C. Wotzasek, Phys. Lett. B **249**, 266 (1990); S. Huang and B. Schreiber, Nucl. Phys. B **426**, 644 (1994).
[7] S. Kawati, G. Konisi, and H. Miyata, Phys. Rev. D **28**, 1537 (1983).
[8] I. L. Buchbinder and E. N. Kirillova, Int. J. Mod. Phys. A **4**, 143 (1989); T. Muta, S. D. Odintsov, and H. Sato, Mod. Phys. Lett. A **7**, 3765 (1992); E. Elizalde, S. Naftulin, and S. D. Odintsov, Phys. Rev. D **54**, 5010 (1996); S. Kanemura, and H.-T. Sato, Mod. Phys. Lett. A **10**, 1777 (1995); Mod. Phys. Lett. A **11**, 785 (1996).
[9] T. Inagaki, T. Muta, and S. D. Odintsov, Prog. Theor. Phys. Suppl. **127**, 93 (1997).
[10] K. G. Klimenko, ''Gross–Neuvue model and optimized expansion method,'' Preprint IHEP 90-95, Protvino, 1990; H. Yamada, Mod. Phys. Lett. A **6**, 3405 (1991); *ibid.* **9**, 1195 (1994); *ibid.* **9**, 5651 (1994); V. E. Rochev and P. A. Saponov, ''The four-fermion interaction in $D=2,3,4$: a nonperturbative treatment,'' http://xxx.lanl.gov/abs/hep-th/9710006.
[11] S. A. Brazovskiĭ, JETP Lett. **28**, 606 (1978); Zh. Éksp. Teor. Fiz. **78**, 677 (1980) [Sov. Phys. JETP **51**, 342 (1980)].
[12] W. P. Su, J. R. Schrieffer, and A. J. Heeger, Phys. Rev. Lett. **42**, 1698 (1979).
[13] L. N. Bulaevskiĭ, Usp. Fiz. Nauk **115**, 263 (1975) [Sov. Phys. Usp. **18**, 131 (1975)]; I. V. Krive and A. S. Rozhavskiĭ, Usp. Fiz. Nauk **152**, 33 (1987) [Sov. Phys. Usp. **30**, 370 (1987)]; A. J. Heeger, S. Kivelson, J. R. Schrieffer, and W. P. Su, Rev. Mod. Phys. **60**, 781 (1988).
[14] V. A. Osipov and V. G. Fedyanin, ''Continuous model of polyacetylene and two-dimensional models of relativistic field theory'' [in Russian], JINR Brief Communications No. 4-84, Dubna, 1984, p. 33; Teor. Mat. Fiz. **73**, 393 (1987).
[15] A. Chodos and H. Minakata, Phys. Lett. A **191**, 39 (1994); Nucl. Phys. B **490**, 687 (1997).
[16] I. V. Krive and A. S. Rozhavskiĭ, Zh. Éksp. Teor. Fiz. **81**, 1811 (1981) [Sov. Phys. JETP **54**, 959 (1981)]; D. K. Campbell and A. R. Bishop, Nucl. Phys. B **200**, 297 (1982); H.-T. Sato and H. Tochimura, Mod. Phys. Lett. A **11**, 3091 (1996).
[17] L. D. Landau and E. M. Lifshitz, *Statistical Physics*, 3rd ed., Pergamon Press, New York, 1980 [Russian original, Nauka, Moscow, 1976, p. 196].
[18] A. S. Vshivtsev, A. K. Klimenko, and K. G. Klimenko, Yad. Fiz. **61**, 543 (1998) [Phys. At. Nucl. **61**, 479 (1998)]; M. A. Vdovichenko, A. S. Vshivtsev, and K. G. Klimenko, Zh. Éksp. Teor. Fiz. **114** (1998) [JETP], in press.

Translated by M. E. Alferieff